UNI[illegible]ITY
OF M[illegible]GAN
FEB [illegible] 1958
ENGINEERING
LIBRARY

# JOURNAL OF FLUID MECHANICS

VOLUME 3 PART 4

JANUARY 1958

Published by

CAMBRIDGE UNIVERSITY PRESS

BENTLEY HOUSE, 200 EUSTON ROAD, LONDON, N.W.1
AMERICAN BRANCH: 32 EAST 57th STREET, NEW YORK 22, N.Y.

*Price* 20*s*. (*U.S.A.* $3.25)

The JOURNAL OF FLUID MECHANICS exists for the publication of theoretical and experimental investigations of all aspects of the mechanics of fluids, and is issued in six parts per volume.

*Editor*

Dr. G. K. BATCHELOR, Cavendish Laboratory, University of Cambridge, Cambridge, England.

*Assistant Editors*

Dr. T. B. BENJAMIN, Dr. I. PROUDMAN, Dr. P. G. SAFFMAN.

*Associate Editors*

Prof. G. F. CARRIER, Pierce Hall, Harvard University, Cambridge 38, Massachusetts, U.S.A.

Dr. W. C. GRIFFITH, Research and Development Laboratory, Missile Systems Division, Lockheed Aircraft Corporation, Palo Alto, California, U.S.A.

Prof. M. J. LIGHTHILL, Department of Mathematics, The University, Manchester, England.

Authors wishing to have papers published in the JOURNAL should communicate them to any one of the persons named above, choosing one in their own country where possible.

Authors are urged to ensure that their papers are written clearly and attractively, in order that their work will be readily accessible to readers.

Manuscripts should be typed in double spacing on one side of the paper only, with references listed at the end in alphabetical order of authors. Drawings should be done on a large scale in Indian ink on tracing cloth or drawing paper, with the list of captions typed at the end of the manuscript. Proofs of papers from overseas will usually be despatched to authors by airmail. Authors are entitled to receive 50 offprints of a paper in the JOURNAL free of charge, and additional offprints can be purchased from the publisher.

## SUBSCRIPTIONS

The subscription price for a volume of six parts is £5 10*s.* net, post free, payable in advance. Separate parts 20*s.* net, plus postage. Subscriptions may be sent to any bookseller, or to the Cambridge University Press, Bentley House, 200 Euston Road, London, N.W.1.

Subscribers in the United States should send their orders to the Cambridge University Press, American Branch, 32 East 57th Street, New York 22. Subscription price per volume $18.50 post free, payable in advance; separate parts $3.25, plus postage.

# Flow past a flat plate at low Reynolds numbers

By E. JANSSEN
*General Electric Company, San Jose, California*

(*Received* 26 *July* 1957)

SUMMARY

The flow past a flat plate at Reynolds numbers in the range 0·1 to 10·0 is investigated by an analogue method. The solution gives the stream function and the vorticity in the flow field surrounding the plate. From these are obtained the local coefficient of friction, the pressure distribution along the plate, and the total drag coefficient. The drag coefficient approaches the analytical values of Haaser (1950) and of Tomotika & Aoi (1953) as the Reynolds number decreases toward 0·1. The drag coefficient approaches the Blasius solution as the Reynolds number increases. At Reynolds number 10·0 the drag coefficient is still above the Blasius value, but is below the value obtained experimentally by Janour (1951). The difference from the experimental result is attributed for the most part to truncation error.

## INTRODUCTION

The Blasius solution of the Prandtl boundary layer equation, for the case of flow past a thin flat plate, is valid only for a boundary layer whose thickness is very small relative to distance from the leading edge. The results of the Blasius analysis are therefore invalid at low Reynolds numbers. Kuo (1953) has investigated the flow past a flat plate for Reynolds numbers as low as 10 by a perturbation method. Tomotika & Aoi (1953), Imai (1954), and others have investigated the flow past a flat plate for Reynolds numbers up to about 1·0, by linearizing the flow equation in accordance with the Oseen approximation. Haaser (1950) has computed the skin friction distribution for this configuration, using Carrier's (1953) modification of the Oseen linearization for Reynolds numbers up to 5·0. The object of this paper is to investigate, by an analogue method, the flow past a finite flat plate at Reynolds numbers in the range 0·1 to 10·0, using the exact non-linear formulation of the problem, and to compare the results with those of the foregoing and with experiment.

The equation governing the two-dimensional motion of an incompressible fluid with constant viscosity is

$$\mathbf{v}.\nabla\zeta = \nu\nabla^2\zeta \tag{1}$$

where $\zeta$ is the scalar vorticity, given by

$$\zeta = \frac{\partial v}{\partial \psi} - \frac{\partial u}{\partial y}. \tag{2}$$

The defining equations of a stream function $\psi$ are

$$u = -\frac{\partial \psi}{\partial y}, \qquad v = \frac{\partial \psi}{\partial x}. \tag{3}$$

In Cartesian coordinates, these equations may be written

$$\nabla^2 \zeta = \frac{1}{\nu}\left\{\frac{\partial \psi}{\partial x}\frac{\partial \zeta}{\partial y} - \frac{\partial \psi}{\partial y}\frac{\partial \zeta}{\partial x}\right\}, \tag{4}$$

$$\nabla^2 \psi = \zeta. \tag{5}$$

Equations (3) satisfy the continuity equation which, therefore, does not need to be expressed explicitly.

Equations (4) and (5) have the form of the Poisson equation. These particular equations have been solved for the case of flow past a circular cylinder with zero circulation at Reynolds numbers in the range 1 to 1000, by numerical techniques (Thom 1933; Kawaguti 1953; and Allen & Southwell 1955). The procedure outlined in this paper gives a method of solution by means of two resistance networks which is applicable to an extensive class of problems in viscous flow. It will be applied here specifically to the case of flow past a flat plate.

*Transformation of equations*

It is convenient at the outset to render the equation dimensionless, and to consider transformation from the physical plane to some other plane. Let the physical plane be the $z$-plane, and let the velocity of the undisturbed flow be parallel to the $x$-axis. Then

$$z' = x' + iy' = r' e^{i\theta}.$$

Here the prime notation signifies dimensional quantities. The hydrodynamic equations, as well as the expression for $z$, are rendered dimensionless by making the following substitutions:

$$z = \frac{z'}{r_0'}, \qquad u = \frac{u'}{u_\infty'}, \qquad v = \frac{v'}{u_\infty'}, \qquad p = \frac{p'}{\rho'(u_\infty')^2},$$

$$\nu = \frac{\nu'}{u_\infty' r_0'}, \qquad \psi = \frac{\psi'}{u_\infty' r_0'}, \qquad \zeta = \frac{\zeta' r_0'}{u_\infty'}, \qquad N_R = \frac{2u_\infty' r_0'}{\nu'},$$

where $r_0'$ is some characteristic length, e.g. a cylinder radius, $u_\infty'$ is the undisturbed velocity parallel to the $x$-axis, $\nu'$ is the kinematic viscosity and $N_R$ is the Reynolds number.

The transformation $t = f(z)$ can be employed to map the field on to the $t$-plane where

$$t = \xi + i\eta. \tag{6}$$

If the transformation is conformal, equations (4) and (5) become

$$\nabla_t^2 \zeta = \frac{N_R}{2}\left\{\frac{\partial \psi}{\partial \xi}\frac{\partial \zeta}{\partial \eta} - \frac{\partial \psi}{\partial \eta}\frac{\partial \zeta}{\partial \xi}\right\} \tag{7}$$

and

$$\nabla_t^2 \psi = \frac{1}{q^2}\zeta, \tag{8}$$

where

$$\nabla_t^2 = \frac{\partial^2}{\partial \xi^2} + \frac{\partial^2}{\partial \eta^2}$$

and $q$, the transformation modulus, is the ratio of a length in the $t$-plane to the corresponding length in the $z$-plane, and is a function of position, that is

$$q = \left|\frac{dt}{dz}\right| = q(x, y) = q(\xi, \eta).$$

*Solution of the Poisson equation by a network analogue*

The general form of the Poisson equation

$$\nabla^2 \phi = f(x, y) \tag{9}$$

may be expressed approximately in the difference form

$$\phi_0 = \phi_M - \tfrac{1}{4} a^2 f(x_0, y_0), \tag{10}$$

where the field has been divided into square meshes of length $a$ on a side (figure 1). $\phi_0$ is the value of the function in question at a particular mesh point, and $\phi_M$ is the average for the nearest four neighbouring mesh points.

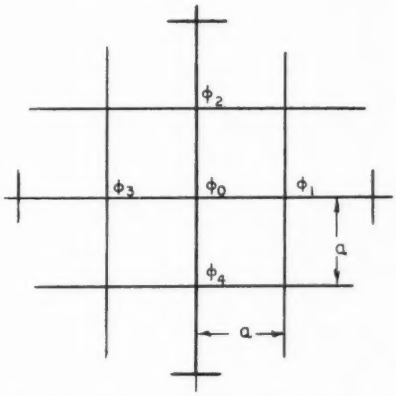


Figure 1. Representation of field by a net.

Now consider a resistance network having a geometrically similar mesh pattern (figure 2), with resistances $R_j$ between adjacent mesh points (nodes) as shown. In addition to the current flowing through these resistors, current flows into each of the nodes from an external source. The sum of the currents flowing into a particular node must be zero from Kirchhoff's law of node currents:

$$\frac{e_0 - e_1}{R_1} + \frac{e_0 - e_2}{R_2} + \frac{e_0 - e_3}{R_3} + \frac{e_0 - e_4}{R_4} - i_0 = 0,$$

$$\delta R_j = R_j - R_1,$$

$$e_0 = e_M - \left[\frac{1}{4}\sum_{j=2}^{4} \frac{\delta R_j}{R_j} e_j - \frac{e_0}{4}\sum_{j=2}^{4} \frac{\delta R_j}{R_j} - \frac{R_1 i_0}{4}\right], \tag{11}$$

where $\delta R_j$ is the deviation of the $j$th resistor with respect to the first resistor. The analogy that exists between the function $\phi$ of the system described by equation (10) and the voltage $e$ of the network is apparent. If a scale factor $K$ is chosen so that $e = K\phi$ at corresponding points, then $i$ can be adjusted so that

$$i_0 = \frac{1}{R_1}\sum_{j=2}^{4}\frac{\delta R_j}{R_j}e_j - \frac{e_0}{R_1}\sum_{j=2}^{4}\frac{\delta R_j}{R_j} - \frac{Ka^2}{R_1}f(x_0, y_0). \tag{12}$$

Note that when the resistor deviation is zero the first two terms on the right of equation (12), which are in fact error terms due to this deviation, drop out. By the method of this paper, however, it is not necessary that the resistor deviation be zero, as the current $i_0$ itself is not measured, and the network resistor deviation contributes nothing to the computational error.

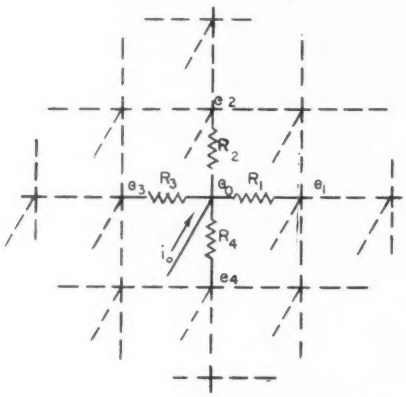


Figure 2. Resistance network pattern geometrically similar to net of figure 1.

The Poisson equations whose solutions are desired are equations (7) and (8). The difference forms of these equations are, respectively,

$$\zeta_0 = \zeta_M - \tfrac{1}{32}N_R\{(\psi_1-\psi_3)(\zeta_2-\zeta_4)-(\psi_2-\psi_4)(\zeta_1-\zeta_3)\} \tag{13}$$

and

$$\psi_0 = \psi_M - \frac{a^2}{4q_0}\zeta_0, \tag{14}$$

where

$$\zeta_M = \tfrac{1}{4}(\zeta_1+\zeta_2+\zeta_3+\zeta_4), \qquad \psi_M = \tfrac{1}{4}(\psi_1+\psi_2+\psi_3+\psi_4).$$

There is a network for each equation. The voltages at the boundaries of the two networks are fixed to correspond to the boundary conditions of the problem. Current must then be supplied to each anode in the $\psi$-network proportional (except for the resistor deviation terms of (12)) to $\zeta$ for that point, and to each node in the $\zeta$-network proportional to $\{(\psi_1-\psi_3)(\zeta_2-\zeta_4)-(\psi_2-\psi_4)(\zeta_1-\zeta_3)\}$ for that point. To accomplish this quantities, called the 'residuals' in relaxation procedures, are defined by

$$\mathscr{R}_\psi = 4\psi_M - 4\psi_0 - \frac{a^2}{q^2}\zeta_0 \tag{15}$$

for the $\psi$-net, and by

$$\mathscr{R}_\zeta = 4\zeta_M - 4\zeta_0 - \tfrac{1}{8}N_R\{(\psi_1-\psi_3)(\zeta_2-\zeta_4)-(\psi_2-\psi_4)(\zeta_1-\zeta_3)\} \qquad (16)$$

for the $\zeta$-net. The current to each node in the $\psi$-network is adjusted manually until $\mathscr{R}_\psi$ goes to zero, and the current to each node in the $\zeta$-network is adjusted manually until $\mathscr{R}_\zeta$ goes to zero. $\mathscr{R}_\psi$ and $\mathscr{R}_\zeta$ may be computed electronically by using components which change sign, add or multiply (the theory is clearly presented in a number of texts, for example see Korn & Korn (1952) or Soroka (1954)). A schematic diagram of the networks and associated voltage sources, current controls, etc., is shown in figure 3. One arrangement of electronic components for computing residuals is shown schematically in figure 4.

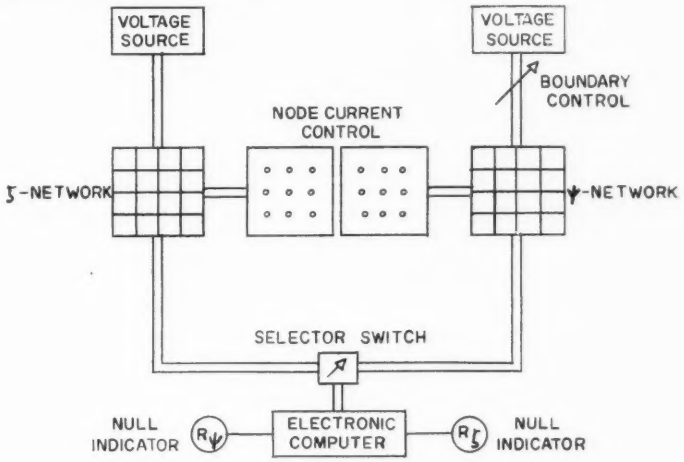


Figure 3. Schematic diagram of analogue.

The solution to equations (13) and (14) is obtained after a relaxation procedure involving the adjustment of the currents to each of the nodes in the two networks in several successive steps. This is the approximate solution to equations (7) and (8), the degree of approximation improving with the fineness of mesh. A mesh size should be used such that any decrease in the size will produce no change in the solution within the desired limits of accuracy.

*Boundary conditions (general)*

In the case of a flat plate located at or near the origin in an otherwise uniform flow field, $\psi$ is essentially at its uniform field value, and $\zeta$ is zero, far away from the origin. Thus, this part of the boundary, henceforth referred to as the outer boundary, is chosen far away and this may be taken care of by making the network quite large. It may also be handled by using a transformation which permits a reasonably small network to be used as was done in obtaining the results reported in this paper.

$\psi$ will be known at every place on the boundary and $\zeta$ will be known at every place except where the boundary is solid (that is, along the flat plate). Consider a solid boundary which is parallel to the $\xi$-axis (figure 5). The

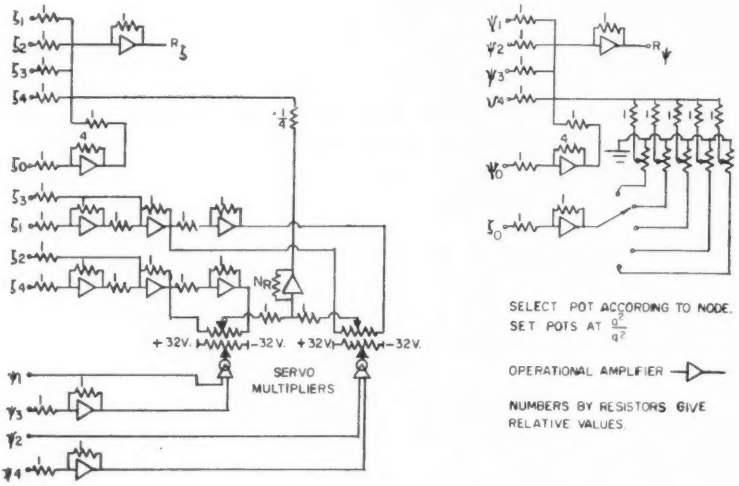


Figure 4. Assembly of electronic components for computing residuals.

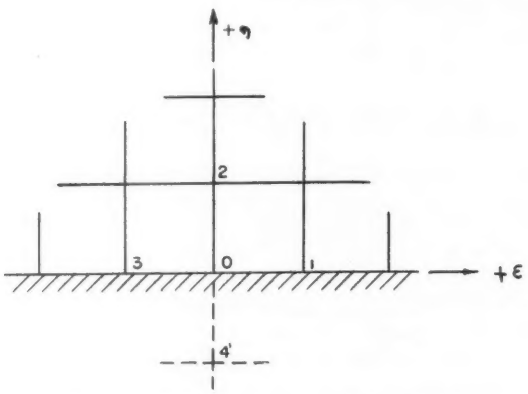


Figure 5. Solid boundary parallel to $\xi$-axis.

value of $\zeta$ at the point 0 on the boundary is desired. Points 1 and 3 are on the boundary and point 2 is a short distance inside the boundary at a position on a normal through point 0. The expression for $\zeta$ in terms of $\psi$ follows from equation (8):

$$\zeta = q_0^2[\nabla_i^2\psi]_0 = q_0^2\left[\left(\frac{\partial^2\psi}{\partial\xi^2}\right)_0 + \left(\frac{\partial^2\psi}{\partial\eta^2}\right)_0\right]. \tag{17}$$

A difference form for equation (17) may be obtained by using a Taylor

series expansion about point 0. The expression for the stream function at point 2 is

$$\psi_2 = \psi_0 + a\left(\frac{\partial\psi}{\partial\eta}\right)_0 + \frac{a^2}{2}\left(\frac{\partial^2\psi}{\partial\eta^2}\right)_0 + \frac{a^3}{6}\left(\frac{\partial^3\psi}{\partial\eta^3}\right)_0 + \frac{a^4}{24}\left(\frac{\partial^4\psi}{\partial\eta^4}\right)_0 + o(a^5).$$

From equation (8),

$$\left(\frac{\partial^2\psi}{\partial\eta^2}\right)_0 = -\left(\frac{\partial^2\psi}{\partial\xi^2}\right)_0 + \frac{1}{q_0^2}\zeta_0,$$

$$\left(\frac{\partial^3\psi}{\partial\eta^3}\right)_0 = -\left[\frac{\partial^2}{\partial\xi^2}\left(\frac{\partial\psi}{\partial\eta}\right)\right]_0 + \left(\frac{\partial(\zeta/q^2)}{\partial\eta}\right)_0,$$

$$\left(\frac{\partial^4\psi}{\partial\eta^4}\right)_0 = \left(\frac{\partial^4\psi}{\partial\xi^4}\right)_0 + \left(\frac{\partial^2(\zeta/q^2)}{\partial\eta^2}\right)_0 - \left(\frac{\partial^2(\zeta/q^2)}{\partial\xi^2}\right)_0.$$

Along the solid boundary $\psi$ is constant and $u$ is zero. Hence, all derivatives of $\psi$ with respect to $\xi$, and the first derivative of $\psi$ with respect to $\eta$, are zero. $\psi_2$ is now given by

$$\psi_2 = \psi_0 + \frac{a^2}{2}\frac{\zeta_0}{q_0^2} + \frac{a^3}{6}\left(\frac{\partial(\zeta/q^2)}{\partial\eta}\right)_0 + \frac{a^4}{24}\left[\left(\frac{\partial^2(\zeta/q^2)}{\partial\eta^2}\right)_0 - \left(\frac{\partial^2(\zeta/q^2)}{\partial\xi^2}\right)_0\right]. \quad (18)$$

Neglecting all terms past the second on the right (that is, all terms of order $a^3$ or higher), and rearranging, one obtains

$$\zeta_0 = \frac{2q_0^2}{a^2}(\psi_2 - \psi_0). \quad (19)$$

Thom (1933) and Allen & Southwell (1955) have used equation (19), and their results check well with experiment. It was possible for them to decrease the mesh constant $a$ in regions where $(\partial\zeta/\partial n)_s$ was large, thus keeping the third (and following) term on the right of equation (18) small and presumably negligible. Woods (1954), on the other hand, takes the third term into account in the following manner. The Taylor series is again employed, this time to obtain an expression for the vorticity at point 2:

$$\frac{\zeta_2}{q_2^2} = \frac{\zeta_0}{q_0^2} + a\left(\frac{\partial(\zeta/q^2)}{\partial\eta}\right)_0 + \frac{a^2}{2}\left(\frac{\partial^2(\zeta/q^2)}{\partial\eta^2}\right)_0 + o(a^3).$$

Rearrangement and multiplication by $\frac{1}{6}a^2$ gives

$$\frac{a^3}{6}\left(\frac{\partial(\zeta/q^2)}{\partial\eta}\right)_0 = \frac{a^2}{6}\frac{\zeta_2}{q_2^2} - \frac{a^2}{6}\frac{\zeta_0}{q_0^2} - \frac{a^4}{12}\left(\frac{\partial^2(\zeta/q^2)}{\partial\eta^2}\right)_0 + o(a^5),$$

and substitution for the third term in (18) then gives

$$\psi_2 = \psi_0 + \frac{a^2}{3}\frac{\zeta_0}{q_0^2} + \frac{a^2}{6}\frac{\zeta_0}{q_2^2} - \frac{a^4}{24}\left[\nabla_l^2\frac{\zeta}{q^2}\right]_0 + o(a^5). \quad (20)$$

Neglect of all terms in (20) of order $a^4$ or higher, and rearrangement, finally gives

$$\zeta_0 = \frac{3q_0^2}{a^2}(\psi_2 - \psi_0) - \frac{q_0^2}{2q_2^2}\zeta_2, \quad (21\,a)$$

or, more generally,

$$\zeta_s = \frac{3q_s^2}{m^2}(\psi_p - \psi_s) - \frac{q_s^2}{2q_p^2}\zeta_p, \tag{21 b}$$

where $\zeta_s$ is the vorticity at any point $s$ on the solid boundary, $\psi_s$ is the stream function at that point, $\zeta_p$ is the vorticity at a point $p$ inside the boundary at a distance $m$ on a normal through $s$, and $\psi_p$ is the stream function at point $p$.

Equation (21) is preferable to (19) for use with networks unless the mesh constant has been reduced in regions of the flow field where the vorticity gradient is steep. Equation (21) was used in obtaining the results reported in this paper.

Values of $\zeta_s$ for every point on the solid boundary are first assumed, then new values are determined after each relaxation of the two networks. If succeeding values of $\zeta_s$ are based on equation (21 b), that is,

$$\zeta_s^{(n+1)} = \frac{3q_s^2}{m^2}(\psi_p^{(n)} - \psi_s) - \frac{q_s^2}{2q_p^2}\zeta_p^{(n)},$$

where the superscript in parentheses refers to the number of the step in the iteration, the process will diverge. To effect convergence a plot of $\{\zeta_s + (q_s^2/2q_p^2)\zeta_p\}^{(n)}$ *vs* $\psi_p^{(n)}$ may be prepared and the graph of equation (21 b) superposed. The intersection of the two curves will give the final value of $\{\zeta_s + (q_s^2/2q_p^2)\zeta_p\}$. A supplementary plot of $\zeta_s^{(n)}$ *vs* $\{\zeta_s + (q_s^2/2q_p^2)\zeta_p\}^{(n)}$ may assist in estimating the correct final value of $\zeta_s$.

*Flow past a flat plate*

Consider the case of a finite flat plate (of infinitesimal thickness) in an infinite flow field, and parallel to the otherwise undisturbed velocity, with leading edge at $(-1, 0)$ and trailing edge at $(+1, 0)$. Let the transformation be

$$z = \cosh t, \tag{22}$$

for which the modulus is

$$q = [\sinh^2 \xi + \sin^2 \eta]^{-1/2}. \tag{23}$$

This transformation has the following features:

(1) the modulus is very small far away from the origin, thus permitting the transformation plane to be relatively small;

(2) the modulus is very large in the region of the leading edge, thus literally magnifying the region of interest.

Because the flow will be symmetrical only the half plane need be used. The transformation is illustrated in figure 6.

The boundary conditions are:

$$\xi = 0, \qquad \psi = 0, \qquad \frac{\partial \psi}{\partial \xi} = 0;$$

$$\xi = \xi_\infty, \qquad \psi = -\sinh \xi_\infty \sin \eta, \qquad \zeta = 0;$$

$$\eta = 0, \pi, \qquad \psi = 0, \qquad \zeta = 0.$$

The solution obtained from the analogue represents $\psi$ and $\zeta$ as functions of position in the flow field (including the solid boundary). The velocity is given by (3). The equation for the pressure is

$$\frac{p-p_\infty}{\frac{1}{2}u_\infty^2} = 1+2\int_\infty \left(\zeta\frac{\partial\psi}{\partial\xi} - \frac{2}{N_R}\frac{\partial\zeta}{\partial\eta}\right)d\xi + 2\int_\infty \left(\zeta\frac{\partial\psi}{\partial\eta} + \frac{2}{N_R}\frac{\partial\zeta}{\partial\xi}\right)d\eta. \quad (24)$$

The shear stress is given by

$$\tau_s = -\frac{2}{N_R}\zeta_s. \quad (25)$$

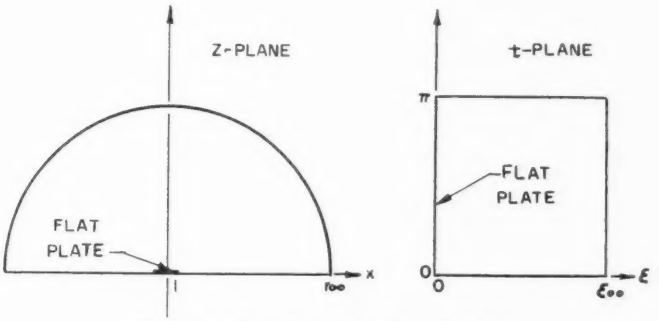


Figure 6. Transformation for a flat plate.

The local coefficient of friction $c_f$ is equal numerically to twice the dimensionless shear stress of equation (25). Let the defining equation for the drag coefficient $C_D$ be

$$D' = C_D\,\tfrac{1}{2}l'\rho' u_\infty'^2,$$

where $D'$ is the drag on both sides of the plate per unit span, and $l'$ is the dimension of the plate parallel to the flow. Then $C_D$ is given by

$$C_D = \frac{1}{2}\int_{-1}^{+1} c_f\,dx = -\frac{1}{2}\int_{\pi}^{0} c_f \sin\eta\,d\eta. \quad (26)$$

*Results and discussion*

Two networks were constructed, with outer boundary at $\xi_\infty = \frac{5}{4}\pi$* and with mesh constant equal to $\frac{1}{8}\pi$† (a transition to $\frac{1}{4}\pi$ was effected beyond $\xi = \frac{1}{4}\pi$). The REAC of the Rand Corporation, Santa Monica, California, was made available to the author for the purpose of computing residuals, its components being connected as indicated in figure 4. Data obtained from the analogue in the form of potentials were readily converted to stream function and vorticity by the application of the appropriate scale factors.

* Location of the outer boundary was based on a consideration of the distance from the plate at which the maximum vorticity in a laminar wake would have become small enough to neglect.

† Considerations based on limiting the truncation error in $\zeta$ led to the value $\frac{1}{40}\pi$ for the mesh constant. This was increased by a factor of 5 for reasons of economy. Any error present in the solution is presumed to be largely truncation error.

Solutions were obtained for Reynolds numbers 0·1, 1·0, and 10·0. The corresponding values of $\psi$ and $\zeta$ are given in tables 1 and 2. The differentation and integration involved in determining the pressure and drag coefficient were done numerically.

The local coefficient of friction is plotted *vs* $x$, for the three Reynolds numbers, in figure 7. $c_f$ as given by the Blasius solution is also plotted. The analogue solution approaches the Blasius solution as the Reynolds number increases. The influence of the trailing edge, significant at very low Reynolds numbers, may be seen distinctly in the analogue solution. The Blasius solution, of course, does not take the effect of the trailing edge into account.

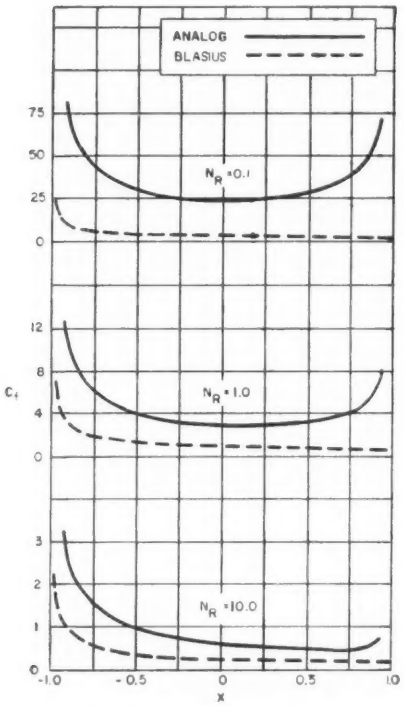


Figure 7. Local friction coefficient *vs* $x$.

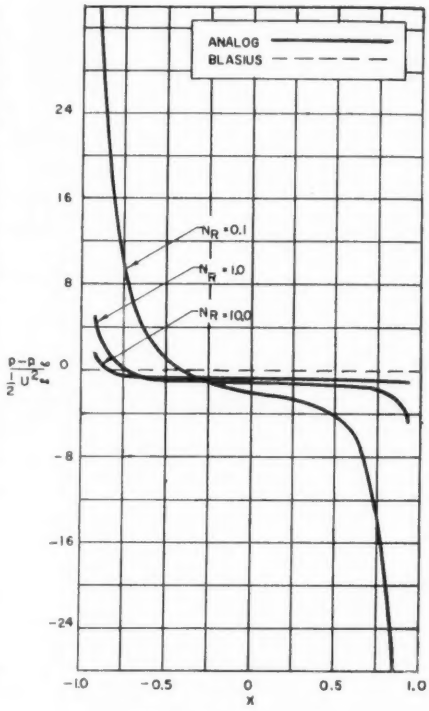


Figure 8. Pressure *vs* $x$.

The pressure at the surface of the plate was found by first integrating the terms of (24) from the outer boundary to the plate along the path $\eta = \frac{1}{2}\pi$ (and thereby determining the pressure at the mid-point of the plate), and then integrating along the surface of the plate (that is, along the path $\xi = 0$). The pressure is plotted *vs* $x$, for the three Reynolds numbers, in figure 8. The value given by the Blasius solution is zero everywhere. It may again be noted that the analogue solution approaches the Blasius solution as the Reynolds number increases.

The drag coefficient $C_D$ is given by (26). One should know $c_f$ at every point along the $x$-axis from $x = -1$ to $x = +1$ in order to evaluate the integral. But the analogue gives values only from $x = -0{\cdot}924$ to $x = +0{\cdot}924$. The fact that $c_f$ is not known in the regions adjacent to the leading and trailing edges is a serious deficiency. However, some correlation is established between the solutions at the three Reynolds numbers by plotting $c_f$ *vs* the 'local' Reynolds numbers $N_{Rx}$ and $N_{R(l-x)}$ in

| $\eta$ | $N_R$ | $\xi = 0$ | $\frac{1}{8}\pi$ | $\frac{1}{4}\pi$ | $\frac{3}{8}\pi$ | $\frac{1}{2}\pi$ | $\frac{3}{4}\pi$ | $\pi$ | $\frac{5}{4}\pi$ |
|---|---|---|---|---|---|---|---|---|---|
| $\frac{7}{8}\pi$ | 0·1 | 0 | −0·022 | −0·08 | −0·21 | — | — | — | — |
| | 1·0 | 0 | −0·030 | −0·11 | −0·28 | — | — | — | — |
| | 10·0 | 0 | −0·076 | −0·27 | −0·57 | — | — | — | — |
| $\frac{3}{4}\pi$ | — | 0 | −0·038 | −0·15 | −0·38 | −0·79 | −2·57 | −7·18 | −17·94 |
| | — | 0 | −0·050 | −0·20 | −0·50 | −1·04 | −3·21 | −8·04 | −17·94 |
| | — | 0 | −0·120 | −0·46 | −1·00 | −1·72 | −3·89 | −8·42 | −17·94 |
| $\frac{5}{8}\pi$ | — | 0 | −0·047 | −0·19 | −0·48 | — | — | — | — |
| | — | 0 | −0·060 | −0·25 | −0·61 | — | — | — | — |
| | — | 0 | −0·131 | −0·54 | −1·21 | — | — | — | — |
| $\frac{1}{2}\pi$ | — | 0 | −0·049 | −0·20 | −0·51 | −1·07 | −3·48 | − 9·86 | −25·36 |
| | — | 0 | −0·060 | −0·25 | −0·62 | −1·30 | −4·14 | −11·10 | −25·37 |
| | — | 0 | −0·116 | −0·49 | −1·16 | −2·20 | −5·39 | −11·89 | −25·37 |
| $\frac{3}{8}\pi$ | — | 0 | −0·045 | −0·18 | −0·46 | — | — | — | — |
| | — | 0 | −0·051 | −0·20 | −0·51 | — | — | — | — |
| | — | 0 | −0·079 | −0·33 | −0·81 | — | — | — | — |
| $\frac{1}{4}\pi$ | — | 0 | −0·035 | −0·14 | −0·34 | −0·71 | −2·31 | −6·63 | −17·94 |
| | — | 0 | −0·036 | −0·14 | −0·35 | −0·70 | −2·20 | −6·27 | −17·94 |
| | — | 0 | −0·042 | −0·17 | −0·41 | −0·79 | −3·64 | −8·38 | −17·94 |
| $\frac{1}{8}\pi$ | — | 0 | −0·020 | −0·07 | −0·19 | — | — | — | — |
| | — | 0 | −0·021 | −0·07 | −0·18 | — | — | — | — |
| | — | 0 | −0·018 | −0·06 | −0·14 | — | — | — | — |

Table 1. Stream function.

figures 9 and 10 respectively. $N_{Rx}$ is the local Reynolds number based on distance from the leading edge and $N_{R(l-x)}$ is the local number based on distance from the trailing edge. On the basis of these plots a straight line extrapolation (on logarithmic coordinates) is employed to obtain values of $c_f$ in the regions $-1 < x < -0{\cdot}924$ and $+0{\cdot}924 < x < +1$, the slope of the straight line being taken as $-0{\cdot}577$.

$C_D$ is now given by

$$C_D = \frac{1}{2}\int_{-1}^{-0{\cdot}924} c_f\,dx - \frac{1}{2}\int_{\frac{1}{8}\pi}^{\frac{7}{8}\pi} c_f \sin\eta\,d\eta + \frac{1}{2}\int_{0{\cdot}924}^{1} c_f\,dx.$$

The first term on the right is the contribution of the 3·8% segment of the surface adjacent to the leading edge, the last term is the contribution of the 3·8% segment adjacent to the trailing edge, and the middle term is the contribution of the 92·4% of the surface which lies between. Let these

| $\eta$ | $N_R$ | $\xi = 0$ | $\frac{1}{8}\pi$ | $\frac{1}{4}\pi$ | $\frac{3}{8}\pi$ | $\frac{1}{2}\pi$ | $\frac{3}{4}\pi$ | $\pi$ | $\frac{5}{4}\pi$ |
|---|---|---|---|---|---|---|---|---|---|
| $\frac{7}{8}\pi$ | 0·1 | −1·99 | −0·76 | −0·34 | −0·15 | — | — | — | — |
| | 1·0 | −2·92 | −1·07 | −0·44 | −0·16 | — | — | — | — |
| | 10·0 | −7·75 | −2·05 | −0·21 | +0·11 | — | — | — | — |
| $\frac{3}{4}\pi$ | — | −0·97 | −0·69 | −0·44 | −0·27 | −0·18 | −0·07 | −0·02 | 0 |
| | — | −1·38 | −0·95 | −0·56 | −0·31 | −0·16 | −0·02 | 0 | — |
| | — | −3·68 | −1·94 | −0·40 | +0·06 | 0 | — | — | — |
| $\frac{5}{8}\pi$ | — | −0·70 | −0·60 | −0·45 | −0·32 | — | — | — | — |
| | — | −0·89 | −0·77 | −0·56 | −0·37 | — | — | — | — |
| | — | −2·21 | −1·62 | −0·58 | −0·04 | | — | — | — |
| $\frac{1}{2}\pi$ | — | −0·61 | −0·56 | −0·45 | −0·33 | −0·23 | −0·11 | −0·04 | 0 |
| | — | −0·74 | −0·68 | −0·54 | −0·39 | −0·25 | −0·07 | +0·01 | 0 |
| | — | −1·53 | −1·34 | −0·72 | −0·17 | 0 | — | — | — |
| $\frac{3}{8}\pi$ | — | −0·66 | −0·58 | −0·44 | −0·32 | — | — | — | — |
| | — | −0·75 | −0·67 | −0·52 | −0·39 | — | — | — | — |
| | — | −1·31 | −1·17 | −0·84 | −0·46 | — | — | — | — |
| $\frac{1}{4}\pi$ | — | −0·90 | −0·65 | −0·42 | −0·27 | −0·19 | −0·09 | −0·04 | 0 |
| | — | −0·94 | −0·72 | −0·49 | −0·34 | −0·25 | −0·14 | −0·08 | 0 |
| | — | −1·20 | −1·05 | −0·85 | −0·66 | −0·80 | 0 | — | — |
| $\frac{1}{8}\pi$ | — | −1·82 | −0·70 | −0·32 | −0·16 | — | — | — | — |
| | — | −2·01 | −0·78 | −0·37 | −0·20 | — | — | — | — |
| | — | −1·84 | −0·91 | −0·64 | −0·58 | — | — | — | — |

Table 2. Vorticity.

| $N_R$ | $C_{D1}$ | $C_{D2}$ | $C_{D3}$ | $C_D$ |
|---|---|---|---|---|
| 0·1 | 7·09 | 30·6 | 6·76 | 44·45 |
| 1·0 | 1·07 | 3·78 | 0·75 | 5·60 |
| 10·0 | 0·28 | 0·79 | 0·07 | 1·14 |

Table 3. Drag coefficient.

contributions to $C_D$ be denoted respectively by $C_{D1}$, $C_{D3}$, and $C_{D2}$, so that $C_D = C_{D1} + C_{D2} + C_{D3}$. The drag coefficient, together with its three parts, is given in table 3.

According to this analysis the contribution of the leading edge segment increases from 16% to 25% of the total drag, the contribution of the trailing

edge segment decreases from 15% to 6%, and the contribution of the surface between stays nearly constant at 68% or 69% as the Reynolds number is increased from 0·1 to 10·0. This is in contrast to the Blasius

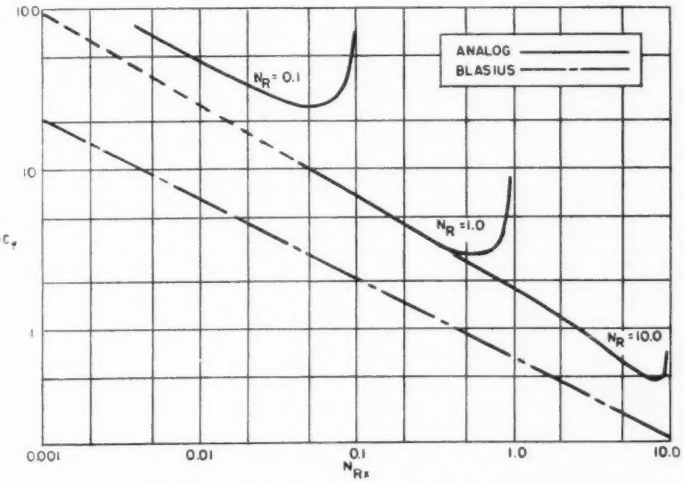


Figure 9. Local coefficient of friction *vs* $N_{rx}$.

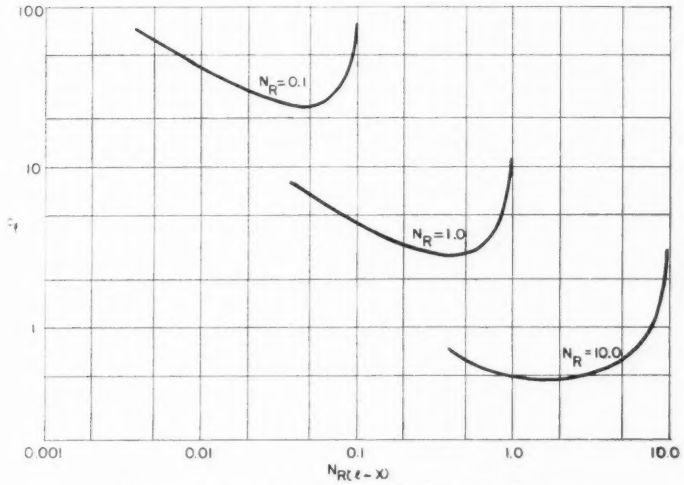


Figure 10. Local coefficient of friction *vs* $N_{R(l-x)}$.

solution according to which the contribution of the same leading edge segment is constant at 13·75% of the total drag and the contribution of the trailing edge segment is constant at 1·35% of the total drag, for all Reynolds numbers.

The drag data of table 3 are compared with the experimental values reported by Janour (1951) in figure 11. Drag data reported by Sherman (1952) are also shown although these were obtained under compressible flow conditions at Mach numbers of approximately 0·2 and 0·6. Also shown are the drag coefficient for the Blasius solution and the drag coefficients as determined by Tomotika & Aoi (1953) and Haaser (1950), the latter two being based respectively on the Oseen approximation and on Carrier's (1953) modification of the Oseen approximation. The drag coefficient as

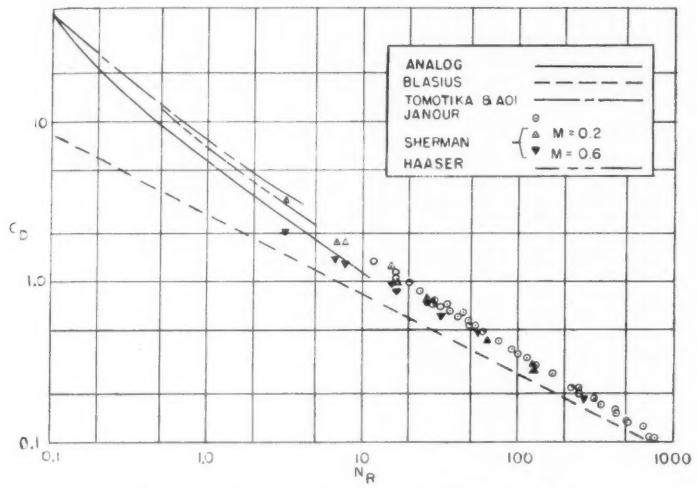


Figure 11. Drag coefficient *vs* Reynolds number.

determined from the analogue solution approaches the Blasius solution as the Reynolds number increases, and approaches the solutions of Haaser and of Tomotika & Aoi as the Reynolds number decreases. In the range where comparison with experiment is possible, the drag coefficient lies below the values of Janour and Sherman. This difference from experiment is believed to be due chiefly to truncation error.

The author wishes to thank the Rand Corporation, Santa Monica, California, for making available to him their analogue computing facilities. The solutions reported here were all obtained at Rand. The resistance networks and associated switching equipment were made possible by the University of California Research Grant No. 1115.

## References

Allen, D. N. & Southwell, R. V. 1955 Relaxation methods applied to determine the motion, in two dimensions, of a viscous fluid past a fixed cylinder, *Quart. J. Mech. Appl. Math.* **8**, 129.

Carrier, G. F. 1953 On slow viscous flow, final report, Office of Naval Research Contract Nonr–653 (00).

HAASER, N. B. 1950 The viscous flow past a flat plate, Ph.D. Thesis, Graduate Division of Applied Mathematics, Brown University.

IMAI, I. 1954 A method of solving Oseen's equations and its application to the flow past an inclined elliptic cylinder, *Proc. Roy. Soc.* A, **224,** 141.

JANOUR, Z. 1951 Resistance of a plate in parallel flow at low Reynolds numbers, *Nat. Adv. Comm. Aero., Wash., Tech. Mem.* no. 1316.

KAWAGUTI, M. 1953 Numerical solution of the Navier–Stokes equations for the flow around a circular cylinder at Reynolds number 40, *J. Phys. Soc. Japan* **8,** 747.

KORN, G. A. & KORN, T. M. 1952 *Electronic Analog Computers.* New York · McGraw-Hill.

KUO, Y. H. 1953 On the flow of an incompressible viscous fluid past a flat plate at moderate Reynolds number, *J. Math. Phys.* **32,** 83.

SHERMAN, F. S. 1952 Skin friction in subsonic low density gas flow, *University of California, IER Report* no. HE–150–105.

SOROKA, W. W. 1954 *Analog Methods in Computation and Simulation.* New York : McGraw-Hill.

THOM, A. 1933 The flow past circular cylinders at low speeds, *Proc. Roy. Soc.* A, **141,** 651.

TOMOTIKA, S. & AOI, T. 1953 The steady flow of a viscous fluid past an elliptic cylinder and a flat plate at small Reynolds numbers, *Quart. J. Mech. Appl. Math.* **6,** 290.

WOODS, L. C. 1954 A note on the numerical solution of fourth order differential equations, *Aero. Quart.* **5,** 176.

# Further space-time correlations of velocity in a turbulent boundary layer

By A. J. FAVRE, J. J. GAVIGLIO and R. J. DUMAS
*Laboratoire de Mécanique de l'Atmosphère, Université de Marseille*

(*Received* 16 *July* 1957)

SUMMARY

This paper describes the results of further experimental investigation of the turbulent boundary layer with zero pressure gradient. Measurements of autocorrelation and of space-time double correlation have been made respectively with single hot-wires and with two hot-wires with the separation vector in any direction. Space-time correlations reach a maximum for some optimum delay. In the case of two points set on a line orthogonal to the plate, the optimum delay $T_i$ is not zero. In the general case it is equal to the corresponding delay $T_i$, increased by compensating delay for translation with the mean flow. Taylor's hypothesis may be applied to the boundary layer at distances from the wall greater than 3% of the layer thickness. Space-time isocorrelation surfaces obtained with optimum delay have a large aspect ratio in the mean flow direction, even if they are relative to a point close to the wall ($0{\cdot}03\delta$); the correlations along the mean flow then retain high values on account of the large scale of the turbulence.

## 1. INTRODUCTION

These experiments, following our previous investigations (Favre, Gaviglio & Dumas 1952, 1953 a, b, 1954 c, 1957), deal with longitudinal components of turbulent velocity in the boundary layer on a flat plate, with zero pressure gradient, set in a low turbulence wind tunnel. The plate is made of a glass 210 cm in length, 80 cm in width, with a profiled leading edge and prolonged with an adjustable flap. Transition is obtained by roughness elements beginning at the leading edge.

The velocity outside the boundary layer is 12·20 msec, and the conventional boundary-layer thickness $\delta$ is 17·5,33 and 34 mm for distances from the leading edge of 79, 185 and 194 cm (Reynolds numbers $R_\delta = 14\,500$, 27 900 and 28 000).

Measurements have been made with hot-wire anemometers, and the apparatus needed for time correlations, autocorrelations, and space-time double correlation coefficients (see Favre 1946, 1948; Favre, Gaviglio & Dumas 1953 a). The space-time correlation coefficient $R_{11}(T, X_1, X_2, X_3)$ for a point $A$ is measured by setting one hot-wire at fixed position $A$ and another at any other position $B$; the two signals are recorded simultaneously

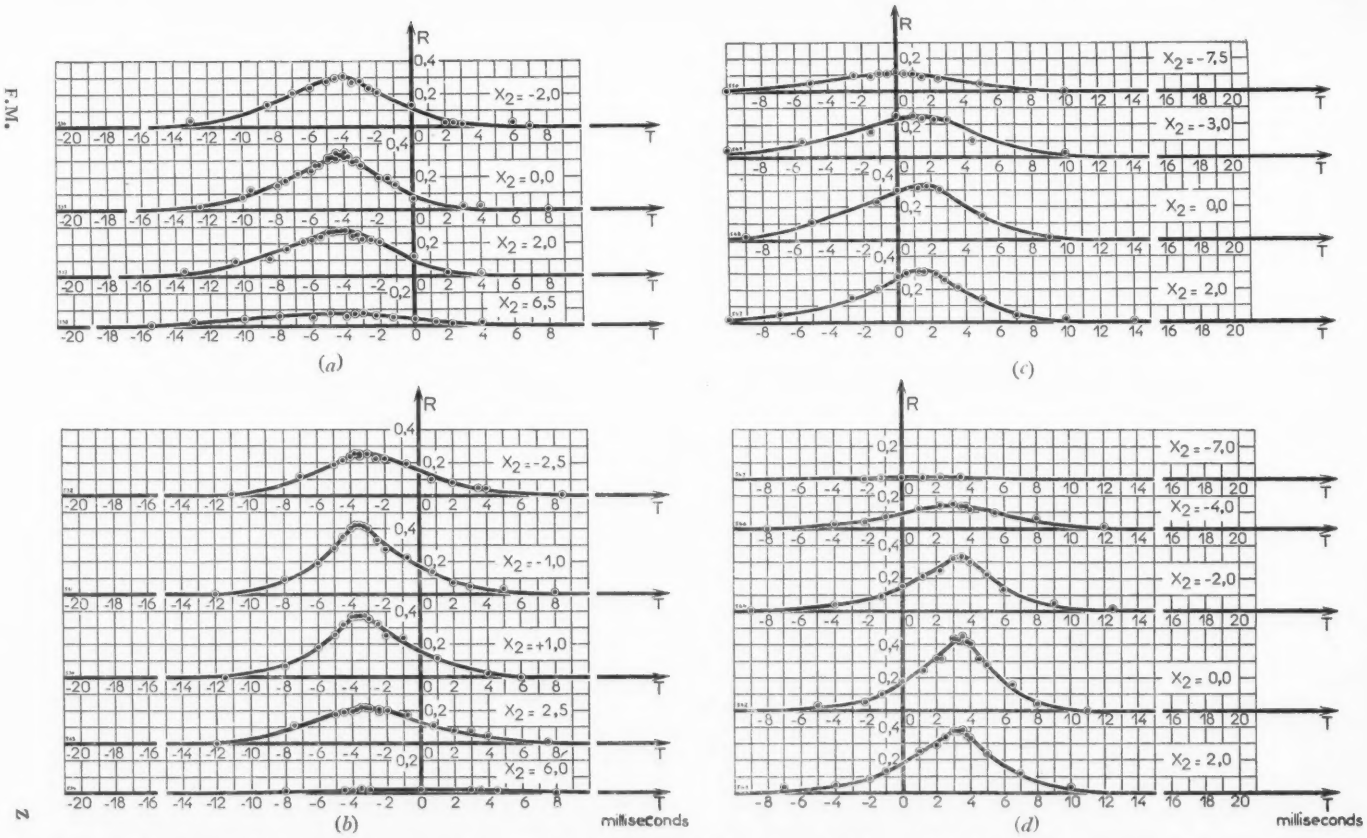


Figure 1. Longitudinal, transverse and lateral space-time correlations in the boundary layer. $\delta = 33$ mm, $R_\delta = 27\,900$, $y' = 1$ mm, $X_2$ variable. (*a*) $X_1 = -25{\cdot}4$ mm, $X_3 = y' - y = -4$ mm; (*b*) $X_1 = -25{\cdot}4$ mm, $X_3 = 0{\cdot}1$ mm; (*c*) $X_1 = 25{\cdot}4$ mm, $X_3 = -4$ mm; (*d*) $X_1 = 25{\cdot}4$ mm, $X_3 = 0$.

and played back with a relative delay $T_0$. The autocorrelation coefficient $R(T, 0, 0, 0)$ is obtained when the points $A$ and $B$ are the same (a single hot-wire). $y'$ and $y$ will be used to denote the distances from the wall of wires $A$ and $B$ respectively. $X_1$ is the component of their separation parallel to the plate (positive in the direction of the mean velocity); $X_3 = y' - y$; $X_2$ is the separation orthogonal to $X_1$ and $X_3$.

The influence on the measurements of the disturbances produced by the upstream probe was checked, and lessened by improvement of probes. With regard to space-time correlations the disturbance reached 13% when the two hot-wires were set on the same mean streamline and close by one another ($X_1/\delta = 0{\cdot}25$ for $y'/\delta = 0{\cdot}77$). No disturbance appeared if the distance $X_1/\delta$ was greater than 0·4 for $y'/\delta = 0{\cdot}03$, and 1·5 for $y'/\delta = 0{\cdot}77$; this is not a certain criterion for disturbances to be negligible, but it may be accepted as such, at least if the upstream wire is a little more distant from the wall than the downstream wire.

The mean velocity profiles are in agreement with the accepted shapes, and the universal profile proposed by Clauser (1954).

## 2. Space-time correlations

The space-time correlation coefficient $R_{11}(T, X_1, X_2, X_3)$ with respect to a point $A$ fixed by its distance $y'$ to the wall and its distance $z'$ to the leading edge, is said to be measured:

'longitudinally' when $X_2 = X_3 = 0$ ($X_1$ and $T$ variable);

'transversely' when $X_1 = X_2 = 0$ ($X_3$ and $T$ variable);

'longitudinally and transversely' when $X_2 = 0$ ($X_1$, $X_3$ and $T$ variable);

'longitudinally, transversely and laterally' when $X_1$, $X_2$, $X_3$ and $T$ are variable.

Numerous measurements were made; figure 1 represents as an example some values of space-time correlations measured longitudinally, transversely and laterally with regard to a fixed point $A$ ($y' = 1$ mm; $z = 185$ cm). It is found that the correlation $R_{11}$ changes with delay $T$ and reaches a maximum for an optimum value of delay to be denoted by $T_m$ in general and by $T_i$ in the particular case of transverse correlations.

*Optimum delay $T_i$ for transverse space-time correlation $R_{11}(T, 0, 0, X_3)$*

Figures 2 and 3 represent $(V_{y'} - V_y)T_i/\delta$ ($V_{y'}$ and $V_y$ are mean velocities at the positions $A$ and $B$) measured when the transition is obtained by preturbulence (Favre, Gaviglio & Dumas 1954a) and by roughness respectively; the differences are small. Comparison at distances $z = 79$ cm and $z = 194$ cm (the difference being about 45 times the mean thickness of boundary layer) shows that for the same values of $y'/\delta$ and $y/\delta$ the delay $T_i$ is proportional to $\delta$. It will be noticed that the variation of $T_i$ as a function of $z$ is very small by comparison with the time required for movement with the mean flow over the same range of $z$. Figure 4 shows values of $T_i$ for other distances $y'/\delta$ of fixed wire from the wall.

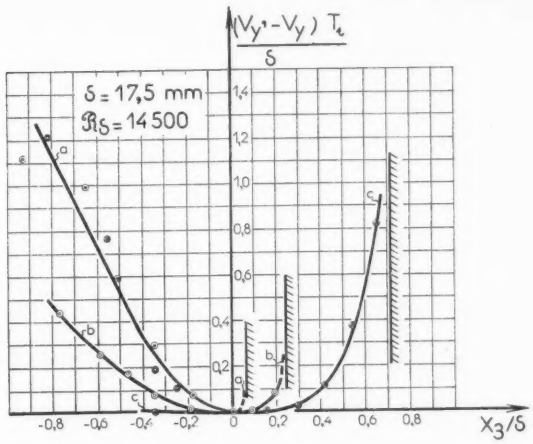


Figure 2. Optimum delay $T_i$ for transverse space-time correlations in the boundary layer on a flat plate (transition by preturbulence).

| | $y'/\delta$ | $Z$ | curve |
|---|---|---|---|
| ◎ | 0·06 | 74 cm | *a* |
| ◉ | 0·06 | 79 cm | |
| ◎ | 0·24 | 79 cm | *b* |
| △ | 0·71 | 79 cm | *c* |

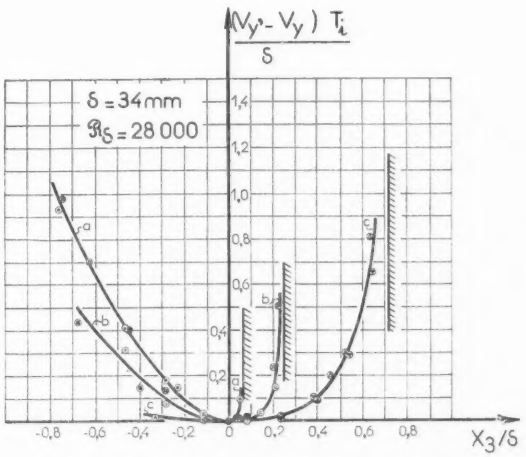


Figure 3. Optimum delay $T_i$ for transverse space-time correlations in the boundary layer on a flat plate (transition by roughness).

| | $y'/\delta$ | $Z$ | curve | | $y'/\delta$ | $Z$ | curve |
|---|---|---|---|---|---|---|---|
| ◉ | 0·06 | 194 cm | *a* | ◎ | 0·06 | 79 cm | *a* |
| ◎ | 0·24 | 194 cm | *b* | ◉ | 0·24 | 79 cm | *b* |
| △ | 0·71 | 194 cm | *c* | ▽ | 0·71 | 79 cm | *c* |

*Optimum delay $T_m$ for transverse and longitudinal space-time correlations $R_{11}(T, X_1, 0, X_3)$*

As previously (Favre, Gaviglio & Dumas 1954b, 1957), we verified in these investigations (especially at distances $X/\delta = 4$) that, as a first approximation, the space-time correlation of velocity fluctuations at the fixed point $A$ and at another point $B$ reaches a maximum for a delay $T_m$ equal to the 'initial' optimum delay $T_i$ (which gives maximum transverse space-time correlation for a point $C$ set on the mean streamline passing

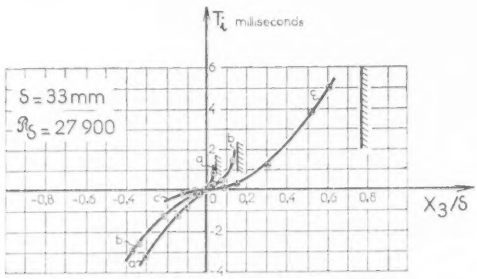


Figure 4. Optimum delay $T_i$ for transverse space-time correlation in the boundary layer on a flat plate (transition by roughness). $Z = 185$ cm.

| curve : | *a* | *b* | *c* |
|---|---|---|---|
| $y'/\delta =$ | 0·03 | 0·15 | 0·77 |

through the point $B$, with $X_1 = 0$) increased by a delay $T_c$ to compensate for the translation due to the mean flow; i.e.

$$T_m \doteq T_i + T_c, \qquad \text{where } T_c \doteq \frac{2X_1}{V_A + V_B}.$$

Then, when we pick out several positions $B'$, $B''$ for point $B$ on the same mean streamline, values of $T_m$ differ from each other by an amount

$$2\left(\frac{CB'}{V_A + V_{B'}} - \frac{CB''}{V_A + V_{B''}}\right) \doteq 2\,\frac{B''B'}{V_A + V_B},$$

since streamlines are close to lines of equal velocity.

We have published (Favre, Gaviglio & Dumas 1957) values of $T_m$ measured and computed from the preceding relation for $y'/\delta = 0{\cdot}06$ in the case of transition obtained by preturbulence, and for $y'/\delta = 0{\cdot}24$ in the case of transition obtained by roughness elements. In figure 5 are given values of $T_m$ corresponding to $y'/\delta$ equal to 0·03, 0·15 and 0·77. The above relation is found to be satisfactory to a first approximation when the upstream wire is a little more distant from the wall than the downstream wire* ($X_1 X_3 > 0$). Yet this relation is lacking in accuracy when the upstream wire is closer to the wall than the downstream wire ($X_1 X_3 < 0$). This may be due to the disturbances produced by the upstream probe.

* Except in the case corresponding to $y'/\delta = 0{\cdot}03$, $X_1 = 76{\cdot}2$ mm, for which the accuracy of measurement of $T_m$ is poor.

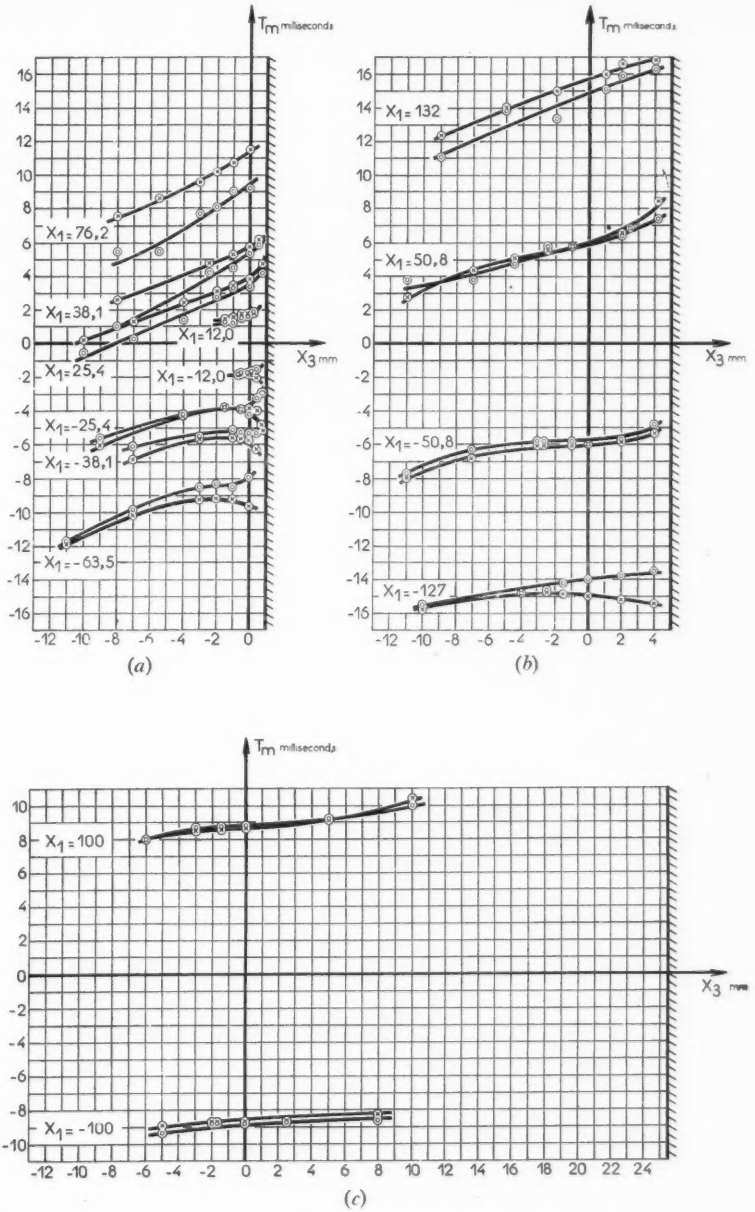


Figure 5. Optimum delays $T_m$ for longitudinal and transverse space-time correlations. $X_2 = 0$, $X_1$ variable. (*a*) $y'/\delta = 0{\cdot}03$, (*b*) $y'/\delta = 0{\cdot}15$, (*c*) $y'/\delta = 0{\cdot}77$. ◎ $T_m$ measured, ⊗ $T_m$ computed.

*Autocorrelation* $R_{11}(T, 0, 0, 0)$ *and longitudinal space correlations* $R_{11}(0, X_1, 0, 0)$; *Taylor's* (1938) *hypothesis*

The previous experiments (Favre, Gaviglio & Dumas 1957) have shown Taylor's hypothesis to be in very satisfactory agreement with autocorrelation curves and longitudinal space correlation curves for the turbulence downstream of a grid of mesh size $M$ when the transformation $T = X_1/V$ is used, at least up to distances beyond which the correlation becomes too small for a conclusive comparison ($X_1/M > 1{\cdot}5$). An analogous comparison has been made for points inside the boundary layer at several distances from the wall, viz. $y'/\delta = 0{\cdot}77$, $0{\cdot}24$*, $0{\cdot}15$ and $0{\cdot}03$ (see figure 6).

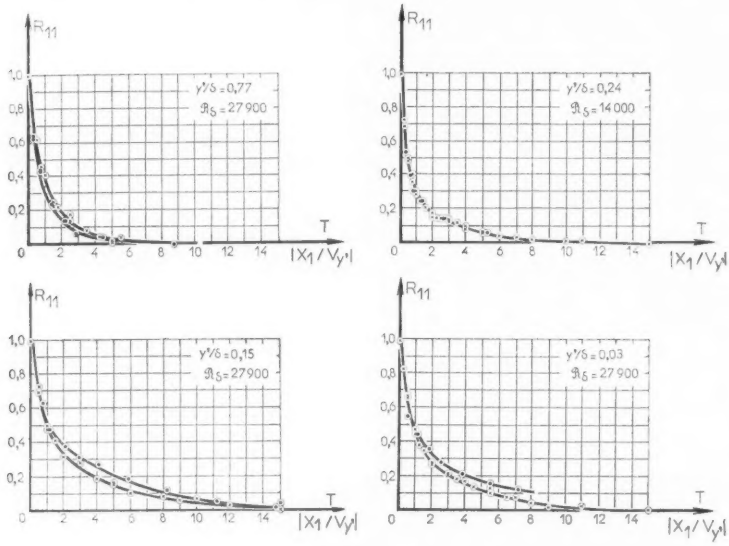


Figure 6. Autocorrelations and longitudinal space correlations; Taylor's hypothesis. ⊗ autocorrelations, ◎ longitudinal space correlations.

The longitudinal space correlation curves (the streamlines are almost parallel to the plate) are seen to lie close to the autocorrelation curves for $y'/\delta \geqslant 0{\cdot}03$ when the transformation $T = X_1/V_{y'}$ is used. The differences noticed, negligible in the central part of boundary layer ($y'/\delta = 0{\cdot}24$), have opposite signs on the two sides of this zone.

It seems that to a first approximation Taylor's hypothesis may be applied to the turbulent boundary layer, for distances from the wall greater than about 6% of the boundary layer thickness.

*Space-time correlations with optimum delay*

We have given in a previous paper (Favre, Gaviglio & Dumas 1957) longitudinal and transverse space-time isocorrelation curves $R_{11}(T_m, X_1, 0, X_3)$

* In this case transition is obtained by preturbulence, but the intermittency factor is negligible.

measured with optimum delay $T_m$ at distances $y'/\delta$ of the fixed wire $A$ from the wall equal to 0·06, 0·24 and 0·71, and also at $y'/\delta \geqslant 1$ in the case of measurements outside the boundary layer downstream of a grid producing the preturbulence.

When $X_1$ is given, the space-time correlation $R_{11}(T_m, X_1, 0, X_3)$ with optimum delay $T_m$ reaches a ***maximum maximorum*** for one value of $X_3$. Corresponding values of $X_1$ and $X_3$ determine the 'maximum space-time line with optimum delay' or 'maximum correlation line' that goes through the fixed point $A$. The present experiments were made in the case of transition obtained by roughness and extended to three space dimensions, longitudinally, transversely, and laterally.

In figures 7, 8, 9 we show space-time isocorrelation surfaces with optimum delay for positions of the fixed point $A$ defined by $y'/\delta = 0{\cdot}03$, 0·15 and 0·77 respectively ($z = 185$ cm). The symmetry with respect to $X_2$ having been checked, we may define as above the line of maximum correlation corresponding to each position of the fixed point $A$. Figure 10 gives the space-time correlation coefficients with optimum delay $T_m$, along the lines of maximum correlations, for positions of the fixed point $A$ defined by $y'/\delta = 0{\cdot}03$, 0·15 and 0·77. These measurements were made with band-passes extending from 1 to 2500 Hz, and from 1 to 275 Hz by cutting off high frequencies.

Space-time isocorrelation surfaces with optimum delay relating to a fixed point $A$ have a great aspect ratio along the mean flow upstream and downstream, even at a small distance of the fixed point $A$ from the wall ($y'/\delta = 0{\cdot}03$). They are symmetrical with respect to $X_2$, and their dimensions are of the same order transversely as laterally. The lines of maximum correlation outside the boundary layer are the same as the mean streamlines, but they differ markedly inside the boundary layer.

| $y'/\delta$ | 1 | 0·77 | 0·71 | 0·24 | 0·15 | 0·06 | 0·03 |
|---|---|---|---|---|---|---|---|
| Transition by preturbulence $R_\delta = 14\,000$ (band-pass 1–2500 Hz) | 7·5 to 12 | | $\doteqdot 8{\cdot}5$ | 2·4 | | 1·2 | |
| Transition by roughness $R_\delta = 27\,900$ (band-pass, 1–2500 Hz) | | $>7$ | | | 2·1 | | 0·65 |
| Transition by roughness $R_\delta = 27\,900$ (band-pass, 1–275 Hz) | | $>10$ | | | 3·6 | | 1·6 |

Table 1. Values of $X_1/\delta$ at which $R_{11} = 0{\cdot}5$.

The correlation coefficient with optimum delay retains high values for distances $X_1/\delta$ along the mean flow upstream and downstream which are appreciable at $y'/\delta \geqslant 0{\cdot}03$ and increase with $y'/\delta$. As an example, the value $R_{11} = 0{\cdot}5$ is preserved as far as the distances indicated in table 1.

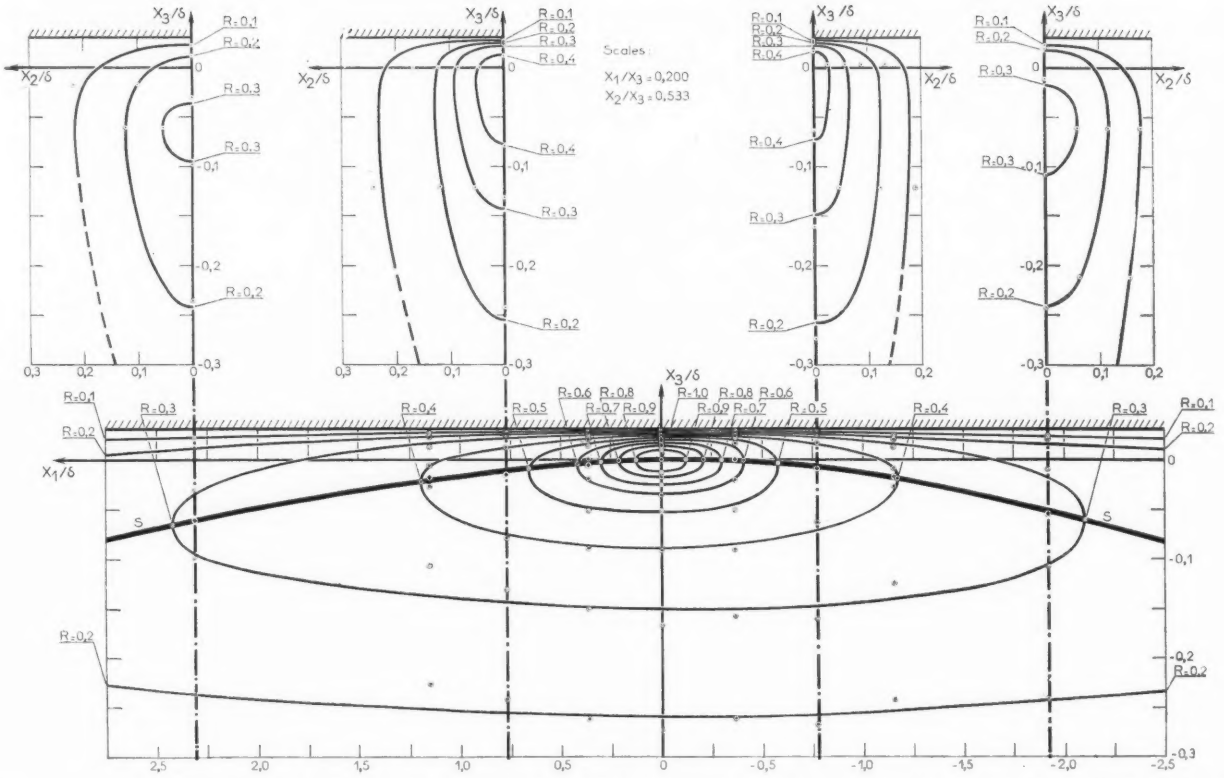


Figure 7. Space-time isocorrelation surfaces with optimum delay in the boundary layer on a flat plate; $\delta = 33$ mm, $R_\delta = 27900$, $y'/\delta = 0{\cdot}03$.

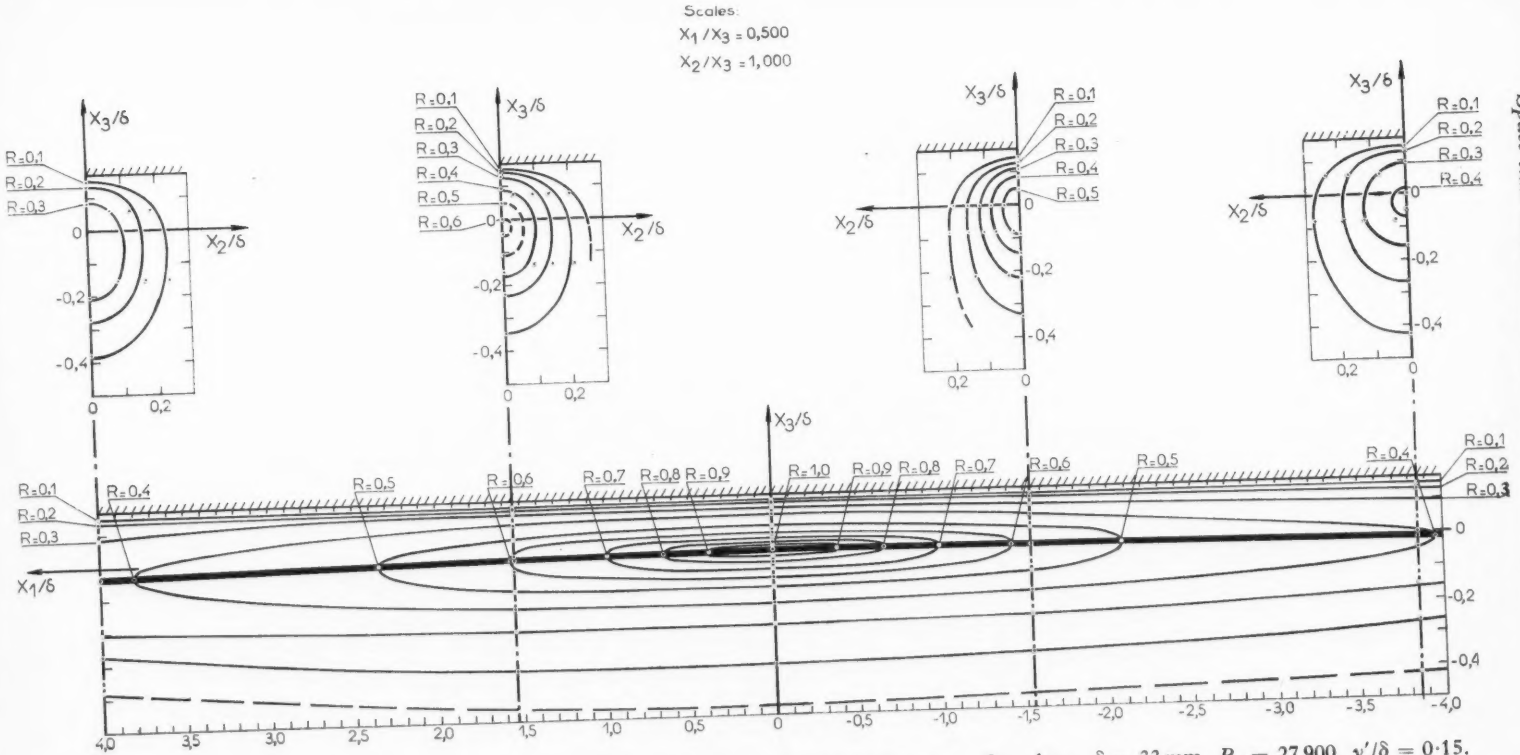


Figure 8. Space-time isocorrelation surfaces with optimum delay in the boundary layer on a flat plate; $\delta = 33$ mm, $R_\delta = 27\,900$, $y'/\delta = 0{\cdot}15$.

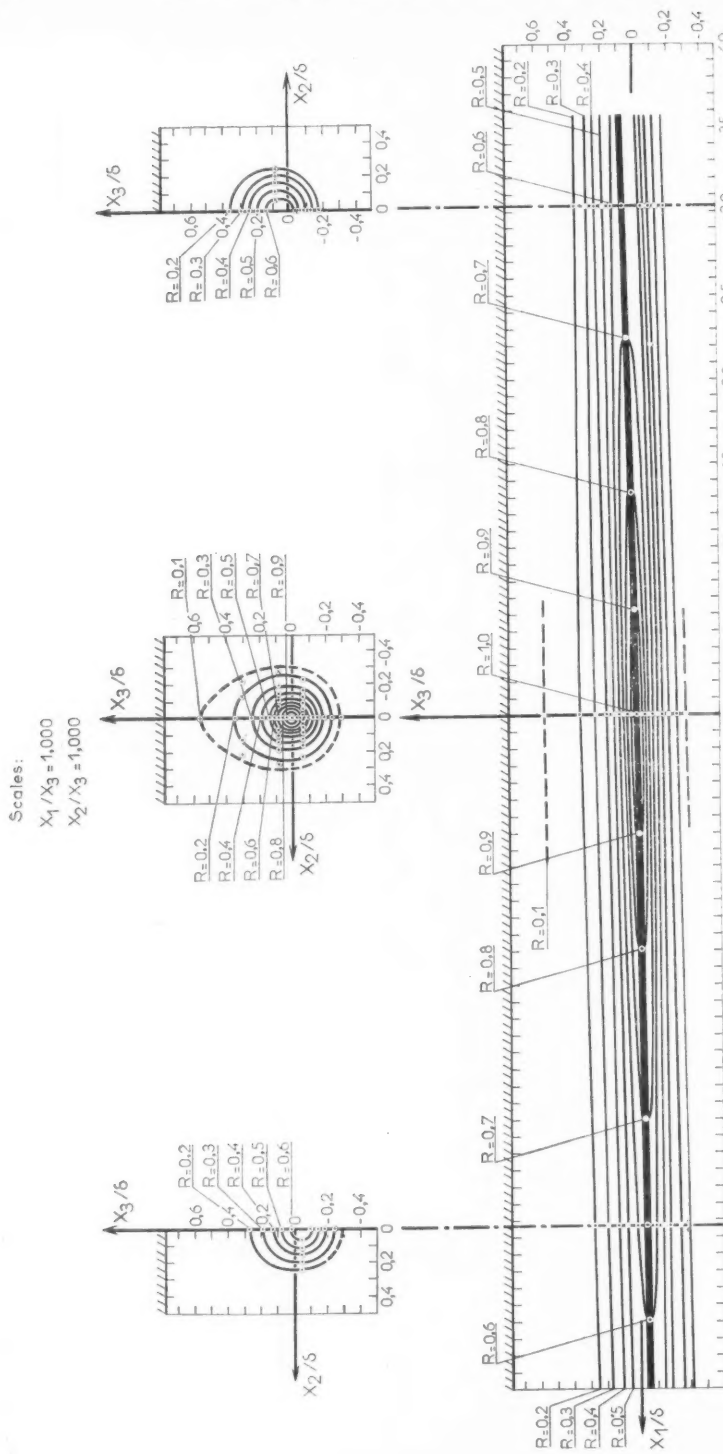


Figure 9. Space-time isocorrelation surfaces with optimum delay in the boundary layer on a flat plate; $\delta = 33$ mm, $R_\delta = 27\,900$, $y'/\delta = 0.77$.

The distances are increased markedly by cutting off frequencies higher than 275 Hz, a result similar to that concerning the turbulence behind a grid (Favre, Gaviglio & Dumas 1954*c*).

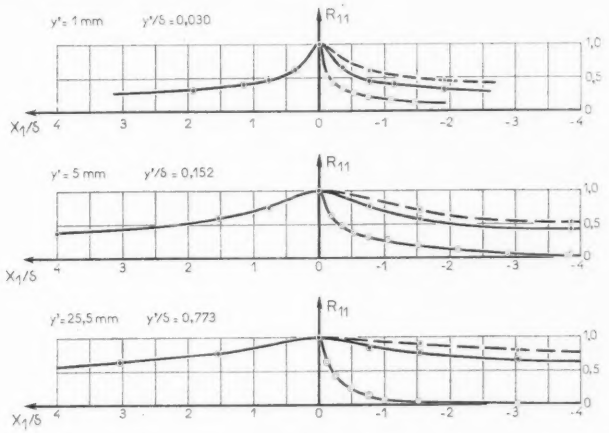


Figure 10. Space-time correlations in the boundary layer on a flat plate.

⦿ Along the line of maximum correlation, with optimum delay $T_m$, band-pass 1–2500 Hz.

⊗ Along the line of maximum correlation, with optimum delay $T_m$, band-pass 1–275 Hz.

◎ Along a mean streamline, with zero delay.

## 3. Conclusions

The space-time correlation reaches a maximum for an optimum delay $T_m$. When several alternative positions $B'$, $B''$ on a mean streamline are chosen for one of the points ($B$), the values of $T_m$ differ from each other by a compensating delay due to the motion from $B'$ to $B''$ with the mean flow, the effective velocity of translation being taken as the average of the mean flow velocity at the point $B$ and at the other point $A$.

The values of the 'initial' optimum delay (corresponding to the case of the two points being set orthogonally to the plate) noted at two stations for which the distances from the leading edge are very different (the distances of the points from the wall being the same fraction of $\delta$) are proportional to the boundary layer thickness $\delta$. Variation of $T_i$ with $x$ is very small compared with the times corresponding to translation with the mean flow over the same range of $x$. This seems to be due to the renewal of turbulence between the two distant positions.

Taylor's hypothesis may be applied, as a first approximation, to the boundary layer, for distances from the wall greater than about 6% of the thickness $\delta$.

Space-time isocorrelation surfaces, with optimum delay relative to a fixed point $A$, have a great aspect ratio along the mean flow, upstream and downstream, even for small distances of the fixed point from the wall

(3% of $\delta$). Their dimensions are of the same order transversely and laterally. The maximum correlation lines and mean streamlines are different inside the boundary layer, but are coincident outside.

The correlation coefficient with optimum delay retains high values for distances upstream and downstream which are significant for $y'/\delta = 3\%$ and increase in proportion to the distance of this fixed point from the wall. These distances are increased by cutting off the high frequency components.

Along the mean streamlines the intensity of turbulence is practically constant and the correlation with optimum delay shows, on the one hand, inasmuch as it retains high values, the long persistence of large scale turbulence translated by the mean motion, and, on the other hand, in the light of its diminution, the evolution of the turbulence and its renewal inside the boundary layer.

These researches were made at the Laboratoire de Mécanique de l'Atmosphère for the Office National d'Etudes et de Recherches Aéronautiques (O.N.E.R.A.) with the aid of the Ministère de l'Air, and of the Centre National de la Recherche Scientifique. The authors are glad to acknowledge Professor L. S. G. Kovásznay's advice in 1956.

## References

Clauser, F. H. 1954 *J. Aero. Sci.* **21,** 91.

Favre, A. 1946 *Proc. 6th Inter. Congr. Appl. Mech.*

Favre, A. 1948 *Proc. 7th Inter. Congr. Appl. Mech.*

Favre, A., Gaviglio, J. & Dumas, R. 1952 *Publ. Sci. Tech. Minist. de l'Air,* no. 296.

Favre, A., Gaviglio, J. & Dumas, R. 1953 a *La Rech. Aéro.*, no. 31.

Favre, A., Gaviglio, J. & Dumas, R. 1953 b *La Rech. Aéro.*, no. 32.

Favre, A., Gaviglio, J. & Dumas, R. 1954 a *La Rech. Aéro.*, no. 38.

Favre, A., Gaviglio, J. & Dumas, R. 1954 b *La Rech. Aéro.*, no. 39.

Favre, A., Gaviglio, J. & Dumas, R. 1954 c *La Rech. Aéro.*, no. 40.

Favre, A., Gaviglio, J. & Dumas, R. 1957 *J. Fluid Mech.* **2,** 313.

Taylor, G. I. 1938 *Proc. Roy. Soc.* A, **164,** 476.

# A simple derivation of Lighthill's heat transfer formula

By H. W. LIEPMANN
*Guggenheim Aeronautical Laboratory, California Institute of Technology*

(*Received* 23*rd July* 1957)

## 1. Introduction and summary

In the following it will be shown that a simple argument based on the use of the energy integral equation of the laminar boundary layer permits the derivation of a heat transfer formula valid for non-uniform temperature distribution and non-zero pressure gradients. The formula is then shown to be identical in structure with Lighthill's (1950) well-known results. Lighthill obtained his formula by solving the boundary layer equations in the von Mises form using operational methods. An elegant way to obtain the same results using exact similarity consideration was given by Lagerstrom (not yet published). The derivation given here is probably the most simple-minded one and the method may be useful for other applications as well. Furthermore, it is shown that the approach can be slightly modified to permit application of the formula to flow near separation. The latter result is applied to the Falkner–Skan solution for just separating flows and is found to be in excellent agreement with the exact solutions.

## 2. Laminar flow far from separation

The energy integral equation relating the heat flux $q_w$ at the surface to the enthalpy distribution $h(y)$ through the boundary layer can be written

$$\frac{d}{dx}\int_0^\delta \rho u(h-h_\infty)\,dy = -q_w, \tag{1}$$

where $\delta$, $\rho$, $u$ are boundary layer thickness, density, and $x$-component of the velocity vector, respectively. Heat produced by dissipation has been neglected.

If the Prandtl number $Pr$ is not very small*, $q_w$ is determined by the velocity distribution in the immediate neighbourhood of the wall. This is a well-known result first used by Fage & Falkner (1931). Thus

$$u \doteq (\partial u/\partial y)_w y = (\tau_w/\mu_w)y, \tag{2}$$

where $\tau_w$ and $\mu_w$ are shearing stress and viscosity at the wall. We will now express $y$ in formula (2) in terms of $h$ and $q$ in the neighbourhood of the wall and then employ a change of variables in (1) such that $q$ is considered as a function of $h$. This transformation is patterned after Crocco's method of using $\tau(x,u)$ instead of $\tau(x,y)$. We write

$$h = h_w + (\partial h/\partial y)_w y = h_w - (c_p/k)_w q_w y,$$

* The opposite case $Pr \ll 1$ is even easier since one can replace $\rho u$ by $\rho_\infty U$ in (1).

and, on combining this with (2), we have near the wall

$$u = Pr^{-1}\tau_w(h_w - h)/q_w. \tag{3}$$

The heat flux $q$ is given by

$$q = -\frac{k}{c_p}\frac{\partial h}{\partial y}. \tag{4}$$

The integration in (1) is performed at constant $x$ and we can replace $dy$ by $dh$ using (4). Thus (1) can be written

$$\frac{1}{Pr}\frac{d}{dx}\left\{\frac{\tau_w}{q_w}\int_{h_w}^{h_\infty}\frac{(h_w - h)(h - h_\infty)\rho k}{qc_p}\,dh\right\} = q_w,$$

or, if we introduce the similarity variable

$$\eta = \frac{h_w - h}{h_w - h_\infty},$$

where $h_\infty$ stands for the enthalpy at the edge of the layer, we have

$$\frac{1}{Pr^2}\frac{d}{dx}\left\{\frac{\tau_w\mu_w\rho_w}{q_w^2}(h_w - h_\infty)^3\int_0^1\left(\frac{\rho\mu}{\rho_w\mu_w}\right)\frac{\eta(1-\eta)}{q/q_w}\,d\eta\right\} = -q_w. \tag{5}$$

We now make the similarity assumptions that $\rho\mu/(\rho_w\mu_w)$ and $q/q_w$ are functions of $\eta$ only, that is

$$q(x, h) = q_w(x)f\left(\frac{h_w - h}{h_w - h_\infty}\right).$$

While this cannot be exact in all cases, it is probably very closely satisfied for a large range of conditions, a fact which will be borne out by a comparison of the final results with known solutions. If the similarity is granted then the integral in (5) is a constant $\alpha$, say, to be evaluated later. The result (5) becomes a very simple differential equation from which $q_w$ as a function of $\tau_w$ and of $\Delta h = h_w - h_\infty$ is easily obtained. We have from (5)

$$-\frac{1}{q_w}\frac{d}{dx}\left(\frac{\tau_w\mu_w\rho_w\Delta h^3}{q_w^2}\right) = \frac{Pr^2}{\alpha}.$$

Multiplication with $\sqrt{(\tau_w\mu_w\rho_w\Delta h^3)}$ makes the left side a perfect differential, and hence we find that

$$-\frac{\sqrt{(\tau_w\mu_w\rho_w\Delta h^3)}}{q_w} = \left(\frac{3}{2\alpha}\right)^{1/3}Pr^{2/3}\left[\int_0^x\sqrt{(\tau_w\mu_w\rho_w\Delta h^3)}\,dx\right]^{1/3},$$

or

$$-q_w = \left(\frac{2\alpha}{3}\right)^{1/3}Pr^{-2/3}\sqrt{(\tau_w\mu_w\rho_w\Delta h^3)}\left[\int_0^x\sqrt{(\tau_w\mu_w\rho_w\Delta h^3)}\,dx\right]^{-1/3}. \tag{6}$$

The result (6) permits the computation of $q_w$ if $\tau_w(x)$ and $T_w(x)$ or $h_w(x)$ are given.

To determine the constant $\alpha$ we have to choose a reasonable distribution of $q\rho_w\mu_w/q_w\rho\mu = f(\eta)$*. However, since only the cube root of $\alpha$ appears,

* One can also use the known solution for a flat plate with uniform temperature to obtain $\alpha$.

the results are very insensitive to the choice of the function $f(\eta)$. If we base our approach again on Crocco's work for the shearing stress we choose

$$f(\eta) = \sqrt{(1-\eta^2)},$$

a simple function with the proper behaviour at the limits. The constant $\alpha$ then has the value $1-\frac{1}{4}\pi \doteqdot 0{\cdot}215$. To compare (6) with Lighthill's (1950) formula it is easiest first to find $q_w(x)$ from (6) if $\Delta h$ vanishes in the range $(0,\xi)$ and then jumps to a constant value $\Delta h_0$ for greater values of $x$. In this way (6) can be written in the form of a Stieltjes integral like Lighthill's formula, and the comparison is as follows.

Lighthill's result (1950, equation (29), with $\rho\mu$ assumed constant) is

$$-q_w(x) = \frac{9^{-1/3}}{\frac{1}{3}!}\, k\left(\frac{\rho Pr}{\mu^2}\right)^{1/3} \sqrt{\{\tau_w(x)\}} \int_0^x \left[\int_\xi^x \sqrt{\{\tau_w(\xi)\}}\, d\xi\right]^{-1/3} dT_0(\xi).$$

Equation (6) transforms into exactly the same form but with a numerical constant $(\frac{2}{3}\alpha)^{1/3}$ instead of $9^{-1/3}/\frac{1}{3}!$. With the value $\alpha = 0{\cdot}215$ determined above we obtain 0·524 for the constant compared with Lighthill's value of 0·539. The agreement is thus better than 3%. Even with the worst possible choice of $f(\eta)$, namely $f(\eta) = 1$, our constant would be reduced to only 0·490.

## 3. Laminar flow near separation

It is now interesting to modify the approach to handle the flow near the separation point where $\tau_w \to 0$. Here (2) obviously fails to represent $u$ and the approximation becomes bad. However, it is an easy matter to try an approximation which represents $u$ near a separation point. Here,

$$u \doteqdot \tfrac{1}{2} y^2 (\partial^2 u/\partial y^2)_w \tag{7}$$

but

$$\mu_w (\partial^2 u/\partial y^2)_w = dp/dx. \tag{8}$$

Hence

$$u = (y^2/2\mu_w)\, dp/dx,$$

and, proceeding as before, we obtain

$$-q_w = (\tfrac{3}{8}\beta)^{1/4} Pr^{-3/4} \left(u_w^2 \rho_w \frac{dp}{dx} \Delta h^4\right)^{1/3} \left[\int_0^x \left(u_w^2 \rho_w \frac{dp}{dx} \Delta h^4\right)^{1/3} dx\right]^{-1/4}, \tag{9}$$

where $\beta$ stands for the integral

$$\int_0^1 \frac{\rho\mu}{\rho_w \mu_w} \frac{\eta^2(1-\eta)}{q/q_w}\, d\eta.$$

The result (9) can be compared with the Falkner–Skan solution for just-separating flow. Lighthill gives a table showing the ratio (Nusselt number)/$\sqrt{}$(Reynolds number) for Falkner Skan flow and $Pr = 0{\cdot}7$. The value given for this ratio for separating Falkner–Skan flow is

$$Nu/\sqrt{(Re_x)} = 0{\cdot}438.$$

The value obtained from (9), again using $f(\eta) = \sqrt{(1-\eta^2)}$ in the evaluation of $\beta$, comes out to be

$$Nu/\sqrt{(Re_x)} = 0{\cdot}448,$$

and agrees also within better than 3%. In addition (9) shows explicitly the dependence of heat transfer on the Prandtl number near separation.

## 4. Extension to high Mach number flow

The exact form of equation (1), valid for arbitrary Mach number, is

$$\frac{d}{dx}\int_0^\delta [h+\tfrac{1}{2}u^2-(h_\infty+\tfrac{1}{2}U^2)]\rho u\,dy = -q_w. \tag{10}$$

Introducing the recovery enthalpy $h_r$, we may write the integral in the form

$$\int_0^\delta [(h-h_r)+(h_r-h_\infty)-\tfrac{1}{2}(U^2-u^2)]\rho u\,dy.$$

It is often possible to neglect the terms

$$h_r-h_\infty-\tfrac{1}{2}(U^2-u^2)$$

and extend the derivations to the high Mach number case simply by replacing $h_\infty$ by $h_r$. It is also possible of course to use the full equation (10), but then the differential equation becomes more difficult and the essential simplicity of the approach is lost.

## References

Fage, A. & Falkner, V. M. 1931 *Aero. Res. Comm., Lond., Rep. & Mem.* no. 1408.

Lagerstrom, P. A. Article in *High Speed Aerodynamics and Jet Propulsion*, Vol. IV, Section B. Princeton University Press.

Lighthill, M. J. 1950 *Proc. Roy. Soc.* A, **202**, 353.

# Turbulent flow in a stably stratified atmosphere

By A. A. TOWNSEND
*Emmanuel College, Cambridge*

(*Received* 2 *July* 1957)

SUMMARY

Fluctuations of velocity and temperature which occur in a turbulent flow in a stably-stratified atmosphere far from restraining boundaries are discussed using the equations for the turbulent intensity and for the mean square temperature fluctuation. From these, an equation is derived for the flux Richardson number in terms of the ordinary Richardson number and some non-dimensional ratios connected with the turbulent motion. It is shown that the interaction between the temperature and velocity fields imposes on the flux Richardson number an upper limit of 0·5, and on the ordinary Richardson number a limit of about 0·08. If these values are exceeded, no equilibrium value of the turbulent intensity can exist and a collapse of the turbulent motion would occur. Although the analysis applies strictly only to a homogeneous non-developing flow, it should have approximate validity for effectively homogeneous, developing flows, and the predictions are compared with some recent observations of these flows.

## 1. INTRODUCTION

The study of turbulent flow in a stably-stratified fluid may be helped by the recognition of some different types of irregular flow which may occur. If the direct influence of the buoyancy forces on the motion is small, the motion will resemble 'ordinary' turbulence and will be characterized by high rates of energy dissipation, and of momentum and mass transport. If the buoyancy forces are dominant, the motion may be an irregular collection of gravity waves with low rates of energy dissipation and transport. In flows unrestrained by boundaries, both types of motion are found, characteristically turbulent motion near the origin of the flow and wave-like motion far downstream. There is here a gradual transition from the region of turbulent flow to the region of wave flow, which makes difficult the definition of the limits of either flow; nevertheless, the two flows are so distinct that no common description is likely to be valid.

In this paper, the characteristically turbulent flow in a stably-stratified fluid far from restraining boundaries is discussed, using ideas and generalizations taken over from our knowledge of turbulent flow of constant density, with the purpose of obtaining a criterion for the continued

existence of fully turbulent flow. Naturally, the results can only be valid while the flow is fully turbulent, and the accuracy of the analysis depends on the occurrence of a breakdown in the mechanism of 'ordinary' turbulent flow before buoyancy forces become dominant.

The methods used are by no means new, and might be described as mutton (mixing-length theory), dressed as lamb by recasting it in terms of similarity hypotheses. The approach is somewhat similar to that used by Ellison (1957) who considered a boundary layer transmitting constant shear stress and constant heat flux. This is an example of the class of turbulent flows which have complete homogeneity in the direction of flow allied to essential inhomogeneity in the direction of shear. All such flows are restrained by the fluid boundaries, while the unrestrained flows considered in this paper are substantially homogeneous in the direction of shear and inhomogeneous in the direction of flow.

Although this paper is concerned primarily with flows in which radiative exchange of heat is negligible, the possibility of radiative transfer has been kept in mind and its effects will be considered in more detail in a following paper.

## 2. Conditions for similarity of the turbulent motion

The attempt to find the criterion which determines whether turbulent flow does or does not occur in a particular flow system is a part of the general problem of establishing the conditions under which flows with geometrically similar boundary conditions are dynamically similar, the independent non-dimensional parameters whose equality permits dynamical similarity losing one degree of freedom when they specify a marginally stable flow. With the earth's atmosphere in mind, we consider only flows of a nearly perfect gas, moving with velocity variations small compared with the local speed of sound, with temperature variations small compared with the absolute temperature, and with a length scale small compared with the scale height of the atmosphere. If effects of the earth's rotation are negligible, it may be shown (Batchelor 1953) that dynamical similarity of flows with geometrically similar boundary conditions, defined quantitatively by the three scales $u_0$, $l_0$, $\theta_0$, referring to velocity variation, length, and potential temperature respectively, depends on equality of the three parameters $u_0 l_0/\nu$ (Reynolds number), $g\theta_0 l_0/(T_0 u_0^2)$ (Richardson number), $\nu/\kappa$ (Prandtl number), and equality or irrelevance of parameters depending on the radiative characteristics of the gas. Here $\nu$ is the kinematic viscosity, $\kappa$ the thermometric conductivity, and $T_0$ the mean absolute temperature. For flows of essentially the same gas the Prandtl number does not vary, and experience of shear flows of high Reynolds numbers shows that viscosity has no effect on the large-scale components of the motion which contain nearly all the energy. It follows that similarity depends only on the scale Richardson number and on the radiation parameters.

No further simplification can be made by dimensional analysis alone without considering the dynamics of the flow. To the approximation

implied by the restrictions set out above, the Navier–Stokes equations of motion are

$$\frac{D(U_i+u_i)}{Dt} = \frac{g_i}{T}\theta - \frac{1}{\rho}\frac{\partial(P+p)}{\partial x_i} + \nu\nabla^2(U_i+u_i), \tag{2.1}$$

and the continuity equation is

$$\frac{\partial(u_e+U_e)}{\partial x_e} = 0, \tag{2.2}$$

where $U_i$ and $u_i$ are the $i$-components of the mean fluid velocity and its fluctuation, $\theta$ is the temperature fluctuation about the mean $T$, $P$ and $p$ are the mean, and the fluctuation about the mean, of the pressure difference from the 'hydrostatic' pressure $P_0$ defined by $\partial P_0/\partial x_i = -\rho g_i$, $-g_i$ is the acceleration vector of the gravitational field, $\rho$ is the mean density.

To this approximation, the direct effects of density variations on the velocity field are completely represented by the bouyancy term $g_i\theta/T$, although the distribution of the buoyancy forces will depend on the interaction of the turbulent motion and the heat sources of the flow. The action of these buoyancy forces may be described in several ways but a fundamental effect is the addition or subtraction of energy from the turbulent motion. The equation for the turbulent kinetic energy per unit mass is

$$\frac{\partial}{\partial t}(\tfrac{1}{2}\overline{q^2}) + \overline{u_i u_e}\frac{\partial U_i}{\partial x_e} + \frac{\partial}{\partial x_e}\left(\tfrac{1}{2}\overline{q^2 u_e} + \frac{1}{\rho}\overline{p u_e}\right) + U_e\frac{\partial(\tfrac{1}{2}\overline{q^2})}{\partial x_e} = \frac{g_i}{T}\overline{\theta u_i} + \nu\overline{u_i\nabla^2 u_i}, \tag{2.3}$$

where $q^2 = u_i u_i$ and repeated suffices indicate summation over the three possible values of the repeated suffix. On the left-hand side of this equation, the first term is zero if the flow is statistically steady and the third and fourth terms represent transport of mechanical energy from one part of the flow to another, repectively transport by diffusive movements and through advection by the mean flow. Diffusive transport is usually effective only in the direction at right angles to the mean flow and can be eliminated from the equation by integrating over a whole section of the flow. Energy transport by advection cannot be eliminated in this way and it is of importance in all developing flows, e.g. boundary layers, jets and mixing layers, but its effects cannot usefully be considered without specifying the flow and it will be neglected in the following discussion. For this reason the results obtained apply strictly only to non-developing flows.

Three terms now remain in equation (2.3), they represent energy production by transfer from the mean flow and energy loss through work done against buoyancy forces and through viscous dissipation. To the extent that energy sources control its nature, the flow depends on the relative magnitudes of these three terms, or the ratio of the total loss of energy by buoyancy forces,

$$-\int \frac{g_i}{T}\overline{\theta u_i}\, dA,$$

to the total production by transfer from the mean flow,

$$-\int \overline{u_i u_e}\frac{\partial U_i}{\partial x_e}\, dA,$$

where the integrals extend over a whole section of the flow. This ratio,

$$[R_f]_I = \int \frac{g_i}{\overline{T}} \overline{\theta u_i}\, dA \Big/ \int \overline{u_i u_e} \frac{\partial U_i}{\partial x_e}\, dA, \tag{2.4}$$

is the flux Richardson number for the whole section of the flow. The ordinary flux form of the Richardson number,

$$R_f = \frac{g_i}{\overline{T}} \overline{\theta u_i} \Big/ \left[ \overline{u_i u_e} \frac{\partial U_i}{\partial x_e} \right], \tag{2.5}$$

is the relevant *local* parameter only if turbulent transport of energy can be neglected. This analysis has been set out here to show that $[R_f]_I$ describes the relative effects of inertial and buoyancy forces on the turbulent motion, whether or not radiative transfer is an important element in the problem.

Since radiative transfer plays no direct part in the dynamics of the turbulent motion or in the turbulent energy balance, it is a plausible assumption that the flux Richardson number will describe the *motion* with or without radiative transfer of heat. It does *not* follow that the condition for the maintenance of turbulent motion must be expressible as a single critical value of the flux Richardson number. Obviously the flux Richardson number cannot exceed one (turbulent dissipation of energy cannot change sign) but laboratory observations of flows unaffected by radiative transfer indicate a critical value of the flux Richardson number substantially less than one. The critical condition appears to arise from a failure to achieve equilibrium in the interactions between the temperature field and the turbulent motion, which may occur in the following way. In a flow with given gradients of mean temperature and velocity, production of turbulent energy is proportional to the Reynolds stress and approximately proportional to the turbulent intensity. Loss of energy through buoyancy forces is proportional to the vertical heat flux or, in the absence of radiation, to the square-root of the turbulent intensity. Turbulent dissipation of energy is proportional to the $\frac{3}{2}$-power of the intensity. Clearly the ratio of the total energy loss to the energy production, considered as a function of the turbulent intensity, has a minimum value, and if this is greater than one no equilibrium intensity exists and the turbulence must decay. Introduction of radiative heat transfer into the system alters the dependence of turbulent heat transport on turbulent intensity and will lead to a change in the critical condition. Although the motion itself may be still determined by the flux Richardson number, the range of possible Richardson numbers will depend on the intensity of the radiative transfer. The next sections are concerned with the quantitative expression of these notions.

## 3. The turbulent heat transfer

To the approximation being used, the equation for the temperature of a fluid element is

$$\frac{D(T+\theta)}{Dt} + (U_i + u_i)\frac{g_i}{c_p} = k\nabla^2(T+\theta) + \frac{\mathscr{R}}{\rho c_p}, \tag{3.1}$$

where $\mathscr{R}$ is the net rate of heat gain by radiative processes. If this equation is multiplied by the temperature fluctuation and the mean value taken, an equation for the intensity of the temperature fluctuations is obtained,

$$\frac{\partial}{\partial t}(\tfrac{1}{2}\overline{\theta^2}) + \overline{u_e\theta}\left(\frac{\partial T}{\partial x_e} + \frac{g_e}{c_p}\right) + U_e\frac{\partial(\tfrac{1}{2}\overline{\theta^2})}{\partial x_e} + \frac{\partial}{\partial x_e}(\tfrac{1}{2}\overline{\theta^2 u_e}) = \kappa\overline{\theta\nabla^2\theta} - \beta\overline{\theta^2}. \quad (3.2)$$

In this equation, the radiation term $\overline{\mathscr{R}\theta}/(\rho c_p)$ has been written as $-\beta\overline{\theta^2}$, where $\beta$ may be regarded as the logarithmic rate of cooling of a fluid element by radiation alone. This radiation term is in general a function of the whole temperature field and its exact value will be considered in a second paper.

From equation (3.2), an estimate of the heat transport by convective movements can be obtained. From this point on, it is convenient to consider a stationary flow with vertical gradients of the horizontal mean velocity and of temperature. In addition, the transport terms will be omitted from the equations for the turbulent energy and for the intensity of the temperature fluctuations, which means that advection is neglected and that the quantities in the equations are suitably defined mean values for the whole flow. Using the ordinary notation with the $Oz$ axis vertical and mean velocities along the $Ox$ axis, equation (3.2) for $\frac{1}{2}\overline{\theta^2}$ becomes

$$\overline{w\theta}\left(\frac{\partial T}{\partial z} + \frac{g}{c_p}\right) = -\tfrac{1}{3}\overline{\theta^2}\frac{(\overline{w^2})^{1/2}}{L_\theta} - \beta\overline{\theta^2}, \quad (3.3)$$

where the conduction term $\kappa\overline{\theta\nabla^2\theta}$ has been replaced by $-\frac{1}{3}\overline{\theta^2}(\overline{w^2})^{1/2}/L_\theta$. This substitution is to some extent formal, but it expresses also the experimentally established result that the large-scale properties of turbulent flows are independent of the magnitudes of the viscosity and conductivity of the fluid. In constant density flows, the length $L_\theta$ is nearly equal to the integral scale of the turbulent motion. From this equation,

$$(\overline{\theta^2})^{1/2} = k_\theta(\overline{w^2})^{1/2}\frac{|\partial T/\partial z + g/c_p|}{\frac{1}{3}(\overline{w^2})^{1/2}/L_\theta + \beta}, \quad (3.4)$$

where

$$k_\theta = |\overline{w\theta}|/[\overline{w^2}\overline{\theta^2}]^{1/2},$$

and the heat transfer by turbulent convection is

$$\overline{\theta w} = -\frac{k_\theta^2}{k_u}|\overline{uw}|\frac{\partial T/\partial z + g/c_p}{\frac{1}{3}(\overline{w^2})^{1/2}/L_\theta + \beta}, \quad (3.5)$$

where $k_u = \overline{uw}/\overline{w^2}$. The flux Richardson number, defined by equation (2.5), is

$$R_f = \frac{k_\theta^2}{k_u}\frac{(g/T)(\partial T/\partial z + g/c_p)}{\partial U/\partial z\,(\frac{1}{3}(\overline{w^2})^{1/2}/L_\theta + \beta)}. \quad (3.6)$$

An expression for the flux Richardson number may be obtained in a form involving only gradients of mean values and some non-dimensional ratios. This is done by using the equation for the kinetic energy of the velocity fluctuations which is, omitting energy transport terms in the same

way as transport terms were omitted in equation (3.3),

$$-\overline{uw}\frac{\partial U}{\partial z} = -\frac{g}{T}\overline{\theta w} + \frac{(\overline{w^2})^{3/2}}{L_\varepsilon} \tag{3.7}$$

where $L_\varepsilon$ is the dissipation length scale and is nearly equal to the integral scale in constant density flows. Combining this equation with (3.5) leads to a quadratic equation for the turbulent heat transport, whose solution may be written in the non-dimensional form

$$R_f = \frac{(g/T)\overline{\theta w}}{\overline{uw}\,\partial U/\partial z} = \tfrac{1}{2}H\left[1-\left(1-12\frac{L_\theta}{L_\varepsilon}\frac{k_\theta^2}{k_u^2}\frac{R_i}{H^2}\right)^{1/2}\right], \tag{3.8}$$

where

$$H = 1+\frac{3}{k_u}\frac{L_\theta}{L_\varepsilon}\frac{\beta}{|\partial U/\partial z|} \tag{3.9}$$

and

$$R_i = \frac{g}{T}\left(\frac{\partial T}{\partial z}+\frac{g}{c_p}\right)\Big/\left(\frac{\partial u}{\partial z}\right)^2.$$

The number $H$ is a measure of the ratio of the logarithmic rate of radiative cooling of a fluid element to the mean rate of shear. In the absence of radiative effects, it equals one.

## 4. Conditions for the maintenance of turbulent motion

In the previous section, an equation was obtained relating the turbulent heat transport to the gradients of mean velocity and potential temperature, to the radiative properties of the fluid, and to some non-dimensional ratios describing the turbulent motion. The validity of conclusions drawn from this equation depends only on further assumptions about the variation of the non-dimensional ratios with stability, since it is derived directly from the equations of motion and of heat. Neither theory nor experiment gives firm guidance on this point, and it will be assumed that the ratios $L_\theta/L_\varepsilon$, $k_u$ and $k_\theta$, are nearly independent of stability. The first of these ratios, $L_\theta/L_\varepsilon$, is simply the ratio of the logarithmic dissipation rates for temperature and velocity fluctuations. The large-scale fluctuations of temperature and vertical velocity are closely correlated and it seems unlikely that the rates of turbulent transfer down the scale of eddy sizes (which determine the magnitudes of the conductive and viscous dissipations) could be very dissimilar (Ellison (1957) makes an equivalent assumption for a constant-stress boundary layer). A more debatable assumption is that the shear coefficient $k_u$ and the temperature–velocity correlation $k_\theta$ are nearly independent of stability, for there are circumstances in which it is certainly not true. In the last stages of decay of a turbulent mixing-layer between two streams of different temperature, most of the motion is in the form of gravity waves at the interface and permanent mixing on the molecular scale is a rarity. Both these coefficients then approach zero although at different rates. Again, in a thick boundary layer of constant stress and constant downward

heat transport, buoyancy has a negligible influence near the ground and an overwhelming influence at great heights. Here, it is not possible to think of $k_u$ and $k_\theta$ except as functions of height. The previous analysis has assumed stationary, non-developing flow and the use of typical or mean values of the velocity and temperature gradients implies that the motion in all parts of the flow is essentially similar, so both these sets of conditions are excluded. If the flow is everywhere characteristically turbulent, it is probable that the correlation factors are always large and near their values in constant density flows.

Returning now to the consideration of equation (3.8), we see that real values of the turbulent heat flux and the flux Richardson number are only possible if

$$R_i < \frac{1}{12}\frac{k_u^2}{k_\theta^2}\frac{L_\varepsilon}{L_\theta} \tag{4.1}$$

assuming, as we do from now, negligible effects of radiative transfer. Accepting the substantial constancy of $k_u$, $k_\theta$ and $L_\varepsilon/L_\theta$, this sets the limit to possible values of the flux Richardson number,

$$R_f < \tfrac{1}{2}. \tag{4.2}$$

This limit to the possibility of turbulent motion arises from an impossibility of finding any real turbulent intensity to satisfy both the equation for the turbulent energy and the equation for the intensity of the temperature fluctuations, and it is additional to the limit set by the energy equation alone,

$$R_f < 1. \tag{4.3}$$

An interesting consequence of a limiting value for the flux Richardson number of one-half is that the turbulent intensity is finite in the critical flow. This can be seen by writing the energy equation (3.7) in the form

$$\frac{(\overline{w^2})^{1/2}}{k_u L_\varepsilon |\partial U/\partial z|} = 1 - R_f. \tag{4.4}$$

At the limit $R_f = \frac{1}{2}$, the turbulent intensity will be about one-quarter of the constant density value, and a sudden collapse of the turbulent motion occurs as the limit is passed.

## 5. Comparison with experiment

For a proper test of the validity of the analysis, it would be desirable to have experimental confirmation that the ratios $k_u$, $k_\theta$, and $L_\theta/L_u$, are nearly independent of stability, but practically no information is available. A few measurements of turbulent flows with stable density gradients do exist and these may be examined for conformity with the proposed criteria for turbulent motion ((4.1) and (4.2)), but nearly all these are of developing flows and in these stability is not a simple concept. In an unconstrained, developing flow, the Richardson number initially increases with distance from the origin of the flow but a comparatively rapid decay of the turbulent

motion sets in downstream of the point where the Richardson number attains a critical value, this decay corresponding with the sudden collapse of the turbulent motion in a non-developing flow. As the decay is not instantaneous, the Richardson number may increase beyond the critical value. This makes the experimental determination of the critical value difficult and measurements of the kind to be discussed can do little more than indicate that the critical Richardson number may be near 0·1.

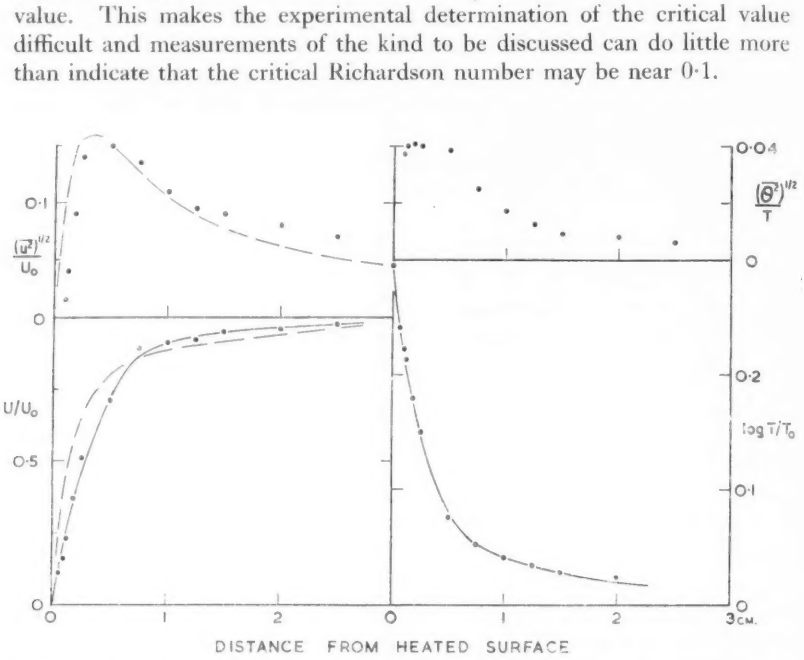


Figure 1. Boundary layer on the underside of a heated surface (C. I. H. Nichol). Free stream velocity $U_0 = 150$ cm sec$^{-1}$, free stream temperature $T_0 = 288°$ K, surface temperature $T_w = 388°$ K, $x = 151$ cm, $(gx/U_0^2)\log(T_w/T_0) = 1{\cdot}94$.

Probably the most accurate and comprehensive measurements in this field are those of C. I. H. Nichol in the turbulent boundary layer on the underside of a heated surface. In these experiments, an artificially-thickened boundary layer was allowed to develop naturally for a distance of 127 cm, beyond which point the wall temperature was maintained at approximately 100° C above the temperature of the free stream. At an air-speed of 150 cm sec$^{-1}$, a nearly complete collapse of the turbulent motion was observed between 151 cm and 202 cm, the flow then having very low values of turbulent intensity and wall stress and a highly inflected form to the mean velocity profile (figures 1 and 2). This last effect is a consequence of the virtual disappearance of Reynolds shear stresses which earlier had kept the air next the wall moving. With their removal, this air slows down and the streamlines expand, displacing the outer flow. The beginnings of this process are clearly visible at $x = 151$ cm (figure 1), although the heat from the wall has not yet spread to the outer parts of the layer, and also

in the measurements at an air-speed of 190 cm sec$^{-1}$ (figure 3). As the individual measurements of velocity and temperature have random errors reflecting the considerable experimental difficulties, the computation of local Richardson numbers is not easy, as is shown by figure 4 in which are plotted local Richardson numbers computed by taking finite differences between neighbouring experimental points. The scatter is very large and only the most docile reader would agree from this that the mean values in the outer part of the layers are all less than 0·1. More representative numbers have been obtained by using the mean gradients over the outer parts of the layers, between 0·5 cm and 2·5 cm from the wall. These numbers are given in table 1 and may be more acceptable evidence that the Richardson number just before collapse is less than 0·1*.

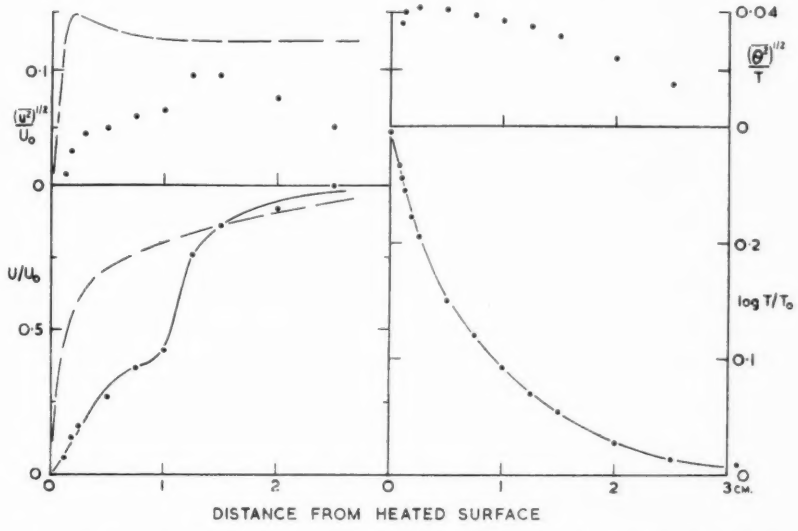


Figure 2. Boundary layer on the underside of a heated surface (C. I. H. Nichol). Free stream velocity $U_0 = 150$ cm sec$^{-1}$, free stream temperature $T_0 = 288°$ K, surface temperature $T_w = 388°$ K, $x = 202$ cm, $(gx/U_0^2)\log(T_w/T_0) = 2{\cdot}60$.

In the second series of experiments, a liquid jet was injected horizontally along the interface between a denser and less dense solution of salt in water. From a ciné record estimates could be made of the velocity and width of the jet. It was found that entrainment of fluid by the jet almost ceased when the Richardson number (which increases with distance from the nozzle) exceeded 0·3. Beyond this point, the velocity and cross-section of the jet remained nearly constant, indicating very little entrainment and

* It should be pointed out that this flow is essentially different from the constant-stress layer considered by Ellison (1957). The flow in this developing layer was not essentially different from that in one-half of the mixing layer between two streams.

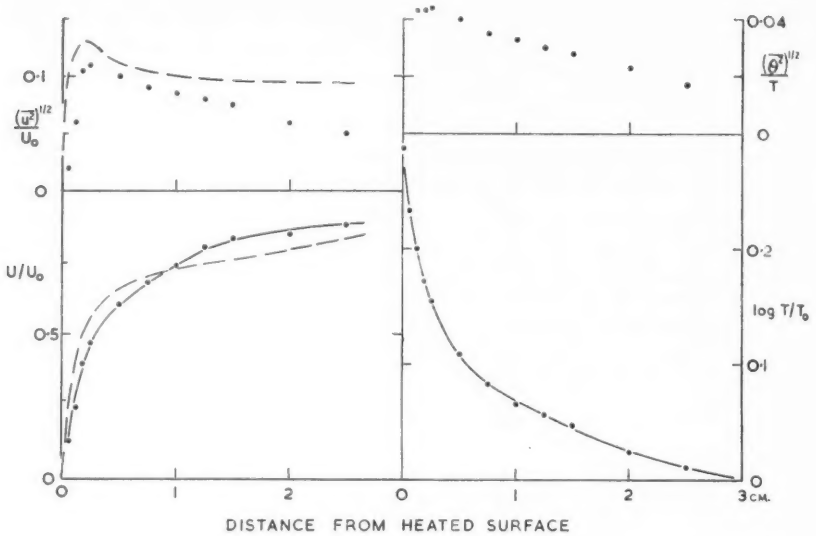


Figure 3. Boundary layer on the underside of a heated surface (C. I. H. Nichol). Free stream velocity $U_0 = 190$ cm sec$^{-1}$, free stream temperature $T_0 = 289°$ K, surface temperature $T_w = 385°$ K, $x = 202$ cm, $(gx/U_0^2)\log(T_w/T_0) = 1{\cdot}57$.

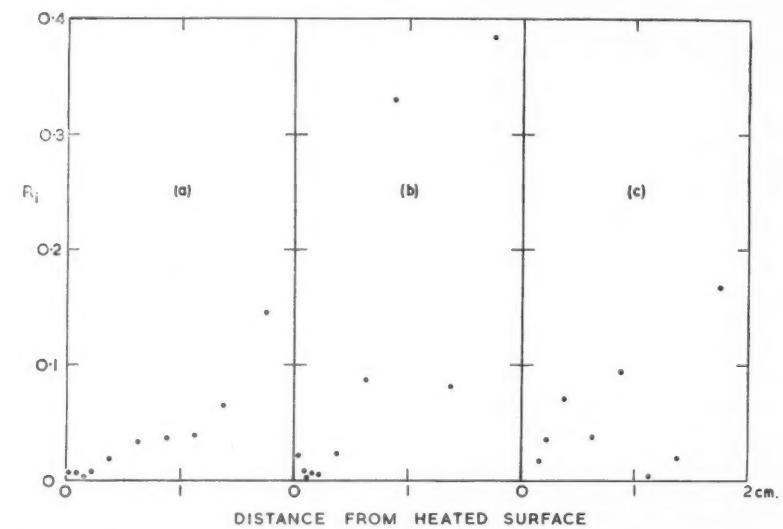


Figure 4. Boundary layer on the underside of a heated surface : local Richardson numbers.

(*a*) $U_0 = 150$ cm sec$^{-1}$, $x = 151$ cm,
(*b*) $U_0 = 150$ cm sec$^{-1}$, $x = 202$ cm,
(*c*) $U_0 = 190$ cm sec$^{-1}$, $x = 202$ cm.

presumably very little turbulent motion. The first signs of a diminution in rate of entrainment appeared at a Richardson number of about 0·05, and the critical number, in the sense used in the theory, is believed to lie between these limits (see figure 5).

| Conditions | $R_i$ | Remarks |
|---|---|---|
| $U_0 = 190$ cm sec$^{-1}$<br>$x = 202$ cm, $T_w - T_0 = 96°$ C. | 0·070 | Collapse just beginning. |
| $U_0 = 150$ cm sec$^{-1}$,<br>$x = 151$ cm, $T_w - T_0 = 100°$ C. | 0·046 | Spread of heat from the wall not yet complete. |
| $U_0 = 150$ cm sec$^{-1}$,<br>$x = 202$ cm, $T_w - T_0 = 100°$ C. | 0·022 | Collapse nearly complete : note low value of $R_i$. |

Table 1.

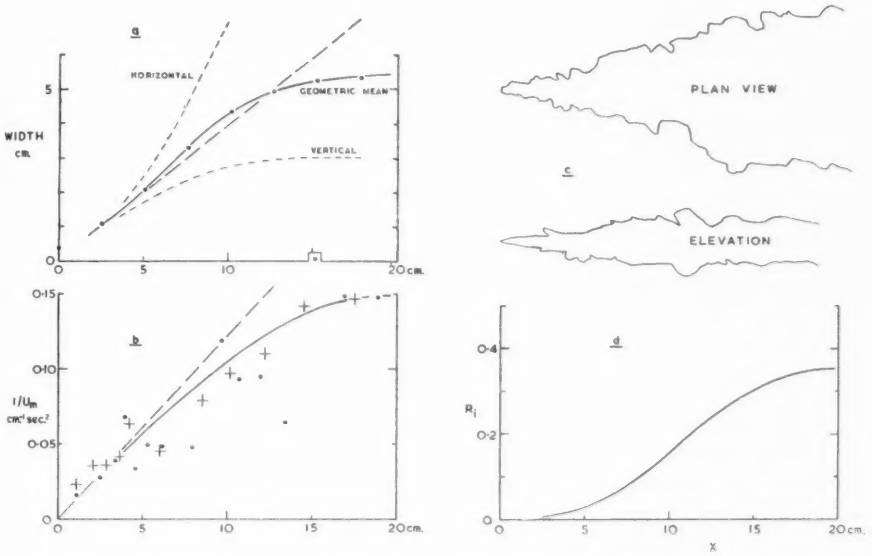


Figure 5. Spreading of a jet injected along the interface between saline solution of densities 1·032 and 1·125 gm cm$^{-3}$. (*a*) Variation of widths with distance from origin. The straight dashed line is the mean of observations of normal, constant-density jets. (*b*) Mean velocities of advance of marked fluid put into the jet. The dashed line is the mean of observations on a normal jet. (*c*) Instantaneous outlines of the jet, traced from enlargements of ciné records. The scale is the same as that of the horizontal scale of the other diagrams. (*d*) Mean Richardson numbers, computed as $R_i = 0{\cdot}064g[(\rho_1 - \rho_2)/\bar{\rho}](D/U_m^2)$, where $D$ is the observed width and $U_m$ is the mean velocity of advance of dye.

The difficulty in all experiments with developing flows is that a failure of the regulating mechanism will cause the turbulence to decay but, while it decays, spreading of the flow and entrainment of ambient fluid continues. For this reason there is a lower critical number at which decay begins and an upper critical number attained when decay is complete. The lower number marks the failure of the normal regulating mechanism of the developing flow and should correspond with the one considered in the theory.

This conclusion that the critical Richardson number is about 0·08 appears to ignore the frequently quoted series of measurements of the flow of fresh-water of salt in the Kattegat, analysed by Taylor (1931) and others. In these measurements, Richardson numbers as high as one hundred were found although the shear stresses and transport of salinity were much larger than could be accounted for by viscosity and molecular diffusion. The observed values of the flux Richardson number were around 0·3. Some observations of a similar flow carried out by Dr J. S. Turner in the Cavendish Laboratory suggest that this apparent anomaly may be due to the non-existence of a critical Richardson number in the ordinary sense for a developing flow. In these experiments, fresh water was caused to flow over salt water which was coloured for easy identification. Near the beginning of the mixing zone, mixing is intense and caused by ordinary turbulent movements but, further downstream, the flow settles down to nearly laminar flow with a sharp interface between the fresh and the salt water. This interface is continuously distorted by irregular gravity waves which occasionally break, projecting coloured salt water upwards and, presumably, fresh water downwards. Most of these jets seem to fall back, losing only a small part of their volume by mixture but clearly transferring a considerable part of their momentum by the formation of 'inviscid' wakes of the vortex sheet type. Transfer of salinity is primarily due to molecular diffusion from the jets but is enhanced by the motion of the jets through the alien fluid. These qualitative considerations show that in this part of the flow 'turbulent' transport of salinity and momentum will each be considerably greater than the molecular rates, but that proportionately momentum transfer is very much more intense than salinity transport. It is probable that the Kattegat measurements were carried out under similar conditions and that the measured Richardson numbers do not refer to turbulent motion but to this random wave motion of the interface.

I am indebted to Mr C. I. H. Nichol for permission to abstract from his unpublished work the measurements that are represented in figures 1–4. I have benefited from observation and discussion of the experiments of Dr J. S. Turner on the flow of fresh water over salt water.

## References

Batchelor, G. K. 1953 *Quart. J. R. Met. Soc.* **80,** 339.

Ellison, T. H. 1957 *J. Fluid Mech.* **2,** 456.

Taylor, G. I. 1931 *Rapports et Procés-Verbaux du Conseil Permanent International pour l'Exploration de la Mer* **76,** 35.

# The minimum Reynolds number for a turbulent boundary layer and the selection of a transition device

By J. H. PRESTON

*Department of Fluid Mechanics, University of Liverpool*

(*Received* 22 *July* 1957)

SUMMARY

In the case of turbulent flow in a pipe there is a lower experimental number to the Reynolds limit for which fully developed turbulent flow occurs. From the similarity and close agreement of the curves showing the coefficient of skin friction $c_f$ as a function of the Reynolds number $R_\theta$ (based on the momentum thickness $\theta$) for the circular pipe and flat plate, it is suggested that there should be a lower limit to $R_\theta$ for fully developed turbulent flow on a flat plate. Rather limited experimental data confirm this and place the lower limit at $R_\theta = 320$. The choice and size of transition device is examined in relation to this minimum $R_\theta$ and an approximate theory leads to a 'wire' Reynolds number in fair agreement with experience.

## 1. INTRODUCTION

In the literature it is common to find a curve depicting the turbulent skin friction coefficient $c_f$ of a flat plate as a function of the Reynolds number $R_x$ based on the distance $x$ from the leading edge. It is assumed that transition occurs at the leading edge and that the boundary layer has zero thickness there, i.e. $R_\theta = 0$. This is an assumption that has a certain analytical convenience, but it has dangers for the experimenter and the engineer. The former is tempted to induce transition at the leading edge by means of a wire or other device without giving much thought as to what are the real conditions just downstream of it, whilst the latter makes estimates of drag for this assumed state which may be considerably in error at low values of $R_x$.

In this connection the recent paper by Dutton (1956) on the turbulent boundary layer of a flat plate brings out clearly the marked effect of the size and type of transition device on the distribution of $c_f$ and $R_\theta$ considered as functions of $R_x$. However, Dutton finds $c_f$ to be an approximately unique function of $R_\theta$ and independent of the transition device used. This is consistent with the assumption of universal 'inner' and 'outer' laws for the velocity distribution which has been the basis of important papers by Landweber (1953) and by Coles (1954) and will also be used in this paper.

In this note, with the aid of pipe flow results and the results obtained by Dutton and earlier investigators on a flat plate, it will be suggested that there is a lower experimental limit to the value of $R_\theta$ for the turbulent boundary layer of a flat plate as for turbulent flow in a pipe. Theoretical support for this suggestion is given and the functions of a transition device in relation to this idea of a lower limit are then considered.

## 2. Flow in circular pipes

Figure 1 shows Nikuradse's (1932, 1933) results for $\tau_w/(\frac{1}{2}\rho U_m)$ as a function of $R = U_m d/\nu$ and the roughness ratio $d/2\epsilon$, where $U_m$ is the mean velocity in the pipe, $d$ is the pipe diameter, $\tau_w$ is the skin friction, and $\epsilon$ is the roughness height. As $R$ is decreased, the various curves tend to that for the smooth pipe (turbulent flow) with the exception of the one for the largest roughness $d/2\epsilon = 15$. At a value of $\log_{10} R$ of about 3·65, all the curves, which have now merged into one, travel down a common

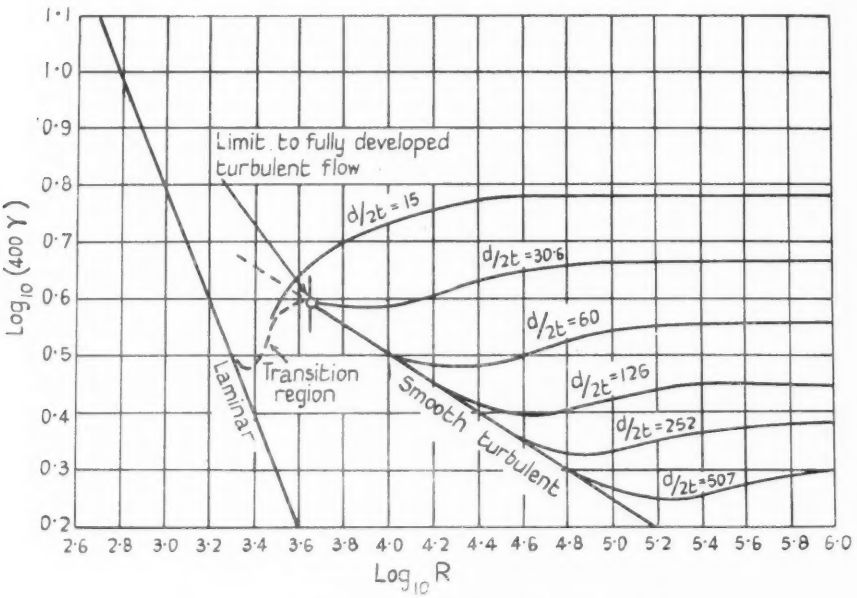


Figure 1. Resistance of rough pipes (after Nikuradse).

transition curve which joins the curve for laminar flow at $\log_{10} R \doteqdot 3{\cdot}32$. This appears to be the maximum value of $R$ for laminar flow with very disturbed entry conditions and, even with comparatively large closely packed roughness, the skin friction has the laminar flow value at Reynolds numbers below this critical value.

Now the significant point from the standpoint of the present note is that it is impossible to obtain results which would extend the smooth pipe

(turbulent flow) curve to values of $\log_{10} R < 3{\cdot}65$ or $R < 4{\cdot}47 \times 10^3$, and this is the lowest Reynolds number for fully developed turbulent flow in a pipe.

Defining the momentum thickness for axisymmetric flow by

$$\theta = \int_0^{d/2} \frac{u}{U_1}\left(1 - \frac{u}{U_1}\right)\left(1 - \frac{2r}{d}\right) dr,$$

where $U_1$ is the velocity of the pipe centre and $u$ is the velocity at radius $r$, it is possible to obtain $2\theta/d$ as a function of the Reynolds number $R$ when the velocity distribution is known. This has been done by Ross (1952)

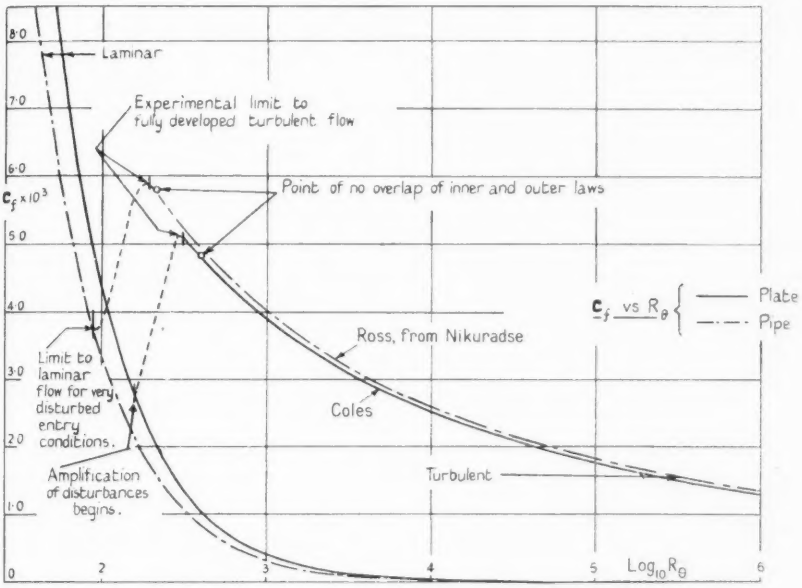


Figure 2. Skin friction coefficient against momentum thickness Reynolds number.

in a re-analysis of Nikuradse's results to yield $R_\theta = U_1\theta/\nu$ as a function of $R$, and $c_f = \tau_w/(\frac{1}{2}\rho U^2)$ as a function of $R_\theta$, for turbulent flow. The result has been expressed in the form

$$c_f^{-1/2} = 3{\cdot}8 \log_{10} R_\theta + 4{\cdot}4. \tag{1}$$

This is shown in figure 2 together with the laminar flow relation

$$c_f = \tfrac{1}{3} R_\theta. \tag{2}$$

The minimum Reynolds number for which equation (1) is applicable is $R = 4{\cdot}47 \times 10^3$, and the corresponding value of $R_\theta$ is 193. The maximum value of $R_\theta$ for laminar flow with very disturbed entry conditions is 87·5,

### 3. The flow along a flat plate

Of a large number of papers dealing with the problem it is proposed in this paper to refer to only three, the paper by Dutton (1956) already referred to, and the papers by Landweber (1953) and Coles (1954), both of which review much of the existing work on the subject. In the calculation of the growth of the turbulent boundary and the distribution of skin friction, both Landweber and Coles start from assumed velocity distributions through the boundary layer.

In a finite region next to the surface, the 'inner' law is assumed to apply and the velocity $u$ is given by

$$\frac{u}{u_\tau} = f\left(\frac{u_\tau y}{\nu}\right), \tag{3}$$

where $u_\tau = (\tau_w/\rho)^{1/2}$ and $y$ is the distance from the surface. In the outer region of the boundary layer, the 'outer' law applies in the form

$$\frac{U-u}{u_\tau} = \phi(y/\delta), \tag{4}$$

where $U$ is the velocity at the edge $y = \delta$ of the boundary layer.

The assumption (supported by experiment) that these laws overlap over a finite region leads to the well-known logarithmic forms of the equations (3) and (4) in this region

$$u/u_\tau = A + B\log(u_\tau y/\nu) \tag{5}$$

$$(U-u)/u_\tau = C - B\log(y/\delta). \tag{6}$$

The 'inner' law equation (5) is assumed to be universal for all flows, but the 'outer' law for the plate differs from that for the pipe in the value of the constant $C$ in equation (6). The assumption of the 'inner' and 'outer' laws leads in both the plate and pipe problems to unique relations between $c_f$ and $R_\theta$.

In the case of the flat plate flow, the momentum equation

$$\tfrac{1}{2}c_f = d\theta/dx \tag{7}$$

enables the distribution of $c_f$ and the growth of $\theta$ to be found for given starting conditions of the turbulent flow. The relations between $c_f$ and $R_\theta$ as obtained by Landweber and Coles differ because of the different values of the constants $A$, $B$, $C$ assumed in the analysis depending on the individual assessment of the available experimental results. The relation obtained by Coles is utilized in this note because Dutton's results are close to it, and in figure 2 it is given for comparison with that for turbulent flow in a pipe, equation (1). The relation for laminar flow over a flat plate

$$c_f = 0{\cdot}441R_\theta^{-1} \tag{8}$$

is also plotted.

The general closeness and similarity of the results for pipe and plate is rather striking and it seems reasonable to expect that, as in the case of

the pipe, there is a minimum value of $R_\theta$ for turbulent flow along a plate. Examination of the results (from various sources) suggests that the minimum value of $R_\theta$ for the turbulent boundary layer of a flat plate is about 320 and Dutton's results, which are discussed later, confirm this.

Now both Landweber and Coles recognized that, in computing the boundary layer development along a plate, some initial starting condition has to be satisfied as there is a constant of integration at disposal. Landweber in fact restricted his solution to large Reynolds numbers $R_x$, so that the starting condition would have negligible effect and he took the constant to be zero. Coles fixed the constant by supposing that $R_\theta = 0$ when $R_x = 0$ and that the skin friction remains finite. Clearly, the constant of integration must be fixed by the value of $R_\theta$ at the transition position and this must equal or exceed the value of 320. The value will be fixed by the extent of laminar flow and the drag of the transition device.

Landweber appears to have been the first to recognize that there is a limit to the application of the 'inner' and 'outer' laws in their logarithmic form, since the amount of overlap decreases as the Reynolds number decreases. His argument is as follows. The 'inner' law equation (3) begins to depart from the logarithmic relation equation (5) as the sub-layer is approached and the value of $y$ $(= y_1)$ when this occurs is often taken as given by

$$u_\tau y_1/\nu \doteqdot 30. \tag{9}$$

The outer law equation (4) has from experimental data a logarithmic behaviour as given by equation (6) up to

$$y_2/\delta \doteqdot 0{\cdot}2. \tag{10}$$

These equations specify the degree of overlap of the two laws. If $y_1 = y_2$ then there is no overlap, and this occurs, from equations (9) and (10), when $u_\tau \delta/\nu = 150$ or

$$\log_{10}(u_\tau \delta/\nu) = 2{\cdot}176. \tag{11}$$

*Pipe flow*

We now apply this idea to turbulent flow in a pipe for which Ross (1952) gives

$$\left.\begin{aligned} u/u_\tau &= 5{\cdot}6 + 5{\cdot}6\log_{10}(u_\tau y/\nu) \\ (U-u)/u_\tau &= 0{\cdot}785 - 5{\cdot}6\log(y/\delta) \end{aligned}\right\}, \tag{12}$$

and, eliminating $u$,

$$U/u_\tau = (2/c_f)^{1/2} = 6{\cdot}385 + 5{\cdot}6\log_{10}(u_\tau \delta/\nu). \tag{13}$$

Inserting the value of $\log_{10}(u_\tau \delta/\nu)$ from equation (11) into equation (13), we find the 'no overlap' condition gives $c_f = 0{\cdot}0058$, and from figure 2 $\log_{10} R_\theta = 2{\cdot}305$, giving $R_\theta = 202$. This limit is marked on figure 2 and it is seen that it is very close to the experimental limit for fully developed turbulent flow $R_\theta = 193$.

*Plate flow*

Coles's relations for the velocity distribution in the overlap region are

$$\left.\begin{aligned} u/u_\tau &= 5{\cdot}10 + 5{\cdot}75\log_{10}(u_\tau y/\nu) \\ (U-u)/u_\tau &= 2{\cdot}80 - 5{\cdot}75\log_{10}(y/\delta) \end{aligned}\right\}, \tag{14}$$

and eliminating $u$

$$U/u_\tau = (2/c_f)^{1/2} = 7{\cdot}9 + 5{\cdot}75\log_{10}(u_\tau\delta/\nu). \tag{15}$$

The 'no overlap' condition gives $c_f = 0{\cdot}0048$, and from figure 2 the corresponding value of $R_\theta$ is given by $\log_{10}R_\theta = 2{\cdot}59$, i.e. $R_\theta = 3{\cdot}89$. The lowest value of $R_\theta$ in the data considered by Coles for which fully developed turbulent flow occurs is 320, which is again close to the $R_\theta$ for no overlap of the 'inner' and 'outer' regions.

It is not clear whether much significance should be attached to this measure of agreement found for both pipe and plate, owing to the rather arbitrary method of defining the limits of the logarithmic region by equations (9) and (10). Slightly different choice of constants in these equations would yield significantly different values of $c_f$ and $R_\theta$ for absence of overlap. But it is clear that, at values of $R_\theta$ of this order, the sub-layer is now an appreciable part of the boundary layer and the viscous stresses are becoming important well away from the wall. Experimentally, it seems that when the overlap region vanishes further reduction of $R_\theta$ leads to the velocity distribution assuming more and more nearly the characteristics of laminar flow with a rapid decrease in skin friction to the laminar flow value.

*Dutton's results*

Dutton's work was carried out at fairly low Reynolds numbers and further evidence of a minimum value of $R_\theta$ for turbulent flow over a flat plate can be gleaned from his results.

Figure 3 is a reproduction of figure 7 of Dutton's report and shows $R_\theta$ as a function of $R_x$ for two transition devices, circular wires and sandpaper strips. The curve for laminar flow has been included in figure 3 and the increments to $R_\theta$ caused by wire drag have been estimated by the theory given in the next section. The estimated total $R_\theta$ immediately behind the wires have been plotted on this figure and are made up as shown in table 1.

In discussing these results we note that $R_\theta$ for the laminar boundary layer just ahead of the wire is 120 and that this is less than the value of $R_\theta = 162$ at which disturbances are first amplified (based on $R_{\theta^*} = 420$, where $R_{\theta^*}$ is the Reynolds number formed by the displacement thickness). It is clear from curve (1) for the 0·013 in. wire that laminar flow is still persisting up to $R_x = 5\times10^5$ and that fully developed turbulent flow does not occur until $R_x = 8\times10^5$. The repeat set for this wire, curve (2), shows fully developed turbulent flow at about $R_x = 3\times10^5$, transition presumably occurring between there and the wire. The difference between these two sets has been explained by Dutton as arising from the sensitivity of the flow

at the leading edge of the plate to small changes in tunnel stream direction. This has probably resulted in the layer approaching the wire being thicker than that predicted by the Blasius theory. We note that, on the basis of the Blasius theory and the estimated $R_\theta$ for the 0·013 in. wire, $R_\theta$ behind the wire is 201 which is slightly greater than that for amplification to occur which is $R_\theta = 162$. Clearly, we cannot regard this value of $R_\theta$ as a lower limit to the $R_\theta$ for fully developed turbulent flow, since amplification must occur before transition occurs and this does not always occur suddenly.

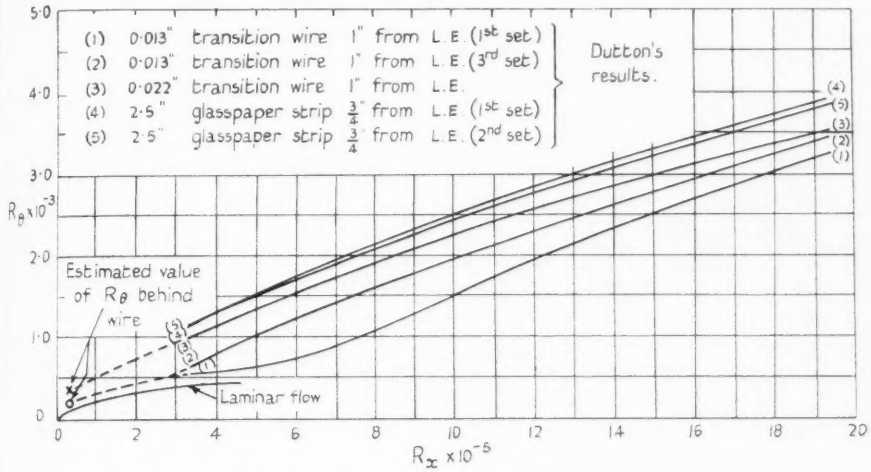


Figure 3. Influence of leading edge conditions on the development of the turbulent boundary layer along a flat plate.

| Wire diameter in inches | $u_d/U$ | $Ud/\nu$ | $\Delta R_\theta$ | Total $R_\theta$ behind wire |
|---|---|---|---|---|
| 0·013 | 0·713 | 423 | 81 | 201 |
| 0·022 | 0·952 | 716 | 244 | 365 |

Table 1. $R_\theta$ (in front of wire) = 120, $d$ = wire diameter, $u_d$ = value of $u$ at $y = d$.

In the case of the larger wire (diameter 0·022 in.) the corresponding curve (3) has fully developed turbulent flow characteristics at the first measuring station ($R_x = 3{\cdot}25 \times 10^5$) and it can be extrapolated to the estimated value at the wire without difficulty as shown. This suggests that transition occurs fairly suddenly at the wire where the estimated $R_\theta$ is 365. Examination of Dutton's curve suggests that a slightly smaller wire than this would still have had transition at the wire, so that the previously quoted value of $R_\theta = 320$, as the lowest value of $R_\theta$ for fully developed turbulent flow, is in agreement with the above assessment of Dutton's results.

The problem of the minimum Reynolds number for fully developed turbulent boundary layers under pressure gradients is more difficult as there appears to be no experimental evidence available. If we take the agreement between the values of $R_\theta$ for 'no overlap' of the inner and outer laws and the minimum values of $R_\theta$ observed for fully developed turbulent flow in the case of the pipe and plate and being true generally, then it is possible to make some predictions. It is known that the outer limit of the logarithmic region in terms of the boundary layer thickness tends to become less in adverse pressure gradients, so that $y_2/\delta$ in equation (10) assumes smaller values than 0·2. Hence in equation (11), the value of $u_\tau\delta/\nu$ for no logarithmic region to exist will increase in adverse pressure gradients. It is also known that $\theta/\delta$ increases progressively towards separation, as does $U/u_\tau$, and hence the value of $U\theta/\nu$ for 'no overlap' of the inner and outer laws will increase. Hence on the basis of the pipe and plate comparisons it is expected that the minimum value of $R_\theta$ for a fully developed turbulent boundary layer will increase in an adverse pressure gradient and decrease in a favourable gradient.

We have noted, from figure 3 of this paper or figure 7 of Dutton's paper, the very considerable influence of the type and magnitude of the transition device on $R_\theta$ in the range of $0 < R_x < 2\times10^6$ and the same is true of the skin friction given by figure 8 of Dutton's paper. This is of importance, not only in fundamental experiments which are often carried out at low to moderate Reynolds numbers, but also in experiments on ships in towing tanks when the Reynolds numbers are of the order of $10^7$–$2\times10^7$. It is also important for compressor blading of gas turbines at high altitudes, when the Reynolds number may be as low as $10^5$, and also in experiments in small high speed wind tunnels and low speed atmospheric tunnels, where Reynolds numbers of the order of $10^6$ are usual. Another point of importance is that, even when transition occurs at the wire, increase in its size naturally leads to an increase in drag and of momentum thickness downstream, but this increase in drag is not equal to the extra drag of the wire. In fact it will be less because, owing to the increased momentum thickness behind the wire, the skin friction will be reduced downstream. Thus allowance for the drag of the wire in profile drag measurements, for example, by subtracting an estimated wire drag is not correct.

## 4. Transition devices

On first thoughts it might appear that the primary function of such devices is to produce disturbances which will cause transition from laminar to turbulent flow. On this basis we could never hope to establish turbulent flow nearer to the leading edge than that position at which disturbances in the laminar boundary layer become amplified. In the case of the flat plate this distance is given by $R_x = 6\times10^4$, corresponding to $R_\theta = 162$. Clearly any transition device has a drag and as a consequence it increases the momentum thickness of the boundary layer flowing over it. The study of Dutton's results in the previous section shows that the drag aspect is

all-important when transition close to the leading edge is desired. It appears from Dutton's results that when $R_\theta < 320$ (the minimum value for a completely turbulent boundary layer) then transition is sudden and close to the wire. If $R_\theta$ is less than this behind the wire, laminar flow may persist to much higher values of $R_\theta$ and transition take place slowly.

On the other hand, provided $R_\theta < 162$, then a transition device producing vigorous disturbances in the right range of frequencies ought to start the transition almost immediately and this should be complete when $R_\theta = 320$. Also for laminar layers with large $R_\theta$ ($> 320$), the production of vigorous disturbances is the important property. Thus any transition device must be considered in terms of both its drag producing and disturbance producing potentialities.

Let us now consider the drag aspect. The drag $D$ per unit span can be related to the increase in momentum thickness $\Delta\theta$ associated with it by

$$D = \rho U^2 \Delta\theta. \tag{16}$$

In this expression we ignore any contribution by the friction in the immediate wake of the device. Now in the case of circular cylinders immersed in thick turbulent boundary layers, Sacks (1956) in an unpublished report found that

$$C_D = D/(\tfrac{1}{2}\rho u_d^2 d) = 0{\cdot}75 \tag{17}$$

over a fairly wide range of $u_\tau d/\nu$. In this relation $u_d$ is the velocity at $y = d$. Hence from equations (16) and (17),

$$\Delta\theta/d = \tfrac{1}{2}C_D(u_d/U)^2,$$

or

$$\frac{U\Delta\theta}{\nu} = \tfrac{1}{2}C_D\left(\frac{u_d}{U}\right)^2 \frac{Ud}{\nu},$$

i.e.

$$\Delta R_\theta = \tfrac{1}{2}C_D(u_d/U)^2 R_d. \tag{18}$$

If $(R_\theta)_L$ is the thickness of the laminar layer in front of the wire and if the minimum $R_\theta$ for a fully developed turbulent layer is 320, then $(R_\theta)_L + R_\theta = 320$, or

$$R_\theta = 320 - (R_\theta)_L. \tag{19}$$

From equations (18) and (19), the Reynolds number based on the wire diameter is found to be

$$R_d = (2/C_D)(U/u_d)^2\{320 - (R_\theta)_L\}. \tag{20}$$

This equation shows how the size of the transition device is determined from momentum considerations. When $(R_\theta)_L$ is small it is clearly necessary to provide this increment $\Delta R_\theta$ in momentum thickness by means of the drag. When $(R_\theta)_L > 320$, then no additional increase in momentum thickness is required, but a transition device is still necessary in order to provide disturbances which will cause a rapid transition.

For a wire placed very close to the leading edge so that $(R_\theta)_L = 0$, $(u_d/U) = 1{\cdot}0$ and, taking $C_D = \frac{3}{4}$, $R_d = U_d/\nu = \frac{8}{3} \times 1 \times 320 = 850$. For a wire placed as in Dutton's experiments so that $(R_\theta)_L = 120$,

we have from laminar boundary layer theory that $u_d/U = 0{\cdot}916$, and hence $R_d = \frac{8}{3} \times (0{\cdot}916)^{-2} \times 200 \doteq 636$. A recommended figure, based on experimental evidence for producing transition at a wire which is placed close to the leading edge, is

$$R_d = 600, \tag{21}$$

which is of the same order. This is further support for the idea of a minimum $R_\theta$ for fully developed turbulent flow.

When the initial $(R_\theta)_L > 320$, the function of the transition device is to produce disturbances which will bring about transition as close to the wire itself as possible and apart from the rough rule equation (21), it is not possible to give further guidance in the selection of the size of the wire.

Circular wires and other bluff obstacles may, as already mentioned, be expected to have a large drag coefficient and to produce considerable disturbances in the form of cast-off eddies. As regards the drag, Sacks (1956) has found the measured drag of circular cylinders resting on the surface in a boundary layer to be given by $C_D = D/(\frac{1}{2}\rho u_d^2 d) = 0{\cdot}75$, which is about $\frac{2}{3}$ of that found for cylinders in a uniform stream. Recent experiments by Arie & Rouse (1956) on normal plates with a splitter plate placed symmetrically behind give $C_D = 1{\cdot}38 - 1{\cdot}4$, which again is about $\frac{2}{3}$ that of a normal plate in a uniform stream. Incidentally, there is in this paper confirmation of the relation between $D$ and $\Delta\theta$ (equation (16)). On the score of drag, the normal plate is to be preferred to the circular cylinder, since, for a given $\Delta R_\theta$, the size of protuberance will be about half that for the circular wire.

As regards the disturbances (when the obstacle is resting on a wall) these do not occur as a regular shedding of eddies in the form of a 'Kármán street'. A separation 'bubble', some 6–8 diameters in length, is formed behind the obstacle. The bubble is composed, in the main, of one large eddy in slow motion, but there is a very disturbed region at the tail of the eddy, which presumably feeds disturbances into the boundary layer.

In the case of the circular wire, when the value of $R_\theta$ just behind the wire is just greater than 162 (the value at which disturbances become amplified), it seems that the disturbances are either of the wrong frequency or are not sufficiently large to bring about immediate transition. In Dutton's paper there is a good example of this where the laminar layer proceeds a considerable distance aft of the wire before transition slowly takes place.

## 5. Choice of transition devices

### *Circular wires*

Circular wires have found favour because of their convenience. They are available in a wide range of sizes and are accurately manufactured. They are fairly easily stuck to the surface, but care is necessary to ensure a uniform spanwise height. From what has been said previously their size is governed both by their ability to thicken the boundary layer and to shed sufficiently strong disturbances.

*Normal plate or strip*

The use of a thin narrow strip has certain attractions aerodynamically. For a given height, it has roughly twice the drag of the circular wire and presumably the disturbances it produces will also be stronger. Thus for a given increment of $\Delta R_\theta$ it need be only half the height of the wire. The fixing would give more trouble than for the wire, as would ensuring spanwise uniformity of height. It might be held in a slot in the surface and accurately milled down to size.

*Slotted or toothed strip*

With this device the drag might possibly be raised above that of the unslotted strip and the teeth would produce strong three-dimensional eddies in the outer part of the boundary layer. This, for fundamental work, may be a disadvantage, as turbulence produced in this region might influence the form of the 'outer' velocity distribution in much the same way as excessive stream turbulence. In the practical problems of suppressing laminar separation by early transition and of delaying turbulent separation by vigorous mixing, they have a definite advantage.

*Sandpaper strip*

This has been used to produce a rapid thickening of the boundary layer and as a transition device. It has disadvantages for fundamental work in that the results with different strips of the same nominal size are not always capable of being repeated and it is difficult to ensure spanwise uniformity. Also Dutton (1955) has found that the outer velocity distribution does not settle to the same distribution as that which occurs when a wire is used. Presumably, this is because eddies are shed from the tips of the largest spikes and these travel down the outer part of the boundary layer.

*Air jets*

These have been used to promote transition but they cannot be regarded as a simple device. There are difficulties in ensuring spanwise uniformity and dangers from over-stimulating the outer part of the boundary layer in fundamental work. Distributed blowing through a strip of uniformly porous material could be effective in thickening a boundary layer.

## 6. Conclusions

In the case of pipe flow there is a lower experimental limit to the Reynolds number for fully developed turbulent flow. From the similarity and close agreement between the curves of $c_f$ *vs* $R_\theta$ for both flat plate and circular pipe, it was anticipated that there would be a lower limit to the Reynolds number $R_\theta$ for fully developed turbulent boundary layer flow on a plate. Rather limited experimental information confirms this and places the lower limit at $R_\theta = 320$.

There is also a lower limit to the Reynolds number for which there is an overlap of the 'inner' and 'outer' laws, the logarithmic region. Estimates of the Reynolds number agree fairly closely with the limiting

Reynolds for turbulent flow in the case of the pipe and flat plate. If this agreement is to be expected generally, then, on this basis of 'no overlap', it would seem that the lower limit of $R_\theta$ for fully developed turbulent flow should decrease in favourable pressure gradients and increase in adverse gradients.

This concept of a minimum Reynolds number for turbulent flow is important when considering the drag of flat plates at medium Reynolds numbers and in considering the size of transition device to be used. For quick transition near the leading edge, the drag of the device and its ability to produce disturbances are both important. An approximate theory has been developed on the basis of a minimum $R_\theta$ for turbulent flow which, in the case of circular wires, leads to a 'wire' Reynolds number in fair agreement with that suggested by experience.

As regards the choice of transition devices, the conclusion is that a normal strip has the least height to achieve transition, but the circular wire is more convenient. When suppression of laminar separation and delay of turbulent separation is important, it is thought that a toothed spoiler or slotted strip should give good results; but the generation of eddies in the outer part of the boundary layer is objectionable in fundamental work, as the 'outer' part of the velocity distribution may be affected.

## References


Arie, M. & Rouse, H. 1956 *J. Fluid Mech.* **1**, 129.

Coles, D. 1954 *Z. angew. Math. Phys.* **5**, 181.

Dutton, R. A. 1955 Ph.D. Dissertation, University of Cambridge.

Dutton, R. A. 1956 The accuracy of the measurement of turbulent skin friction by means of surface pitot tubes and the distribution of skin friction on a flat plate, *Aero. Res. Counc., Lond., Rep. & Mem.* (to be published).

Landweber, L. 1953 *Trans. Soc. Nav. Archit.*, N.Y., **61**, 5.

Nikuradse, J. 1932 *Forschungsh. Ver. dtsch. Ing.* 356.

Nikuradse, J. 1933 *Forschungsh. Ver. dtsch. Ing.* 361.

Ross, D. 1952 Turbulent flow in smooth pipes (a reanalysis of Nikuradse's experiments), Pennsylvania State College, Report Nord. 7958–246.

Sacks, G. M. 1956 M.Sc. Dissertation, University of Cambridge.

# Two-dimensional flow at high subsonic speeds past wedges in channels with parallel walls

By J. B. HELLIWELL

*Department of Mathematics, The Royal College of Science and Technology, Glasgow*

(*Received 6 September* 1957)

SUMMARY

Investigations are made of the plane flow of an inviscid isentropic gas at high subsonic and sonic speeds past a finite wedge of small angle set at zero incidence in a channel with parallel walls. Hodograph methods are applied to the determination of the stream function, which, under the usual transonic approximation, is a solution of Tricomi's equation. In § 2 a brief summary is given of the derivation of the fundamental solution of this equation in terms of Bessel functions.

Two models of the flow pattern are discussed. The model of Cole is examined in § 3 with the sonic line from the shoulder extending completely across the channel at right angles to the wall. In § 4 the Helliwell–Mackie model is taken in which there is a free stream breakaway at sonic velocity from the shoulder of the wedge and the velocity far downstream may be either uniformly subsonic or sonic. Values are obtained for the drag coefficient in both cases and a high degree of both qualitative and quantitative agreement is found. On the basis of the free streamline theory explicit formulae are given relating, in terms of the channel width and upstream Mach number, the drag of the wedge in the channel to that of the same wedge in the free stream.

Attention is drawn in § 5 to certain properties of plane jet flows that may be deduced from the investigation of the flow with free stream breakaway past a wedge in a channel.

## 1. INTRODUCTION

The two-dimensional steady flow of an inviscid isentropic gas at high subsonic and sonic speeds past a finite wedge profile in a free stream has been investigated by many workers, employing various methods based upon the hodograph transformation by which the resulting differential equation for the stream function $\Psi$ is made linear. A common procedure, which will be followed in the present paper, is to use the so-called transonic approximation in which this differential equation becomes the well-known Tricomi equation

$$\frac{\partial^2\Psi}{\partial u^2} + u\frac{\partial^2\Psi}{\partial v^2} = 0,$$

where $U = a^*(1-u/(\gamma+1))$ and $V = a^*v/(\gamma+1)$ are the cartesian components of velocity, the axes being taken parallel and perpendicular to the uniform flow at infinity, $a^*$ is the velocity of the gas when the Mach number is 1 and $\gamma$ is the adiabatic index of the gas. In this approximation $V = 0$ at infinity upstream of the wedge and $u$, $v$ are small. Henceforth the suffix 1 will refer to conditions at infinity upstream. Furthermore, it is known that $\Psi$ is proportional to the $y$-coordinate.

It should be remarked* that recent work by Vincenti, Wagoner & Fisher (1956) shows that even more accuracy may be expected from the transonic approximation if solutions of Tricomi's equation

$$\frac{\partial^2\Psi''}{\partial u^2} + u\frac{\partial^2\Psi''}{\partial v^2} = 0$$

are used in which $u$ is interpreted in a somewhat different manner from that in the present paper, and $\Psi''$ is the stream function $\Psi$ multiplied by a certain other function of $u$.

Guderley & Yoshihara (1950), Cole (1951) and Helliwell & Mackie (1957) have obtained solutions of Tricomi's equation under different hypotheses regarding the flow pattern downstream of the shoulder of the wedge. In each model the flow, accelerating from zero velocity at the tip of the wedge, attains sonic velocity at the shoulder. The solution of Guderley & Yoshihara is of considerable complexity since it includes a determination of the flow field between the sonic line and the limiting characteristic of the Prandtl–Meyer expansion at the shoulder. Less difficult analysis is involved in Cole's solution in which the supersonic region degenerates into a sonic line straight and normal to the direction of the flow far upstream; the flow pattern is investigated upstream of this line. In the work of Helliwell & Mackie the sonic line is specified as a free streamline starting from the shoulder and the velocity is subsonic or sonic throughout the entire field of flow. A comparison of these various models shows a close similarity in the pressure distribution over the wedge nose upstream of the shoulder and hence correspondingly small variations in the estimate of the drag coefficient of the wedge.

An extension of the approach of Guderley & Yoshihara to the situation when the wedge is placed symmetrically in a wind tunnel has been carried out recently by Marschner (1956). However, he only investigates the case of the choked tunnel. In the present paper similar investigations are made of the flow past a wedge at zero incidence in a two-dimensional channel with parallel walls under more general conditions of downstream flow. In §3 the basic model of Cole is used with the sonic line extending from the shoulder of the wedge normally to the channel wall. In §4 the Helliwell–Mackie model is taken with the sonic line appearing as a free streamline from the shoulder. Expressions are obtained for the drag coefficient in each case and the channel walls are found to produce similar

* The author is indebted to a referee for drawing his attention to these results.

effects upon its value, as compared with that in a free stream, for both models of the flow. In the free streamline model, equation (25) taken in conjunction with figure 8 gives correction terms which yield explicitly, in terms of the upstream Mach number and the channel width, the relation between the drag of the wedge in the channel and of the same wedge in a free stream with the same Mach number. When using these results it should be ensured that the channel width has been taken sufficiently large for the flow far downstream not to become supersonic; the limiting relationship between channel width and upstream Mach number for uniform sonic velocity downstream is shown in figure 6.

Finally in § 5 attention is drawn to a result concerning jet flows that may be deduced from the investigations of the flows with free streamlines past the wedge in a channel.

## 2. Flow patterns in a subsonic stream

In the subsequent analysis we shall be concerned with flow nowhere supersonic. In this section we summarize briefly the equations relating the variables which define the flow patterns. These relationships only hold, of course, within the limits of the transonic approximation.

The dimensionless velocity variables $u$ and $v$ have already been defined. The Mach number $M$ is given by $1-M^2=u$. The polar angle $\theta$ of the velocity is related to $v$ by $v=(\gamma+1)\theta$. The local pressure coefficient is defined by

$$c_p=(p-p_1)/(\tfrac{1}{2}\rho_1 U_1^2),$$

where $p$ is the pressure and $\rho$ is the density. It is straightforward to show that, according to the linearized transonic theory,

$$c_p=2(u-u_1)/(\gamma+1). \tag{1}$$

The equation of continuity and the condition for irrotational flow are respectively

$$uu_x-v_y=0, \qquad u_y+v_x=0,$$

which may be inverted to yield the hodograph equations

$$uy_v-x_u=0, \qquad x_v+y_u=0. \tag{2}$$

If $x$ is eliminated these lead to the equation of Tricomi

$$y_{uu}+uy_{vv}=0,$$

in which $u>0$ represents subsonic flow. If we set

$$r=\tfrac{2}{3}u^{3/2}=\tfrac{2}{3}(1-M^2)^{3/2}, \tag{3}$$

then, on solving Tricomi's equation by the method of separation of variables, simple solutions are obtained of the type

$$y=r^{1/3}e^{\pm\lambda v}\mathscr{C}_{\pm 1/3}(\lambda r), \tag{4}$$

where $\mathscr{C}_{\pm 1/3}(\lambda r)$ is any linear combination of Bessel functions of the order indicated and $\lambda$ is any constant, real or imaginary.

### 3. Model 1. Sonic line normal to channel wall

In this section we employ the model of Cole for flow at near sonic velocity past a wedge profile. The basic feature of this model is that the sonic line from the shoulder is straight and normal to the flow at infinity upstream. It is pointed out by Cole in his original paper that, so far as the flow over the front portion of the wedge is concerned, it is a good approximation to replace the actual shape of the sonic line in this way, and hence a good estimate should be obtained for the drag coefficient. At low subsonic Mach numbers the supersonic region is small and so the approximation is close to being correct; for larger Mach numbers, whilst the actual sonic line is by no means straight away from the wedge, yet the upstream influence of the errors in the supersonic region introduced by the approximation is weaker.

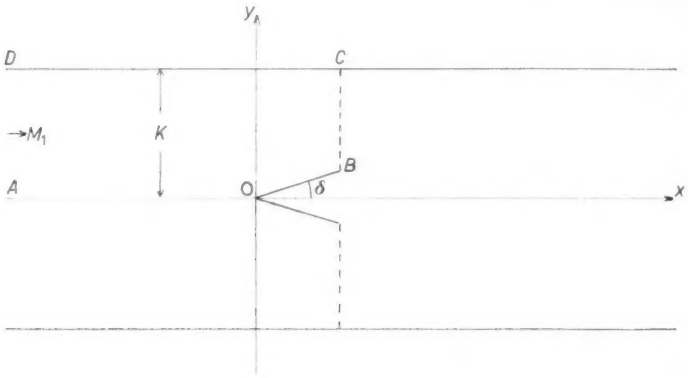


Figure 1. Model 1. Physical plane.

Consider then a wedge of semi-angle $\delta$ placed symmetrically in a channel of semi-width $K$ as shown in figure 1. The $x$-axis is taken as the axis of symmetry and the $y$-axis passes through the tip of the wedge. Hence, we need only consider the flow in the upper half-plane $y \geqslant 0$. The channel is supposed to be blocked by the sonic line which extends normally from the channel wall to the shoulder of the wedge. This is represented by $BC$. $AOB$ is the dividing streamline $\Psi = 0$ on which at $A$, the point at infinity upstream, the velocity is subsonic with Mach number $M_1$, at $O$, the wedge tip, the velocity is zero and along the wedge face $OB$ the flow accelerates to attain sonic velocity at $B$, the shoulder of the wedge. $DC$ is the streamline $\Psi = k$ with associated $y = K$ corresponding to the channel wall along which the flow accelerates steadily from its subsonic upstream velocity to sonic speed at $C$. Along the wedge face $OB$ we also have $\tau = \tau_0 = (\gamma + 1)\delta$.

The boundary value problem may now be established in the hodograph plane, as shown in figure 2. $CD$ is the line $y = K$. $AOB$ is the line $y = 0$. $BC$ is the sonic line $x =$ constant, from which it follows, since $u = 0$, that

$x_r = 0$, whence using (2) we have $y_r = 0$. Two other lines of constant $y$ are shown. Clearly there is a finite singularity at the point $DA$.

The problem is now stated in terms of $r$ and $v$. The condition along $BC$ becomes $r^{1/3}y_r = 0$ when $r = 0$ for all $0 \leqslant v \leqslant v_0$ which is automatically satisfied provided that $y_r$ remains bounded at $r = 0$. The simple solutions (4) show that we must take $y_r = 0$ at $r = 0$ as the condition to fit this requirement. Hence we have

$$\begin{aligned} y &= K, \quad & v &= 0, \quad & 0 \leqslant r < r_1, \\ y &= 0, \quad & v &= 0, \quad & r > r_1, \\ y &= 0, \quad & v &= v_0, \quad & r \geqslant 0, \\ y_r &= 0, \quad & 0 \leqslant v &\leqslant v_0, \quad & r = 0. \end{aligned}$$

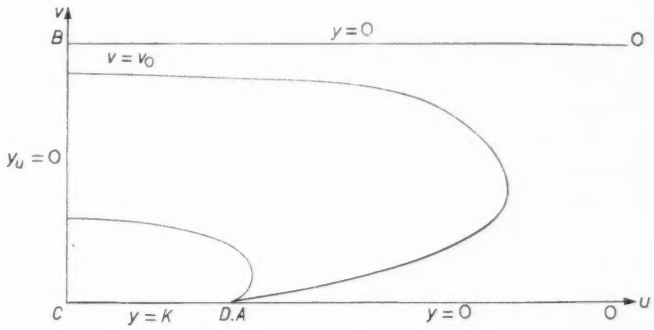


Figure 2. Model 1. Hodograph plane.

The linearization principle, applied to the stagnation condition at the tip $O$, leads to

$$x = 0, \qquad y = 0, \qquad \text{as } r \to \infty.$$

Finally, taking the wedge to be of unit length,

$$x = 1 \quad \text{at } v = v_0, \qquad r = 0.$$

A solution of the problem is obtained by taking a combination of the simple solutions (4) in the form

$$y = \int_0^\infty f(\lambda) r^{1/3} J_{-1/3}(\lambda r) \frac{\sinh \lambda(v_0 - v)}{\sinh \lambda v_0} \, d\lambda. \tag{5}$$

Differentiating under the sign of integration, we have

$$y_r = -\int_0^\infty \lambda f(\lambda) r^{1/3} J_{2/3}(\lambda r) \frac{\sinh \lambda(v_0 - v)}{\sinh \lambda v_0} \, d\lambda.$$

Here $f(\lambda)$ is an arbitrary function of $\lambda$ that is to be determined so that (5) satisfies the first two boundary conditions, since it is immediately apparent

that the last two are satisfied automatically. Hence $f(\lambda)$ is given by

$$\int_0^\infty f(\lambda) r^{1/3} J_{-1/3}(\lambda r)\, d\lambda = K, \qquad 0 \leqslant r < r_1,$$

$$= 0, \qquad r > r_1.$$

An application of the Hankel inversion theorem and a simple integration then yields the result that

$$f(\lambda) = \lambda \int_0^{r_1} K r^{2/3} J_{-1/3}(\lambda r)\, dr = K r_1^{2/3} J_{2/3}(\lambda r_1).$$

Inserting this in (5), the solution of the problem becomes

$$y = K r_1^{2/3} r^{1/3} \int_0^\infty J_{2/3}(\lambda r_1) J_{-1/3}(\lambda r) \frac{\sinh \lambda(v_0 - v)}{\sinh \lambda v_0}\, d\lambda. \tag{6}$$

That this form has a singularity of the correct type at $r = r_1$ may be confirmed in the usual way. It may also be noted that (6) simplifies into Cole's solution for the wedge in the sonic free stream if $K r_1^{4/3}$ tends to a finite constant as $r_1 \to 0$ so that the channel becomes infinitely wide as the upstream Mach number tends to unity. This behaviour of $K$ is confirmed in a later result (equation (9)).

The $x$-coordinate is now obtained from equation (2). After a little analysis we find that

$$x = 1 - (\tfrac{3}{2})^{1/3} K r^{2/3} r_1^{2/3} \int_0^\infty J_{2/3}(\lambda r_1) J_{2/3}(\lambda r) \frac{\cosh \lambda(v_0 - v)}{\sinh \lambda v_0}\, d\lambda. \tag{7}$$

The unit additive constant in this expression arises from the condition that the sonic line on which $r = 0$ is $x = 1$ when the wedge is taken to have unit length.

In the subsequent work a series representation for the $x$-coordinate on the face of the wedge will be useful. To obtain this we set $v = v_0$ in (7) and expand $\operatorname{cosech} \lambda v_0$ in partial fractions by

$$\operatorname{cosech} \lambda v_0 = \frac{1}{\lambda v_0} + 2 \sum_{n=1}^{\infty} \frac{(-1)^n \lambda v_0}{(\lambda v_0)^2 + (n\pi)^2}.$$

After some manipulation and use of standard results concerning integrals involving Bessel functions, we ultimately derive the series

$$x = 1 - \frac{(\tfrac{3}{2})^{1/3} K r^{2/3} r_1^{2/3}}{v_0} \left\{ \frac{3}{4} \left( \frac{r}{r_1} \right)^{2/3} + 2 \sum_{n=1}^{\infty} (-1)^n K_{2/3}\left( \frac{n\pi r_1}{v_0} \right) I_{2/3}\left( \frac{n\pi r}{v_0} \right) \right\}, \qquad 0 < r \leqslant r_1,$$

$$= 1 - \frac{(\tfrac{3}{2})^{1/3} K r^{2/3} r_1^{2/3}}{v_0} \left\{ \frac{3}{4} \left( \frac{r_1}{r} \right)^{2/3} + 2 \sum_{n=1}^{\infty} (-1)^n I_{2/3}\left( \frac{n\pi r_1}{v_0} \right) K_{2/3}\left( \frac{n\pi r}{v_0} \right) \right\}, \qquad r \geqslant r_1. \tag{8}$$

Because of the asymptotic behaviour of $K_\nu(z)$ for large $z$, the stagnation condition, $x = 0$ as $r \to \infty$, applied to the latter representation gives

$$Kr_1^{4/3} = 2(\tfrac{2}{3})^{4/3} v_0. \tag{9}$$

Writing $r_1$ in terms of $M_1$ through (3) and replacing $v_0$ by $(\gamma+1)\delta$, we thus have the result.

$$\{\delta(\gamma+1)\}^{1/3} K = 2[(1-M_1^2)\{\delta(\gamma+1)\}^{-2/3}]^{-2}.$$

This is the relation between the semi-channel width and the upstream Mach number that, on account of continuity of the flow, holds for the present model, if the channel is of such a width that sonic velocity is attained everywhere across a section through the wedge shoulder.

The drag coefficient is defined in the customary way as

$$C_D = D/(\tfrac{1}{2}\rho_1 U_1^2),$$

where $D$ is the drag on the upper face of the wedge and, according to the linearized theory, is given by

$$D = \delta \int C_p \, dx,$$

the integrations being taken over the length of the wedge. Introducing the relations (1) and (3) it can then be shown that

$$C_D = -2\frac{(\frac{3}{2})^{2/3}\delta}{\gamma+1}\left\{\int_0^\infty r^{2/3}\left(\frac{\partial x}{\partial r}\right)_{v=v_0} dr + r_1^{2/3}\right\}. \tag{10}$$

The series representations (8) may now be substituted into (10) and after considerable algebra, in which (9) is used to replace $K$ in terms of $r_1$, an expression for $C_D$ in the form of an infinite series is obtained as

$$\frac{(\gamma+1)^{1/3}}{\delta^{5/3}} C_D = \frac{16}{3^{2/3}\Gamma(\frac{2}{3})\pi^{4/3}}\left(\frac{3r_1}{2v_0}\right)^{-2/3} \sum_{n=1}^{\infty}\left\{\frac{(-1)^n}{n^{4/3}} K_{2/3}\left(\frac{n\pi r_1}{v_0}\right)\right\} + \\ + \frac{4\zeta(2)}{\pi^2}\left(\frac{3r_1}{2v_0}\right)^{-4/3} - \frac{2}{3}\left(\frac{3r_1}{2v_0}\right)^{2/3},$$

where $\zeta(z)$ is the zeta function of Riemann. For values of the upstream Mach number $M_1$ little different from unity, a series expansion in powers of $(1-M_1^2)$ may be obtained for $C_D$ in which the leading terms are

$$C_D = C_D^* - \frac{2\delta}{\gamma+1}(1-M_1^2) + O(1-M_1^2)^3, \tag{11}$$

where $C_D^*$ is the finite value of the drag coefficient in Cole's model for the wedge in the sonic free stream. As $M_1$ decreases from unity, the value of $C_D$ for a wedge in a channel diverges from the corresponding value of $C_D$ for an identical wedge in a free stream with the same upstream Mach number, but reference to equation (72) of Cole's paper shows that the difference is of the order $(1-M_1^2)^3$. A specific comparison is shown graphically in figure 3.

### 4. Model 2. Sonic line a section of a free streamline

We now turn to investigate the flow pattern past a wedge profile symmetrically placed in a channel, employing the model incorporating a free streamline proposed by Helliwell & Mackie. For the wedge in a channel the following general properties of the flow are laid down. The dividing streamline $\Psi = 0$ is straight from infinity upstream, where the velocity is subsonic with Mach number $M_1$, to the tip of the wedge where there is a stagnation point. The upper branch of $\Psi = 0$ then follows the upper face of the wedge, the gas accelerating to attain sonic velocity at the shoulder at which point the

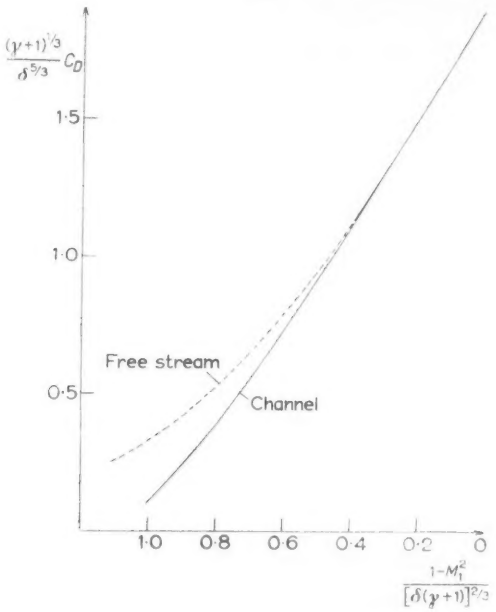


Figure 3. Model 1. Drag coefficient.

streamline breaks away from the wedge, retaining sonic velocity until it again becomes parallel to the channel walls. Thereafter it remains straight, the velocity of the gas along it meantime decelerating from sonic speed to some high subsonic velocity with Mach number $M_2$ ($> M_1$). The critical case of a channel with uniform sonic velocity everywhere in the flow field far downstream is merely a special case of the above with $M_2 = 1$. More generally, the model describes a flow pattern with uniform subsonic velocity upstream, a local sonic region in the neighbourhood of the shoulder of the wedge and ultimately a uniform subsonic velocity downstream in addition to the wake, regarding which certain information may be deduced. From a theoretical point of view there is the added advantage that throughout the whole flow field the velocity is nowhere supersonic and hence limit lines

cannot occur to render invalid the transformation back to the physical plane.

The pattern described in the preceding paragraph is shown in figure 4. The semi-channel and semi-wake widths are $K$ and $H$ respectively. The upstream portion of the dividing streamline $\Psi = 0$ is taken as the line of the $x$-axis with origin at the tip of the wedge. The channel walls are thus the straight lines $y = \pm K$. Because of symmetry only the flow in the upper

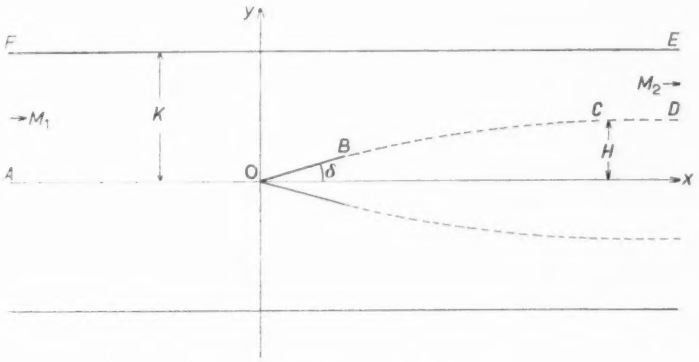


Figure 4. Model 2. Physical plane.

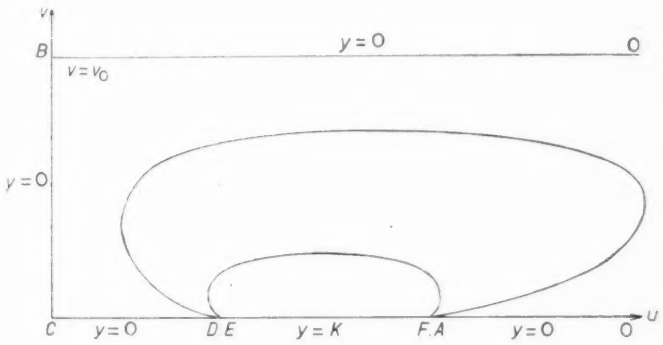


Figure 5. Model 2. Hodograph plane.

half-plane $y \geqslant 0$ need be considered. $AOBCD$, then, is the dividing streamline. At the point $A$ far upstream the Mach number is $M_1$ with associated $r = r_1$; at $O$ the velocity is zero. Along $OB$, the wedge face, the component $v = v_0 = (\gamma+1)\delta$, where $\delta$ is the semi-angle of the wedge; the gas accelerates to sonic velocity at $B$ and retains this speed along the section $BC$. At $C$ the velocity is again parallel to the $x$-axis and along $CD$

the gas decelerates until at $D$ far downstream the Mach number is $M_2$ with associated $r = r_2$ ($< r_1$). $FE$ is the upper channel wall along which the gas velocity varies from Mach number $M_1$ at $F$ to $M_2$ at $E$.

The boundary value problem is now set up in the hodograph plane which is shown in figure 5. It is recalled that, to the order of the transonic approximation, $\Psi$ is proportional to $y$. $AOBCD$ is the line $y = 0$, $EF$ is the line $y = K$, and two other lines of constant $y$ are shown. Finite singularities occur at the two pairs of coincident points $AF$ and $DE$, corresponding to upstream and downstream conditions, respectively. The remaining boundary conditions, in terms of $r$ and $v$, are

$$\begin{aligned}
&y = 0, \qquad v = 0, \qquad && 0 \leqslant r < r_2,\\
&y = K, \qquad v = 0, \qquad && r_2 < r < r_1,\\
&y = 0, \qquad v = 0, \qquad && r > r_1,\\
&y = 0, \qquad v = v_0, \qquad && r \geqslant 0,\\
&y = 0, \qquad 0 \leqslant v \leqslant v_0, \qquad && r = 0.
\end{aligned}$$

The stagnation condition at the tip of the wedge is, according to the transonic approximation,

$$x = 0, \qquad y = 0 \quad \text{as } r \to \infty.$$

For a wedge of unit length, we also have the further condition

$$x = 1, \qquad v = v_0 \quad \text{at } r = 0.$$

The solution of the present problem may be derived from a combination of the simple solutions (4) of the type

$$y = \int_0^\infty g(\lambda) r^{1/3} J_{1/3}(\lambda r)\, \frac{\sinh \lambda(v_0 - v)}{\sinh \lambda v_0}\, d\lambda.$$

Whereas this automatically satisfies the last two boundary conditions for any $g(\lambda)$, it only satisfies them all if $g(\lambda)$ is a solution of the equations

$$\begin{aligned}
\int_0^\infty g(\lambda) r^{1/3} J_{1/3}(\lambda r)\, d\lambda &= 0, \qquad && 0 \leqslant r < r_2,\\
&= K, \qquad && r_2 < r < r_1,\\
&= 0, \qquad && r > r_1.
\end{aligned}$$

The function $g(\lambda)$ may be determined by an application of the Hankel inversion theorem and we obtain

$$g(\lambda) = K\{r_2^{2/3} J_{-2/3}(\lambda r_2) - r_1^{2/3} J_{-2/3}(\lambda r_1)\}.$$

Hence the formal solution of the problem is

$$y = K r^{1/3} \int_0^\infty \{r_2^{2/3} J_{-2/3}(\lambda r_2) - r_1^{2/3} J_{-2/3}(\lambda r_1)\} J_{1/3}(\lambda r)\, \frac{\sinh \lambda(v_0 - v)}{\sinh \lambda v_0}\, d\lambda. \quad (12)$$

This has singularities at $r = r_1$ and $r = r_2$ when $v = 0$. That they are of the correct type may easily be seen by an investigation of the form of $y$ in the neighbourhood of $r = r_1$, $r = r_2$. We also note that if we let $r_2 \to r_1$ and $K \to \infty$ simultaneously, we derive the special case of the flow in a free stream. In fact, by carrying through this limiting process on $y$ in equation (12) using the relation (14) between $K$, $r_1$ and $r_2$, we find that we recover the solution for flow past a wedge of unit length in a free stream given by equation (3) of the paper of Helliwell & Mackie.

The $x$-coordinate of the solution is next determined. A direct substitution from (12) into (2) and the resulting integrations yield

$$x = (\tfrac{3}{2})^{1/3} K r^{2/3} \int_0^\infty \{r_2^{2/3} J_{-2/3}(\lambda r_2) - r_1^{2/3} J_{-2/3}(\lambda r_1)\} J_{-2/3}(\lambda r) \frac{\cosh \lambda(v_0 - v)}{\sinh \lambda v_0} \, d\lambda. \tag{13}$$

The constant which appears as a result of the integrations may be shown to be zero as a consequence of the stagnation condition at the tip of the wedge.

The wedge will be taken to be of unit length and we have therefore $x = 1$ at the shoulder where $v = v_0$ as $r \to \infty$. Thus, from (13), we find

$$1 = \frac{(\frac{3}{2})^{1/3} 2^{2/3} K}{\Gamma(\frac{1}{3})} \int_0^\infty \frac{\lambda^{-2/3}}{\sinh \lambda v_0} \{r_2^{2/3} J_{-2/3}(\lambda r_2) - r_1^{2/3} J_{-2/3}(\lambda r_1)\} \, d\lambda.$$

On expanding the Bessel functions, setting $\lambda v_0 = t$, and interchanging orders of integration and summation, it follows that

$$1 = \frac{(\frac{3}{2})^{1/3} K}{\Gamma(\frac{1}{3}) v_0} \sum_{n=1}^\infty \frac{(-1)^n}{n! \Gamma(n + \frac{1}{3})} \left\{ r_2^{1/3} \left( \frac{r_2}{2v_0} \right)^{2n - 4/3} - r_1^{1/3} \left( \frac{r_1}{2v_0} \right)^{2n - 4/3} \right\} \int_0^\infty \frac{t^{2n - 4/3} \, dt}{\sinh t}.$$

This is simplified by the use of a well-known integral representation of the Riemann zeta function $\zeta(z)$, giving

$$1 = \frac{2(3)^{1/3} K v_0^{1/3}}{\sqrt{\pi} \Gamma(\frac{1}{3})} \sum_{n=1}^\infty \frac{(-1)^{n+1}}{n!} \Gamma(n - \tfrac{1}{6})(2^{2n - 1/3} - 1) \zeta(2n - \tfrac{1}{3}) \times \\ \times \left\{ \left( \frac{r_1}{2v_0} \right)^{2n} - \left( \frac{r_2}{2v_0} \right)^{2n} \right\}. \tag{14}$$

This equation determines the relationship between upstream and downstream Mach numbers $M_1$ and $M_2$ for a wedge of unit length placed in a channel of semi-width $K$, where

$$r_1 = \tfrac{2}{3}(1 - M_1^2)^{3/2}, \qquad r_2 = \tfrac{2}{3}(1 - M_2^2)^{3/2}. \tag{15}$$

Figure 6 shows this result graphically in the important and limiting case of a channel when the velocity is uniformly sonic downstream ($r_2 = 0$). For purposes of comparison the corresponding result (9) for the model of the previous section is also shown.

In the subsequent work series representations for the coordinates will be required. We shall obtain these by means of intermediate contour

integral forms. First let us investigate the $y$ coordinate. Setting $\lambda v_0 = t$, the result (12) becomes

$$y = \frac{K\pi r^{1/3}}{v_0} \int_0^\infty \left\{ r_2^{2/3} J_{-2/3}\left(\frac{t\pi r_2}{v_0}\right) - r_1^{2/3} J_{-2/3}\left(\frac{t\pi r_1}{v_0}\right) \right\} \times$$
$$\times J_{1/3}\left(\frac{t\pi r}{v_0}\right) \frac{\sinh \pi t(1 - v/v_0)}{\sinh \pi t}\, dt. \quad (16)$$

There are three distinct cases of this integral to be discussed, depending upon the value of $r$.

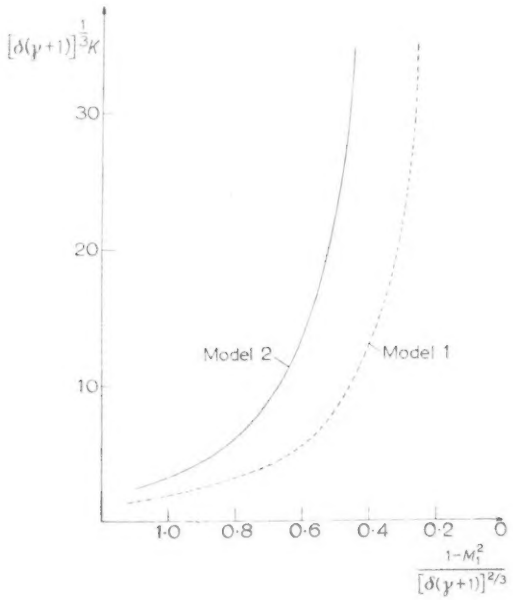


Figure 6. Upstream Mach number and critical channel width.

For $0 \leqslant r < r_2 < r_1$, consider the contour integral

$$W = -\frac{iKr^{1/3}}{v_0} \int_C \left\{ r_2^{2/3} K_{2/3}\left(\frac{\nu\pi r_2}{v_0}\right) - r_1^{2/3} K_{2/3}\left(\frac{\nu\pi r_1}{v_0}\right) \right\} I_{1/3}\left(\frac{\nu\pi r}{v_0}\right) \frac{e^{i\nu\pi(1-v/v_0)}}{\sin \nu\pi}\, d\nu,$$

where $C$ is the contour in the complex $\nu$ plane going from $-i\infty$ to $+i\infty$, indented at the origin, and closed by the right-hand infinite semi-circle. The integrand has a branch point at the origin but is single-valued in the whole plane cut along the negative real axis. The contributions to $W$ from the infinite semi-circle and origin indentation can be both shown to be zero by using the asymptotic and power series expansions of $K_{2/3}(z)$ and $I_{1/3}(z)$ in the respective calculations. If now we write $W = W_1 + W_2$,

where $W_1$ is the part of the integral along the imaginary axis from 0 to $i\infty$, and set $\nu = te^{i\pi/2}$, $\nu = te^{-i\pi/2}$ in $W_1$ and $W_2$, respectively, we find after some manipulation that

$$y = \mathscr{I} W.$$

Since the poles of the integrand of $W$ occur at the integer values of $\nu$, the residue theorem of Cauchy applied to $\mathscr{I}W$ will yield a series form for $y$. We obtain

$$y = \frac{2Kr^{1/3}}{v_0} \sum_{n=1}^{\infty} \left\{ r_2^{2/3} K_{2/3}\left(\frac{n\pi r_2}{v_0}\right) - r_1^{2/3} K_{2/3}\left(\frac{n\pi r_1}{v_0}\right) \right\} I_{1/3}\left(\frac{n\pi r}{v_0}\right) \sin\left(\frac{n\pi v}{v_0}\right). \quad (17)$$

In the case when $r > r_1 > r_2$, considerations similar to the above may be used to show that

$$y = \mathscr{I} \frac{iKr^{1/3}}{v_0} \int_C \left\{ r_2^{2/3} I_{-2/3}\left(\frac{\nu\pi r_2}{v_0}\right) - r_1^{2/3} I_{-2/3}\left(\frac{\nu\pi r_1}{v_0}\right) \right\} K_{1/3}\left(\frac{\nu\pi r}{v_0}\right) \frac{e^{i\nu\pi(1-v/v_0)}}{\sin \nu\pi}\, d\nu,$$

where $C$ is the same contour as before. The Cauchy residue theorem applied to this expression gives

$$y = -\frac{2Kr^{1/3}}{v_0} \sum_{n=1}^{\infty} \left\{ r_2^{2/3} I_{-2/3}\left(\frac{n\pi r_2}{v_0}\right) - r_1^{2/3} I_{-2/3}\left(\frac{n\pi r_1}{v_0}\right) \right\} K_{1/3}\left(\frac{n\pi r}{v_0}\right) \sin\left(\frac{n\pi v}{v_0}\right). \quad (18)$$

Over the range $r_2 < r < r_1$, the two forms of $y$ already obtained suggest that we consider

$$W' = \frac{iKr^{1/3}}{v_0} \int_C \left\{ r_2^{2/3} I_{-2/3}\left(\frac{\nu\pi r_2}{v_0}\right) K_{1/3}\left(\frac{\nu\pi r}{v_0}\right) + r_1^{2/3} K_{2/3}\left(\frac{\nu\pi r_1}{v_0}\right) I_{1/3}\left(\frac{\nu\pi r}{v_0}\right) \right\} \times \frac{e^{i\nu\pi(1-v/v_0)}}{\sin \nu\pi}\, d\nu,$$

with $C$ the contour described previously. Once again, the contribution from the infinite semi-circle is zero, but we now find that the imaginary part of the contribution from the origin indentation is

$$-K(1-v/v_0).$$

Hence, proceeding as before, we discover that

$$y = \mathscr{I} W' + K(1-v/v_0),$$

and an application of the residue theorem of Cauchy yields

$$y = -\frac{2Kr^{1/3}}{v_0} \sum_{n=1}^{\infty} \left\{ r_2^{2/3} I_{-2/3}\left(\frac{n\pi r_2}{v_0}\right) K_{1/3}\left(\frac{n\pi r}{v_0}\right) + r_1^{2/3} K_{2/3}\left(\frac{n\pi r_1}{v_0}\right) I_{1/3}\left(\frac{n\pi r}{v_0}\right) \right\} \sin\left(\frac{n\pi v}{v_0}\right) + K\left(1 - \frac{v}{v_0}\right). \quad (19)$$

The required series representations for $y$ are given by equations (17), (18), (19). The discontinuities when $v \neq 0$ at $r = r_1$, $r = r_2$ are only

apparent; continuity may be shown to exist at these points by use of a result concerning Bessel functions (Erdélyi 1953) and the Fourier series representation

$$1-\frac{v}{v_0}=\sum_{n=1}^{\infty}\frac{2}{n\pi}\sin\frac{n\pi v}{v_0}, \qquad v\neq 0.$$

Of course, the value of $y$ is still undefined at $r=r_1$, $r=r_2$ when $v=0$.

Series representations for $x$ may now be obtained by the use of equations (2). The constants of integration are determined by the stagnation condition at the tip of the wedge and by the necessary continuity of the $x$-coordinate everywhere. The three forms corresponding to equations (17), (18) and (19) are the following. For the range $0\leqslant r<r_2<r_1$,

$$x=\frac{2(\frac{3}{2})^{1/3}Kr^{2/3}}{v_0}\sum_{n=1}^{\infty}\left\{r_2^{2/3}K_{2/3}\left(\frac{n\pi r_2}{v_0}\right)-r_1^{2/3}K_{2/3}\left(\frac{n\pi r_1}{v_0}\right)\right\}\times$$

$$\times I_{-2/3}\left(\frac{n\pi r}{v_0}\right)\cos\left(\frac{n\pi v}{v_0}\right)+\frac{(\frac{3}{2})^{4/3}K}{2v_0}(r_1^{4/3}-r_2^{4/3}); \quad (20)$$

for $r>r_1>r_2$,

$$x=\frac{2(\frac{3}{2})^{1/3}Kr^{2/3}}{v_0}\sum_{n=1}^{\infty}\left\{r_2^{2/3}I_{-2/3}\left(\frac{n\pi r_2}{v_0}\right)-\right.$$

$$\left.-r_1^{2/3}I_{-2/3}\left(\frac{n\pi r_1}{v_0}\right)\right\}K_{2/3}\left(\frac{n\pi r}{v_0}\right)\cos\left(\frac{n\pi v}{v_0}\right); \quad (21)$$

and for the range $r_2<r<r_1$,

$$x=\frac{2(\frac{3}{2})^{1/3}Kr^{2/3}}{v_0}\sum_{n=1}^{\infty}\left\{r_2^{2/3}I_{-2/3}\left(\frac{n\pi r_2}{v_0}\right)K_{2/3}\left(\frac{n\pi r}{v_0}\right)-\right.$$

$$\left.-r_1^{2/3}K_{2/3}\left(\frac{n\pi r_1}{v_0}\right)I_{-2/3}\left(\frac{n\pi r}{v_0}\right)\right\}\cos\left(\frac{n\pi v}{v_0}\right)+\frac{(\frac{3}{2})^{4/3}K}{2v_0}(r_1^{4/3}-r_2^{4/3}). \quad (22)$$

We are now in a position to calculate the drag coefficient, $C_D$, which, as indicated in the previous section, is given to the order of the transonic approximation by equation (10). The evaluation is quite straightforward. The series representations (20), (21) and (22), with $v=v_0$, are inserted into the infinite integral and orders of summation and integration are interchanged. The resulting integrals involving Bessel functions are all standard types and after their evaluation a little algebra leads to the expression,

$$C_D=\tfrac{3}{2}K\delta^2\left\{\left(\frac{r_1}{v_0}\right)^2-\left(\frac{r_2}{v_0}\right)^2\right\}-\frac{2(\frac{3}{2})^{2/3}\delta^{5/3}(r_1/v_0)^{2/3}}{(\gamma+1)^{1/3}}. \quad (23)$$

For a wedge of unit length, we express $K$ in terms of $r_1$ and $r_2$ by equation (14)

and thereby obtain

$$\frac{(\gamma+1)^{1/3}C_D}{\delta^{5/3}} = -2\left(\frac{3r_1}{2r_0}\right)^{2/3} + \frac{\sqrt{\pi}\Gamma(\frac{1}{3})3^{-4/3}\{(3r_1/2v_0)^2-(3r_2/2v_0)^2\}}{\sum_{n=1}^{\infty}[(-1)^{n+1}/n!]3^{-2n}\Gamma(n-\frac{1}{6})(2^{2n-1/3}-1)\zeta(2n-\frac{1}{3})\{(3r_1/2v_0)^{2n}-(3r_2/2v_0)^{2n}\}}.$$

This may be written in terms of the upstream and downstream Mach numbers $M_1$ and $M_2$. For flow sufficiently near sonic this may be expanded as a Taylor series in powers of $(1-M_1^2)$ and $(1-M_2^2)$. The leading terms of such an expansion are

$$C_D = C_D^{**} - \frac{2\delta}{\gamma+1}(1-M_1^2) + O\{(1-M_1^2)^3,\ (1-M_2^2)^3\}, \tag{24}$$

where $C_D^{**}$ is the finite value of the drag coefficient of this model for the flow past the wedge in a sonic free stream. The result (24) should be compared

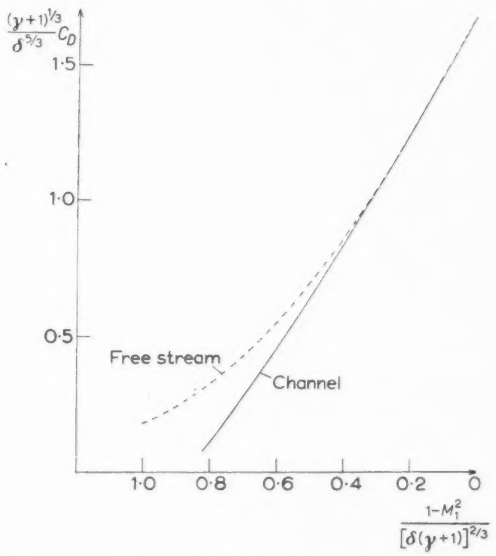


Figure 7. Model 2. Drag coefficient (critical channel).

with that for the previous model as given in equation (11). The special case of the drag coefficient for a wedge in a critical channel with variable subsonic upstream velocity and sonic velocity along the entire free streamline and uniformly far downstream is shown in figure 7. This should be compared with figure 3 for the corresponding case of the previous section. The effect of the channel walls is seen to be very similar for the two models of the flow.

A more useful form for the drag coefficient in the general case is, however, obtained if the asymptotic expansion of equation (23) is taken for large $K$.

The drag coefficient is then written as a series expansion in ascending powers of $K^{-1}$ where the relation (14) has been previously used to express $r_2$ in terms of $K$ and $r_1$. After considerable algebra we obtain an expansion of the type

$$\frac{(\gamma+1)^{1/3}}{\delta^{5/3}}\{C_{D_{\text{free}}}-C_{D_{\text{channel}}}\}=\frac{a(M_1)}{\bar{K}}+\frac{b(M_1)}{\bar{K}^2}+\frac{c(M_1)}{\bar{K}^3}+\ldots, \quad (25)$$

where $\bar{K}=K(1-M_1^2)^3/[\delta(\gamma+1)]^{5/3}$. The coefficients $a, b, c, \ldots$ are extremely complicated and inelegant functions of $M_1$ which increase slowly as $M_1$ decreases from unity. The first two are shown graphically in figure 8. $C_{D_{\text{free}}}$ and $C_{D_{\text{channel}}}$ denote the drag coefficient of the same wedge in a free stream and channel, respectively, with the same upstream gas velocity. The expression (25) is thus essentially one yielding correction terms to be

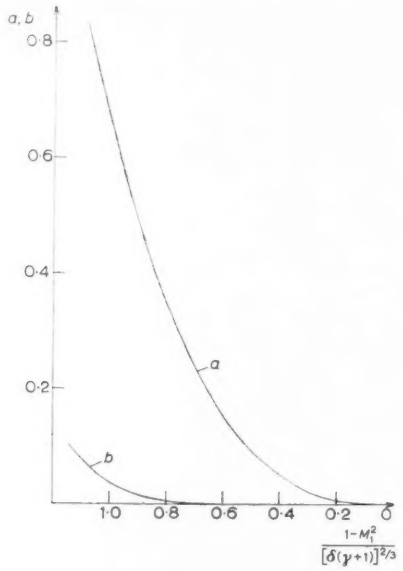


Figure 8. Model 2. Drag correction coefficients.

applied to the drag coefficient in the channel in order to obtain the corresponding value for the drag in the free stream. It is remarked that the correction to be applied is, in general, small within the range of validity of the present theory which does not apply unless the channel is wider than the length of the wedge by a factor of the order of 10. That this is so may be noted from the fact that, for a given value of $M_1$, the value of $K$ yielded by figure 6 is that corresponding to uniform sonic velocity across the channel far downstream. In general, however, the velocity will be subsonic and considerations of continuity of the flow show that the value of $K$ thus determined is a lower bound.

The location of the end of the sonic line is the point $C$ in figure 4. Here the wake becomes parallel to the channel walls. The $x$-coordinate of this point is obtained by setting $r = 0$ and $v = 0$ in (20) and has the value

$$x_C = \frac{2(\frac{3}{2})^{1/3}K}{\Gamma(\frac{1}{3})v_0} \sum_{n=1}^{\infty} \left(\frac{n\pi}{2v_0}\right)^{-2/3} \left\{ r_2^{2/3} K_{2/3}\left(\frac{n\pi r_2}{v_0}\right) - r_1^{2/3} K_{2/3}\left(\frac{n\pi r_1}{v_0}\right) \right\} + \\ + \frac{(\frac{3}{2})^{4/3}K}{2v_0} (r_1^{4/3} - r_2^{4/3}). \quad (26)$$

This is finite for all $r_1$, $r_2 \neq 0$ so that the wake becomes parallel at a finite distance downstream of the wedge, as was laid down in the flow pattern for this model. It is of considerable interest to note that this result remains true when $r_2 = 0$, so that uniformly sonic conditions in a parallel flow would be attained at a finite distance downstream in the case when the channel width is critical.

Finally, the semi-width of the wake can be calculated. From figure 4, for a wedge of unit length, we have

$$H - \delta = \int_{y_B}^{y_C} dy = \int_{x_B}^{x_C} \theta \, dx,$$

where $\theta$ is here the slope of the sonic line. Integration by parts leads to

$$(\gamma + 1)H = \int_0^{v_0} x \, dv,$$

where $x$ is to be taken along $BC$. The appropriate series representation of $x$ to be inserted in this integral is the limiting form of (20) as $r \to 0$. Thus, after the integration is performed, we find

$$H = \frac{(\frac{3}{2})^{4/3}K}{2(\gamma + 1)} (r_1^{4/3} - r_2^{4/3}),$$

which by means of equations (15) may be written

$$H = K \frac{(M_2^2 - M_1^2)(2 - M_1^2 - M_2^2)}{2(\gamma + 1)}. \quad (27)$$

It should be recalled that this value is not independent of $\delta$, as appears at first sight, since $K$, $M_1$ and $M_2$, are interrelated with $\delta$ through equations (14) and (15).

## 5. Jet flows

It is apparent that if we redraw figure 4 with $FE$ as axis of symmetry and take the flow region bounded by the dividing streamline $AOBCD$ and its image $A'O'B'C'D'$ in $FE$ we obtain figure 9. The physical problem portrayed is then that of a two-dimensional jet flowing from a convergent nozzle through a region of constant pressure into a duct with parallel walls. Far upstream in the channel of semi-width $K$, the Mach number of the flow is $M_1$. At the orifice $BB'$ sonic velocity is attained at the boundary,

and the gas issues as a jet with free boundaries $BC$, $B'C'$ along which sonic velocity is maintained. At $CC'$ the gas enters a duct with straight, parallel walls in which the flow decelerates to a subsonic velocity with Mach number $M_2$ ($> M_1$).

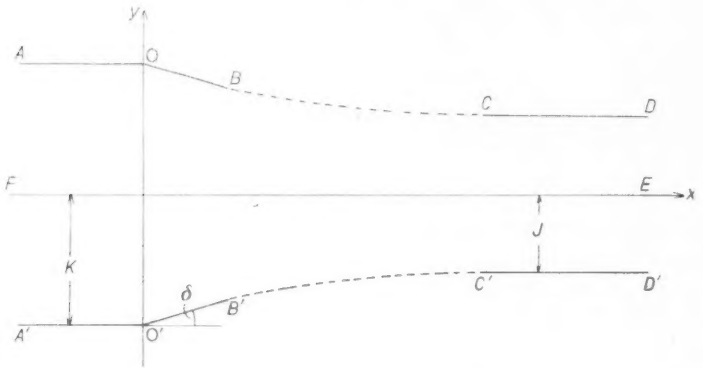


Figure 9. Physical plane for jet flow.

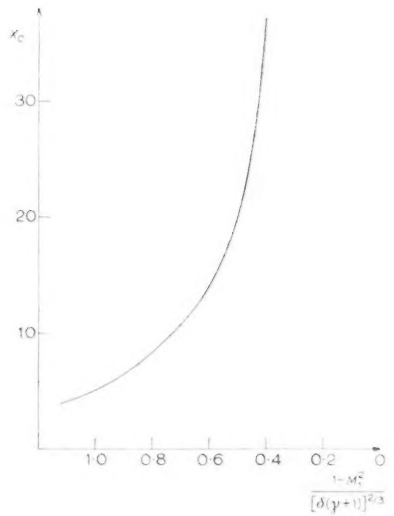


Figure 10. Downstream position of parallel sonic jet.

The case when $M_2 = 1$ is of particular interest since then the duct may be dispensed with and we have the problem of a two-dimensional jet flowing through a convergent nozzle into a region of constant pressure which has the value associated with the sonic velocity. The flow in the jet

has a uniform sonic velocity far downstream, where the ultimate semi-width of the jet is $J\ (=K-H)$. The results of the previous section in the special case when $r_2=0$ are thus appropriate for the solution of this problem. We take $FE$ as $x$-axis and $OO'$ as $y$-axis. Then, as has already been remarked, the jet becomes parallel at the point $C$ located a finite distance downstream of the orifice. For a nozzle of unit length the value of $x_C$, the $x$-coordinate of $C$, is given by equation (26) with $r_2=0$. We recall that the relationship between the channel semi-width $K$ and upstream mach number $M_1$ is shown graphically in figure 6. The variation of $x_C$ with $M_1$ is shown in figure 10. Finally, it follows from equation (27) that the value of $J$, the semi-width of the jet, is given by

$$\frac{J}{K}=1-\frac{(1-M_1^2)^2}{2(\gamma+1)}.$$

As remarked at the conclusion of the previous section, it should be noted that this result is not independent of $\delta$ since $K$ and $M_1$ are interrelated with this angle.

This research has been sponsored by the Air Research and Development Command U.S. Air Force under Contract AF 61(514)-1170, through the European Office A.R.D.C.

## References

Cole, J. D. 1951 *J. Math. Phys.* **30,** 79.

Erdélyi, A. (Ed.) 1953 *Higher Transcendental Functions*, Vol. 2. New York: McGraw-Hill.

Guderley, G. & Yoshihara, H. 1950 *J. Aero. Sci.* **17,** 723.

Helliwell, J. B. & Mackie, A. G. 1957 *J. Fluid Mech.* **3,** 93.

Marschner, B. W. 1956 *J. Aero. Sci.* **23,** 368.

Vincenti, W. G., Wagoner, C. B. & Fisher, N. H. 1956 *Nat. Adv. Comm. Aero., Wash., Tech. Note* no. 3723.

# Slow motion of a paraboloid of revolution in a rotating fluid

By L. V. K. VISWANADHA SARMA
*Indian Institute of Technology, Kharagpur*

(*Received* 7 *August* 1957)

SUMMARY

The slow uniform motion, after an impulsive start from relative rest, of a paraboloid of revolution along the axis of a rotating fluid is investigated by using a perturbation method. The principal purpose of the note is to illustrate the mechanism by which the fluid is not subjected to any substantial radial displacement, which is a direct consequence of the requirement that the circulation round material circuits should be constant when the perturbation velocities due to the motion of the paraboloid remain small. It appears that the mechanism is an oscillatory one in which the distance between any fluid particle and the axis of rotation oscillates sinusoidally in time with small amplitude. As time progresses, the amplitude of the oscillation decays to zero everywhere except on the paraboloid. The ultimate motion is then a rigid body rotation everywhere except on the paraboloid and the axis of rotation, where the perturbation velocities continue to oscillate indefinitely with small amplitude.

## 1. INTRODUCTION

The motion of bodies in a rotating fluid has been a subject for a series of investigations in recent years. The perturbation caused by the motion of a body in an inviscid fluid exhibits different characteristics according as the fluid is at rest at infinity or is rotating about an axis there. Thus if the fluid is at rest at infinity, the flow is everywhere irrotational and dependent only on the instantaneous velocity of the body. But if the fluid is rotating about an axis, the perturbation in the fluid velocity depends not only on the instantaneous velocity of the body but also on its past history and is in general neither steady nor irrotational; and even in cases where a steady solution of the governing equation can be found, there is no guarantee that the flow can be set up by starting the body from rest relative to the rotating system. For these reasons it is necessary to consider an initial-value problem while dealing with this type of fluid motion.

When the body moves slowly it has been customary to use a small perturbation theory. Using this method Stewartson (1952, 1953) has investigated the slow uniform motion, after an impulsive start from relative rest, of a sphere and an ellipsoid along the axis of a rotating liquid. In both

these cases he found that ultimately the fluid inside the circumscribing cylinder $C$ with its generators parallel to the axis of rotation is pushed along in front of the body as if it were solid, while outside the cylinder there is a shearing motion parallel to the axis of rotation. There is also a swirling motion about the axis inside the cylinder $C$. The ultimate velocity distribution in the fluid is in general steady and two-dimensional (in the sense that the motion is the same in all planes perpendicular to the axis of rotation) everywhere except on the body and on its axis, where it oscillates finitely. In fact the linearized equations show that every slow and steady motion must also be two-dimensional.

There is, however, an *a priori* difficulty with any theory which supposes that the perturbation remains small. Since the circulation round any material circular circuit concentric with the axis must remain constant, the radius of such a circuit must always be nearly equal to its initial radius. At first sight this restriction on the total strain of the fluid seems unlikely to be satisfied since it is inconsistent with any prolonged general streaming (however small) past the body. Nevertheless, Stewartson's (1952, 1953) solutions do show that the perturbation can remain small, and these solutions must therefore contain an explanation of the mechanism by which the circulation is maintained at a constant level, though Stewartson does not point this out. Moreover, his solution is very complicated, largely due to the formation of the singular surface at the cylinder $C$, and this rather obscures the mechanism of the flow. In this note, therefore, a much simpler solution which does not have a surface corresponding to $C$ is obtained, the primary aim being to illustrate the mechanism by which the circulation remains constant even when the perturbation remains small.

The flow considered is that due to the slow uniform motion, started impulsively from relative rest, of a paraboloid of revolution along the axis of a rotating liquid. It is found that the radius of any material circuit concentric with the axis of rotation executes small oscillations which are 180° out of phase with the corresponding oscillations in the azimuthal velocity component. As time progresses, the amplitude of these oscillations decays to zero everywhere except on the paraboloid. The ultimate flow is then steady and two-dimensional everywhere except on the paraboloid and on the axis of rotation. On the paraboloid the velocity oscillates finitely and on the axis the velocity component parallel to the axis oscillates finitely and the other components are zero. The swirling motion about the axis found in the case of the sphere and ellipsoid is absent here.

It may be pointed out that the results obtained here can be deduced from Stewartson's (1953) solution for an ellipsoid by carrying out the usual limiting process. But the procedure adopted here is found to be simpler.

## 2. Solution to the problem

We choose cylindrical polar coordinates, $Oz$ along the axis of rotation and $(r, \theta)$ polar coordinates in a plane normal to $Oz$. Let the unperturbed motion of the fluid consist of a uniform angular velocity $\Omega$ about the $z$-axis.

A paraboloid of revolution (whose axis of symmetry coincides with the $z$-axis) impulsively starts to move along the axis at $t = 0$ with uniform velocity $V$. If we choose the origin of coordinates to be in the body, we have in effect superposed a uniform velocity $-V$ on the system and brought the body to rest. Let the components of the fluid velocity along the directions of increasing $r$, $\theta$, $z$, be $u$, $\Omega r + v$, $w$, respectively, where $u$, $v$, $w$ are small. Then the linearized equations of motion are

$$\left.\begin{aligned} \frac{\partial u}{\partial t} - 2\Omega v &= -\frac{\partial P}{\partial r}, \\ \frac{\partial v}{\partial t} + 2\Omega u &= 0, \\ \frac{\partial w}{\partial t} &= -\frac{\partial P}{\partial z}, \end{aligned}\right\} \tag{2.1}$$

$$\frac{1}{r}\frac{\partial}{\partial r}(ru) + \frac{\partial w}{\partial z} = 0, \tag{2.2}$$

where

$$P = \frac{p}{\rho} - \frac{1}{2}\Omega^2 r^2.$$

The boundary conditions are that

$$u \to 0, \qquad v \to 0, \qquad w \to -V, \qquad \text{as } z \to \infty \text{ for fixed } r, t, \tag{2.3}$$

and, on the body, the component of the fluid velocity normal to the body is zero.

As Morgan (1953) pointed out, the initial disturbance travels with infinite velocity and the initial motion relative to the rotating system must be the irrotational motion with the given boundary conditions. Taking the velocity potential of this irrotational flow to be

$$\phi(r, z) = -Vz + \chi(r, z),$$

we have at $t = 0$

$$u = \frac{\partial \chi}{\partial r}, \qquad v = 0, \qquad w = -V + \frac{\partial \chi}{\partial z}.$$

Now to take the Laplace transforms of $u$, $v$, $w$, and $P$, we put

$$\bar{u} = \int_0^\infty e^{-st} u(r, z, t)\, dt, \quad \text{etc.}$$

Then (2.1) and (2.2) become

$$\left.\begin{aligned} s\bar{u} - 2\Omega\bar{v} &= -\frac{\partial \bar{N}}{\partial r}, \\ s\bar{v} + 2\Omega\bar{u} &= 0, \\ s\bar{w} + V &= -\frac{\partial \bar{N}}{\partial z}, \end{aligned}\right\} \tag{2.4}$$

$$\frac{1}{r}\frac{\partial}{\partial r}(r\bar{u}) + \frac{\partial \bar{w}}{\partial z} = 0, \tag{2.5}$$

where $$\overline{N} = \overline{P} - \chi,$$

and the boundary conditions (2.3) become

$$\overline{u} \to 0, \qquad \overline{v} \to 0, \qquad \overline{w} \to -\frac{V}{s} \qquad \text{as } z \to \infty. \tag{2.6}$$

Solving (2.4) we get

$$\left.\begin{aligned} \overline{u} &= -\frac{s}{s^2+4\Omega^2}\frac{\partial \overline{N}}{\partial r}, \\ \overline{v} &= \frac{2\Omega}{s^2+4\Omega^2}\frac{\partial \overline{N}}{\partial r}, \\ \overline{w} &= -\frac{V}{s} - \frac{1}{s}\frac{\partial \overline{N}}{\partial z}, \end{aligned}\right\} \tag{2.7}$$

so that the continuity condition (2.5) becomes

$$\frac{1}{r}\frac{\partial}{\partial r}\left(r\frac{\partial \overline{N}}{\partial r}\right) + \frac{s^2+4\Omega^2}{s^2}\frac{\partial^2 \overline{N}}{\partial z^2} = 0, \tag{2.8}$$

and the boundary condition (2.6) becomes

$$\frac{\partial \overline{N}}{\partial z} \to 0 \quad \text{as } z \to \infty. \tag{2.9}$$

If the section of the paraboloid in the $(z, r)$-plane is $z = -ar^2$, the condition on the body is

$$2aru + w = 0, \qquad \text{or } 2ar\overline{u} + \overline{w} = 0,$$

or, in view of (2.7),

$$2ar\frac{s^2}{s^2+4\Omega^2}\frac{\partial \overline{N}}{\partial r} + \frac{\partial \overline{N}}{\partial z} = -V. \tag{2.10}$$

So equation (2.8) is to be solved with boundary conditions (2.9) and (2.10).

Now we can easily formulate the problem in a coordinate system in which (2.8) can be solved simply and in which the body is a coordinate surface, by taking a suitable transformation of independent variables. We introduce new coordinates $(\xi, \eta)$ defined by

$$z + \frac{K^2}{4a} = K(\xi^2 - \eta^2), \qquad r = 2\xi\eta, \tag{2.11}$$

where

$$K^2 = \frac{s^2+4\Omega^2}{s^2}.$$

On the paraboloid we have

$$\xi = \xi_0 = (K/4a)^{1/2}.$$

With the above transformation equation (2.8) becomes

$$\frac{\partial^2 \overline{N}}{\partial \xi^2} + \frac{1}{\xi}\frac{\partial \overline{N}}{\partial \xi} + \frac{\partial^2 \overline{N}}{\partial \eta^2} + \frac{1}{\eta}\frac{\partial \overline{N}}{\partial \eta} = 0, \tag{2.12}$$

and the boundary condition (2.10) becomes

$$\frac{\partial \overline{N}}{\partial \xi^2} = -2KV\xi_0 \quad \text{on } \xi = \xi_0. \tag{2.13}$$

The appropriate solution of (2.12) is

$$\bar{N} = (A + B\log\xi)(C + D\log\eta),$$

and using (2.13) we get

$$\bar{N} = -2KV\xi_0\log\xi. \tag{2.14}$$

Now

$$\frac{\partial\bar{N}}{\partial z} = \frac{1}{2K(\xi^2+\eta^2)}\left(\xi\frac{\partial\bar{N}}{\partial\xi} - \eta\frac{\partial\bar{N}}{\partial\eta}\right) = -\frac{V\xi_0^2}{\xi^2+\eta^2}.$$

Therefore $\partial\bar{N}/\partial z \to 0$ as $\xi \to \infty$, in agreement with (2.9). Thus (2.14) is the appropriate solution.

The results for $\bar{u}$, $\bar{v}$, $\bar{w}$ follow immediately from (2.7). Finally, inverting these Laplace transforms, we find that the velocity components at any point of the fluid are given by

$$\left.\begin{aligned} u &= \frac{V}{8ar\pi i}\int_{\gamma-i\infty}^{\gamma+i\infty}\left(1 - \frac{(1+4az)s^2+4\Omega^2}{\omega^2}\right)\frac{e^{st}}{s}\,ds,\\ v &= -\frac{\Omega V}{4ar\pi i}\int_{\gamma-i\infty}^{\gamma+i\infty}\left(1 - \frac{(1+4az)s^2+4\Omega^2}{\omega^2}\right)\frac{e^{st}}{s^2}\,ds,\\ w &= -V + \frac{V}{2\pi i}\int_{\gamma-i\infty}^{\gamma+i\infty}\frac{s^2+4\Omega^2}{\omega^2}e^{st}\,ds, \end{aligned}\right\} \tag{2.15}$$

where $\gamma > 0$ and

$$\left.\begin{aligned} \omega^2 &= \{(1+4az)^2 + 16a^2r^2\}^{1/2}(s^2+4\Omega^2l_1^2)^{1/2}(s^2+4\Omega^2l_2^2)^{1/2},\\ l_1^2 &= \frac{1+4az+8a^2r^2-8ar(a^2r^2+az)^{1/2}}{(1+4az)^2+16a^2r^2},\\ l_2^2 &= \frac{1+4az+8a^2r^2+8ar(a^2r^2+az)^{1/2}}{(1+4az)^2+16a^2r^2}. \end{aligned}\right\} \tag{2.16}$$

These results represent a complete formal solution to the problem. For the present purpose of ascertaining the general features of the flow, however, it is only necessary to consider certain special cases of the formulae (2.15).

## 3. General features of the flow

On the surface of the paraboloid the integrals (2.15) simplify considerably and it is possible to evaluate them in the forms

$$\left.\begin{aligned} u &= \frac{2Var}{1+4a^2r^2}\cos\frac{2\Omega t}{(1+4a^2r^2)^{1/2}},\\ v &= -\frac{2Var}{(1+4a^2r^2)^{1/2}}\sin\frac{2\Omega t}{(1+4a^2r^2)^{1/2}},\\ w &= -\frac{4Va^2r^2}{1+4a^2r^2}\cos\frac{2\Omega t}{(1+4a^2r^2)^{1/2}}. \end{aligned}\right\} \tag{3.1}$$

Thus we find that the motion never becomes steady on the paraboloid. More important, perhaps, these results show very simply the way in which the circulation round circular material circuits, concentric with the axis of rotation and lying on the paraboloid, remains constant. Since the radial

velocity $u$ oscillates sinusoidally in time, the radius of such a circuit must oscillate in a similar way, and the primary rotation then makes an oscillatory contribution to the circulation round the circuit. This must, in turn, be counterbalanced by an oscillatory contribution from the azimuthal perturbation velocity $v$, in accordance with (3.1). As far as the validity of the linearized analysis is concerned, the essential feature of this mechanism is that no fluid particle is displaced appreciably in a radial direction from its initial position.

Similarly, on the axis of rotation we find

$$u = 0, \qquad v = 0, \qquad w = -\frac{4Vaz}{1+4az}\cos\frac{2\Omega t}{(1+4az)^{1/2}}. \tag{3.2}$$

Here again the oscillatory axial velocity implies that small material circuits surrounding the axis of rotation are never swept on to the surface of the paraboloid, thereby increasing their perimeter by a large factor; an essential result if the azimuthal perturbation velocity is to remain small.

From these special cases it is reasonable to infer that the same oscillatory mechanism is responsible for maintaining the radial positions of all fluid particles, and this may be verified directly when the motion is approaching its ultimate form. Thus, for large values of $t$, the integrals in (2.15) may be evaluated by inserting cuts in the $s$-plane from $s = \pm 2i\Omega l_1$ and $s = \pm 2i\Omega l_2$ along lines on which the imaginary part of $s$ is constant and the real part decreases. The path of integration may now be replaced by a path round the infinite semicircle $\mathscr{R}\{s\} < 0$ and round the four cuts. For example, the contribution from the branch point $s = 2i\Omega l_1$ to the integral in the first of the equations (2.15) is found to be

$$e^{2i\Omega l_1 t}\frac{1-(1+4az)l_1^2}{l_1(l^2-l_1^2)^{1/2}(4i\Omega l_1)^{1/2}}\frac{\Gamma(\frac{1}{2})}{t^{1/2}}$$

for large $t$. In this way we find that

$$u \sim -\frac{V}{16(ar)^{3/2}(a^2r^2+az)^{1/4}}\left[\frac{1-(1+4az)l_1^2}{l_1(\Omega l_1)^{1/2}}\sin(2\Omega l_1 t-\tfrac{1}{4}\pi)+\right.$$
$$\left.+\frac{1-(1+4az)l_2^2}{l_2(\Omega l_2)^{1/2}}\sin(2\Omega l_2 t+\tfrac{1}{4}\pi)\right]\frac{1}{(\pi t)^{1/2}},$$

$$v \sim \frac{V}{16(ar)^{3/2}(a^2r^2+az)^{1/4}}\left[\frac{1-(1+4az)l_1^2}{l_1^2(\Omega l_1)^{1/2}}\cos(2\Omega l_1 t-\tfrac{1}{4}\pi)+\right.$$
$$\left.+\frac{1-(1+4az)l_2^2}{l_2^2(\Omega l_2)^{1/2}}\cos(2\Omega l_2 t+\tfrac{1}{4}\pi)\right]\frac{1}{(\pi t)^{1/2}},$$

$$w \sim \frac{V}{4(ar)^{1/2}(a^2r^2+az)^{1/4}}\left[\frac{1-l_1^2}{l_1(\Omega l_1)^{1/2}}\sin(2\Omega l_1 t-\tfrac{1}{4}\pi)+\right.$$
$$\left.+\frac{1-l_2^2}{l_2(\Omega l_2)^{1/2}}\sin(2\Omega l_2 t+\tfrac{1}{4}\pi)\right]\frac{1}{(\pi t)^{1/2}}.$$

Thus the only significant difference here is that the amplitude of the oscillations decreases to zero, so that the ultimate motion is in general steady and two-dimensional and the axial velocity of the fluid is ultimately the same as that of the paraboloid.

In view of the ultimate singularity in the velocity gradients on the axis and body it seems that the detailed form (but probably not the general nature) of the solution is of doubtful validity in this neighbourhood.

In conclusion, I wish to thank Professor B. R. Seth for his kind guidance throughout the preparation of this paper.

## References

Morgan, G. W. 1953 *Proc. Camb. Phil. Soc.* **49,** 362.
Stewartson, K. 1952 *Proc. Camb. Phil. Soc.* **48,** 168.
Stewartson, K. 1953 *Quart. J. Mech. Appl. Math.* **6,** 141.

# On the series that represent tides and surges in an estuary

By J. PROUDMAN
*Edgemoor, Verwood, Dorset*

(*Received* 13 *August* 1957)

SUMMARY

This paper is concerned with a progressive wave of general form in an infinitely long estuary of uniform cross-section when there is a permanent current independent of the wave. The only approximation is the neglect of friction. Explicit formulae in the form of infinite series are found for the surface-elevation and for the current.

In the special case in which there is no permanent current and when the oscillation at the mouth of the estuary reduces to a single harmonic constituent, the first five harmonic shallow water constituents at any place up the estuary are evaluated.

## 1. INTRODUCTION

In the making of tide-tables for a port, the basis of the method usually employed is that of a series of harmonic constituents. When the port is on an estuary, a number of these constituents are of the type usually called 'shallow water' constituents. For many years Doodson (1957) has used his method of 'harmonic shallow water corrections' in predicting the times and heights of high and low water. This method implies the existence of a much larger number of shallow water constituents than the number of harmonic units on any predicting machine.

It is the object of the present paper to examine the series in the case of an infinitely long estuary of uniform cross-section when there is a permanent current down the estuary and no friction. This is an ideal problem in the three respects of infinity, uniformity and absence of friction. But, because precise results are obtained, the investigation appears to be of value in spite of the limitations indicated.

As the cross-section of the estuary is uniform, the permanent current is also uniform. Owing to the absence of reflection, the motion takes the form of a progressive wave, and no serious limitation is placed on the shape of this wave at the mouth of the estuary.

The simple basin specified is that which was taken by Saint-Venant (1871), McCowan (1892) and Fjeldstad (1941) when they evolved their accurate finite solutions of the fundamental equations. Saint-Venant did not include a permanent current, but McCowan did. Their solutions show that the heights of high and low water at any place up the estuary are the

same as at the mouth, and this gives a complete answer to the most important question regarding a combination of tide and surge. They also show that a bore will always form, the position of its formation depending on the size and shape of the oscillation at the mouth.

But the solutions of Saint-Venant, McCowan and Fjeldstad do not express the surface-elevation as an explicit function of position and time, and it is just such a function which is required in tidal prediction and which is provided by series.

I first obtained the general formulae of the present paper by substituting series with unknown coefficients into the fundamental differential equations. But Dr M. S. Longuet-Higgins then pointed out that the results could be obtained much more shortly from the implicit solutions by means of Lagrange's theorem on implicit functions. I now follow this method.

The early terms of the series have an interest in themselves, and they take simple forms when there is no permanent current. Taking the special case in which the oscillation at the mouth reduces to a single harmonic constituent, the first five harmonic shallow water constituents are evaluated for any place up the estuary. The first three of these were given by Airy in 1842.

## 2. Notation and general equations

Denote by:

- $g$ the acceleration of gravity;
- $h$ the undisturbed depth of water;
- $x$ distance up the estuary from the mouth;
- $t$ the time;
- $\zeta$ the elevation of the water-surface above its undisturbed level;
- $u$ the current up the estuary;
- $u_0$ the permanent current down the estuary, assumed constant and uniform;
- $F(t)$ the ratio $\zeta/h$ at the mouth of the estuary;

and write

$$c = (gh)^{1/2}, \qquad \theta = x/(c-u_0), \qquad \eta = t-\theta.$$

The equation of continuity is

$$\frac{\partial}{\partial x}\{(h+\zeta)u\} + \frac{\partial \zeta}{\partial t} = 0, \tag{1}$$

and the equation of motion is

$$\frac{\partial u}{\partial t} + u\frac{\partial u}{\partial x} + g\frac{\partial \zeta}{\partial x} = 0, \tag{2}$$

while a stationary solution of these equations is given by

$$\zeta = 0, \qquad u = -u_0. \tag{3}$$

Following Lamb (1932, § 187), multiply (1) by $[g/(h+\zeta)]^{1/2}$ and subtract from (2); the resulting equation may be written

$$\frac{\partial u}{\partial t} - \left(\frac{g}{h+\zeta}\right)^{1/2}\frac{\partial \zeta}{\partial t} + \{u - [g(h+\zeta)]^{1/2}\}\left\{\frac{\partial u}{\partial x} - \left(\frac{g}{h+\zeta}\right)^{1/2}\frac{\partial \zeta}{\partial x}\right\} = 0,$$

and this will be satisfied when

$$\frac{\partial u}{\partial t} - \left(\frac{g}{h+\zeta}\right)^{1/2}\frac{\partial \zeta}{\partial t} = 0, \tag{4}$$

$$\frac{\partial u}{\partial x} - \left(\frac{g}{h+\zeta}\right)^{1/2}\frac{\partial \zeta}{\partial x} = 0. \tag{5}$$

Both (4) and (5) may be integrated to give

$$u + u_0 = 2[g(h+\zeta)]^{1/2} - 2c, \tag{6}$$

where the constant of integration has been chosen so as to satisfy (3). Equation (6) may be written in the forms

$$\frac{u+u_0}{c} = 2\left(1+\frac{\zeta}{h}\right)^{1/2} - 2, \tag{7}$$

$$\frac{\zeta}{h} = \frac{u+u_0}{c} + \frac{1}{4}\left(\frac{u+u_0}{c}\right)^2. \tag{8}$$

Substitution from (8) into (2) gives

$$\frac{\partial u}{\partial t} + (c + \tfrac{1}{2}u_0 + \tfrac{3}{2}u)\frac{\partial u}{\partial x} = 0$$

and into (1) gives

$$\left(1 + \frac{u+u_0}{2c}\right)\left\{\frac{\partial u}{\partial t} + (c + \tfrac{1}{2}u_0 + \tfrac{3}{2}u)\frac{\partial u}{\partial x}\right\} = 0,$$

and hence both (1) and (2) reduce, in effect, to

$$\frac{\partial u}{\partial t} + U\frac{\partial u}{\partial x} = 0, \tag{9}$$

where

$$U = c - u_0 + \tfrac{3}{2}(u+u_0). \tag{10}$$

Substitution from (4), (5) for $\partial u/\partial t$, $\partial u/\partial x$ into (9) gives

$$\frac{\partial \zeta}{\partial t} + U\frac{\partial \zeta}{\partial x} = 0, \tag{11}$$

and from (7) into (10) gives

$$\frac{U}{c} = 3\left(1+\frac{\zeta}{h}\right)^{1/2} - \frac{u_0}{c} - 2. \tag{12}$$

The velocity $U$ is that of propagation of an element of the wave up the estuary.

It is easily verified that solutions of the differential equations (11) and (9) are given respectively by

$$\zeta/h = F(t-x/U), \tag{13}$$

$$(u+u_0)/c = f(t-x/U), \tag{14}$$

where $F(\ )$, $f(\ )$ are any differentiable functions. Since $x=0$ at the mouth of the estuary, the function $F$ is that which has been defined above. The function $F(t)$ will be regarded as prescribed, and from its physical meaning it follows that $F(t) > -1$. From (7) it follows that

$$\tfrac{1}{2}f = (1+F)^{1/2} - 1, \tag{15}$$

the arguments of $F$, $f$ being the same.

Equation (13) is equivalent to McCowan's solution (1892), and when $u_0 = 0$ it is equivalent to Saint-Venant's solution (1871).

It is seen from (12) and (13) that, for the same time, the effect of the permanent current is to make a specified surface-elevation occur at a shorter distance up the estuary than when there is no such current.

## 3. The series

The equations (13) and (14) give $\zeta$ and $u$ as implicit functions of $t$ and $x$, but it is the object of this paper to obtain $\zeta$ and $u$ as explicit functions. Such explicit functions, in the form of infinite series, may be derived from (13) and (14) by means of Lagrange's theorem on the expansion of a function which is defined implicitly (Edwards 1896, p. 451).

Lagrange's theorem may be stated as follows. Let $\phi(y)$, $\psi(y)$ be functions which may be expanded in powers of $y-\eta$, and let

$$y = \eta + \theta\,\phi(y);$$

then

$$\psi(y) = \psi(\eta) + \sum_{n=1}^{\infty} \frac{\theta^n}{n!} [\{\phi(\eta)\}^n\, \psi^{(1)}(\eta)]^{(n-1)}, \tag{16}$$

where the bracketed indices denote derivatives with respect to $\eta$.

Now, in the present application of the theorem, the parameters $\eta$ and $\theta$ are given the meanings indicated at the beginning of § 2, so that

$$t - \frac{x}{U} = \eta + \theta\left(1 - \frac{c-u_0}{U}\right) = y,$$

on taking

$$\phi(y) = 1 - \frac{c-u_0}{U}; \tag{17}$$

thus (13) and (14) may be written as

$$\zeta/h = F(y), \tag{18}$$

$$(u+u_0)/c = f(y). \tag{19}$$

From (12), (17) and (18) it follows that

$$\phi(y) = 1 - \frac{c-u_0}{3c[1+F(y)]^{1/2} - u_0 - 2c}$$

$$= \frac{[1+F(y)]^{1/2} - 1}{[1+F(y)]^{1/2} - \frac{1}{3}u_0/c - \frac{2}{3}}, \tag{20}$$

and from (15) that

$$f^{(1)}(y) = \frac{F^{(1)}(y)}{[1+F(y)]^{1/2}}. \tag{21}$$

It will be supposed that $F(y)$ and $f(y)$ satisfy the condition imposed on $\psi(y)$ in Lagrange's theorem. From (18) and (20), the expansion (16), with $F$ in place of $\psi$, becomes

$$\frac{\zeta}{h} = F(\eta) + \sum_{n=1}^{\infty} \theta^n Z_n(\eta), \tag{22}$$

where

$$Z_n(\eta) = \frac{1}{n!}\left[\left\{\frac{[1+F(\eta)]^{1/2}-1}{[1+F(\eta)]^{1/2}-\frac{1}{3}u_0/c-\frac{2}{3}}\right\}^n F^{(1)}(\eta)\right]^{(n-1)} \tag{23}$$

for $n = 1, 2, 3, \ldots$, and from (15), (19), (20) and (21), the expansion (16), with $f$ in place of $\psi$, becomes

$$\frac{u+u_0}{c} = 2[1+F(\eta)]^{1/2} - 2 + \sum_{n=1}^{\infty} \theta^n U_n(\eta), \tag{24}$$

where

$$U_n(\eta) = \frac{1}{n!}\left[\left\{\frac{[1+F(\eta)]^{1/2}-1}{[1+F(\eta)]^{1/2}-\frac{1}{3}u_0/c-\frac{2}{3}}\right\}^n \frac{F^{(1)}(\eta)}{[1+F(\eta)]^{1/2}}\right]^{(n-1)}. \tag{25}$$

The series (22) and (24), with their coefficients given by (23) and (25), constitute the required solution of the fundamental equations in terms of $F(\ )$, which itself gives the prescribed elevation at the mouth of the estuary.

The condition imposed on $\phi(y)$ in Lagrange's theorem requires that $\phi(y)$ shall not be infinite, and, by (17), this requires that $U$ shall not vanish. Assuming that $U$, the velocity of propagation up the estuary, is once positive, it follows that, for the validity of the expansions (22) and (24), it must always be positive. From (12) and (18) this requires that

$$3[1+F(y)]^{1/2} - u_0/c - 2 > 0. \tag{26}$$

When the expressions (23) and (25) for the coefficients $Z_n(\eta)$ and $U_n(\eta)$ are expanded in ascending powers of $F(\eta)$, the first term in each is

$$\frac{1}{n!}\left[\left\{\frac{3F(\eta)}{2(1-u_0/c)}\right\}^n F^{(1)}(\eta)\right]^{(n-1)},$$

and this is equal to

$$\frac{1}{(n+1)!}\left\{\frac{3}{2(1-u_0/c)}\right\}^n [\{F(\eta)\}^{n+1}]^{(n)}.$$

Examples of this will occur in § 4.

The expansion of $(1+F)^{1/2}$ in ascending powers of $F$ requires that $|F| \leqslant 1$. On combining this with the condition (26) it follows that, for the validity of the expansions,

$$\frac{1}{9}\left(\frac{u_0}{c}+2\right)^2 < 1+F(\eta) \leqslant 2. \tag{27}$$

At the mouth of the estuary, the relationships (27) give the lower and upper bounds of the ratio of the total disturbed depth of water to the undisturbed depth.

4. EARLY TERMS OF THE SERIES WHEN THERE IS NO PERMANENT CURRENT

When $u_0 = 0$, then

$$\theta = x/c, \qquad \eta = t - x/c,$$

and the early terms of the series (22) and (24) may be written as

$$\frac{\zeta}{h} = F + \frac{x}{c}Z_1 + \frac{x^2}{c^2}Z_2 + \frac{x^3}{c^3}Z_3 + \frac{x^4}{c^4}Z_4, \tag{28}$$

$$\frac{u}{c} = U_0 + \frac{x}{c}U_1 + \frac{x^2}{c^2}U_2 + \frac{x^3}{c^3}U_3 + \frac{x^4}{c^4}U_4, \tag{29}$$

respectively, where $U_0 = 2(1+F)^{1/2} - 2$, and the arguments of $F$, $Z_n$, $U_n$ are $t - x/c$.

On using (23) and (25) and expanding $Z_n$, $U_n$ in ascending powers of $F$ as far as $F^5$, the following results are obtained:

$$\left.\begin{aligned}
Z_1 &= \left[\frac{3}{4}F^2 - \frac{7}{8}F^3 + \frac{75}{64}F^4 - \frac{1077}{640}F^5\right]^{(1)}, \\
Z_2 &= \left[\frac{3}{8}F^3 - \frac{63}{64}F^4 + \frac{1341}{640}F^5\right]^{(2)}, \\
Z_3 &= \left[\frac{9}{64}F^4 - \frac{189}{320}F^5\right]^{(3)}, \\
Z_4 &= \left[\frac{27}{640}F^5\right]^{(4)}, \\
U_0 &= F - \frac{1}{4}F^2 + \frac{1}{8}F^3 - \frac{5}{64}F^4 + \frac{7}{128}F^5, \\
U_1 &= \left[\frac{3}{4}F^2 - \frac{9}{8}F^3 + \frac{105}{64}F^4 - \frac{1563}{640}F^5\right]^{(1)}, \\
U_2 &= \left[\frac{3}{8}F^3 - \frac{9}{8}F^4 + \frac{1647}{640}F^5\right]^{(2)}, \\
U_3 &= \left[\frac{9}{64}F^4 - \frac{207}{320}F^5\right]^{(3)}, \\
U_4 &= \left[\frac{27}{640}F^5\right]^{(4)}.
\end{aligned}\right\} \tag{30}$$

These results may also be obtained from the fundamental equations by the method of successive approximations.

5. HARMONIC CONSTITUENTS

When there is no surge, the surface-elevation at the mouth of the estuary is given by a series of the form

$$F(t) = \sum_{n=1}^{\infty} A_n \cos(\sigma_n t + \alpha_n), \tag{31}$$

where $A_n$, $\sigma_n$, $\alpha_n$ are constants. When (31) is substituted into the formulae of § 3, the surface-elevation at any place up the estuary is given by a triple series of harmonic constituents.

When the series (31) reduces to one term, so that $F(t) = A\cos(\sigma t + \alpha)$, then $F(t - x/c) = A\cos\theta$, where $\theta = \sigma(t - x/c) + \alpha$. Substitution into the

results of §4 then gives

$$\left.\begin{aligned}
\frac{Z_1}{\sigma} &= -\frac{3}{4}A^2\sin 2\theta+\frac{21}{32}A^3(\sin\theta+\sin 3\theta)-\\
&\quad-\frac{75}{128}A^4(2\sin 2\theta+\sin 4\theta)+\frac{1077}{2048}A^5(2\sin\theta+3\sin 3\theta+\sin 5\theta),\\
\frac{Z_2}{\sigma^2} &= -\frac{9}{32}A^3(\cos\theta+3\cos 3\theta)+\frac{63}{32}A^4(\cos 2\theta+\cos 4\theta)-\\
&\quad-\frac{1341}{2048}A^5(2\cos\theta+9\cos 3\theta+5\cos 5\theta),\\
\frac{Z_3}{\sigma^3} &= \frac{9}{16}A^4(\sin 2\theta+2\sin 4\theta)-\frac{189}{1024}A^5(2\sin\theta+27\sin 3\theta+25\sin 5\theta),\\
\frac{Z_4}{\sigma^4} &= \frac{27}{2048}A^5(2\cos\theta+81\cos 3\theta+125\cos 5\theta).
\end{aligned}\right\}\quad(32)$$

The terms of the above formulae in $A^2$ and $A^3$ are equivalent to formulae given by Airy in (1842).

Rearrangement of the series (28) so as to group together terms with the same function of $\theta$ gives

$$\begin{aligned}
\frac{\zeta}{h} = A&\left\{1-\frac{9}{32}A^2\left(\frac{\sigma x}{c}\right)^2\left[1+\frac{1}{32}A^2\left\{149-3\left(\frac{\sigma x}{c}\right)^2\right\}\right]\right\}\cos\theta+\\
&+\frac{1}{32}A^3\frac{\sigma x}{c}\left\{21+\frac{1}{32}A^2\left[1077-378\left(\frac{\sigma x}{c}\right)^2\right]\right\}\sin\theta+\\
&+\frac{63}{32}A^4\left(\frac{\sigma x}{c}\right)^2\cos 2\theta-\\
&-\frac{3}{4}A^2\frac{\sigma x}{c}\left\{1+\frac{1}{4}A^2\left[\frac{25}{4}-3\left(\frac{\sigma x}{c}\right)^2\right]\right\}\sin 2\theta-\\
&-\frac{27}{32}A^3\left(\frac{\sigma x}{c}\right)^2\left\{1+\frac{3}{64}A^2\left[149-27\left(\frac{\sigma x}{c}\right)^2\right]\right\}\cos 3\theta+\\
&+\frac{3}{32}A^3\frac{\sigma x}{c}\left\{7+\frac{3}{32}A^2\left[\frac{359}{2}-567\left(\frac{\sigma x}{c}\right)^2\right]\right\}\sin 3\theta+\\
&+\frac{63}{32}A^4\left(\frac{\sigma x}{c}\right)^2\cos 4\theta-\frac{3}{8}A^4\frac{\sigma x}{c}\left\{\frac{25}{16}-3\left(\frac{\sigma x}{c}\right)^2\right\}\sin 4\theta-\\
&-\frac{45}{2048}A^5\left(\frac{\sigma x}{c}\right)^2\left\{149-75\left(\frac{\sigma x}{c}\right)^2\right\}\cos 5\theta+\\
&+\frac{3}{1024}A^5\frac{\sigma x}{c}\left\{\frac{359}{2}-1575\left(\frac{\sigma x}{c}\right)^2\right\}\sin 5\theta.
\end{aligned}\quad(33)$$

## References


Airy, G. B. 1842 *Tides and Waves.* Article in *Encyclopaedia Metropolitana.*

Doodson, A. T. 1957 *Internat. Hydrog. Rev.*, Monaco, **34,** 85.

Edwards, J. 1896 *Differential Calculus.* London : Macmillan & Co.

Fjeldstad, J. E. 1941 *Astrophys. Norvegica*, Oslo, **3,** 223.

Lamb, H. 1932 *Hydrodynamics*, 6th Ed. Cambridge University Press.

McCowan, J. 1892 *Phil. Mag.* (5), **33,** 250.

Saint-Venant, B. de 1871 *Comptes Rendus* **73,** 147 & 237.

# Some properties of boundary layer flow during the transition from laminar to turbulent motion

By S. DHAWAN and R. NARASIMHA
*Department of Aeronautics, Indian Institute of Science, Bangalore*

(*Received* 28 *August* 1957)

SUMMARY

Transition in the boundary layer on a flat plate is examined from the point of view of intermittent production of turbulent spots. On the hypothesis of localized laminar breakdown, for which there is some experimental evidence, Emmons' probability calculations can be extended to explain the observed statistical similarity of transition regions. Application of these ideas allows detailed calculations of the boundary layer parameters including mean velocity profiles and skin friction during transition. The mean velocity profiles belong to a universal one-parameter family with the intermittency factor as the parameter. From an examination of experimental data the probable existence of a relation between the transition Reynolds number and the rate of production of the turbulent spots is deduced. A simple new technique for the measurement of the intermittency factor by a Pitot tube is reported.

## 1. INTRODUCTION

The stability of laminar shear flows and the transition to turbulent motion has received and continues to attract much attention because of its fundamental importance to the study of fluid motions. A great deal of theoretical and experimental work has been done on the instability of laminar boundary layers and in determining criteria for transition. It is known that in general transition can be influenced by the following factors: surface roughness; free stream turbulence; surface curvature; pressure gradient; surface temperature; Reynolds number; Mach number; acoustic radiation; injection or suction of fluid at the wall. Because of the complex manner in which the various factors affect transition, no satisfactory theory for the transition process has been possible so far, and the origin of turbulence is still largely an unsolved problem in fluid mechanics.

Recently, recognition of the intermittent character of laminar breakdown in a boundary layer has directed attention towards the fundamental processes involved. The observations and theoretical work of Emmons (1951) and the experiments of Mitchener (1954), Schubauer & Klebanoff (1955), Tani & Hama (1953), Hama *et al.* (1957) and others have shown that

the transition phenomenon in a boundary layer is characterized by the intermittent appearance of turbulent spots which move downstream with the fluid. The mechanics of spot creation and growth is as yet not completely clear. Experimental observations with flow visualization techniques suggest that the amplification of Tollmein–Schlichting waves becomes associated at some stage with the concentration of vorticity along discrete lines, which subsequently distort into vortex loops in the boundary layer. The vortex loops themselves go through a process of distortion and extension finally resulting in the creation of 'spots' of turbulence. Once created these spots are swept along with the mean flow, growing laterally as well as axially with laminar flow in their trail. The spots originate in a more or less random fashion and increasingly overlap as they enlarge during their transit downstream, finally covering the entire plate and resulting in fully turbulent motion. Passage of the spots over points on the surface results in alternations of laminar and turbulent flow.

These alternations can be quantitatively described by an intermittency factor $\gamma$ which represents the fraction of time any point spends in turbulent flow. Flow at zero pressure gradient over a flat plate is the only case so far studied in any detail. For this case, when transition occurs naturally or due to a disturbing agency which causes the spots to appear at some distance downstream, the spots grow laterally in a nearly linear manner sweeping 'turbulence wedges' on the plate. The angle of these wedges is approximately the same as that for transverse contamination found by Charters (1943). During the initial period the spot growth is non-linear, and envelopes of spot growth exhibit a characteristic curved shape.

The existence of turbulent spots in boundary layer flow has been confirmed experimentally by Mitchener (1954), Schubauer & Klebanoff (1955) and in this laboratory, and it appears to be quite certain that their occurrence plays a fundamental role in the mechanics of boundary layer transition and probably also in the breakdown of laminar motion in general. In this paper the transition region of a boundary layer on a flat plate is examined from a viewpoint which keeps the intermittency of flow as the central feature of the process. It is then sought to utilize the available experimental and analytical information to explain details of the flow in the boundary layer during transition. The main sources of experimental information on the mechanics of transition utilized for analysis here are the experiments by Schubauer & Klebanoff (1955) at the Bureau of Standards, Washington, D.C., and those conducted at the Indian Institute of Science, Bangalore. Both sets were carried out in low-turbulence wind tunnels under carefully controlled environmental conditions.

In the literature it is indeed rare to find transition measurements which provide sufficiently complete information. The most serious omission in the older studies is usually the intermittency factor whose significance was probably not recognized earlier. It is hoped that such measurements will become more common in the future, and will provide more extensive data on transition flows.

## 2. Distribution of intermittency during transition

Experimentally, distributions of the intermittency factor during a transition zone can be measured by placing a hot-wire close to the surface and recording the amplified output on an oscillograph. Typical records obtained in this manner are shown in figure 1 (plate 1). The passage of each spot over the hot-wire is characterized on the oscillographs by random high-frequency fluctuations in contrast to the relatively regular, smooth laminar regions. The factor $\gamma$ is easily calculated from such records by counting the intervals of time for which the traces show turbulent flow.

For a quantitative description of the transition process, Emmons (1951) has formulated a theory based on probability considerations. This theory assumes the existence of a turbulence spot production function $g(x, y, t)$, and Emmons shows how this can be related to the probability of the flow being turbulent at some point, i.e. to the intermittency factor $\gamma$. It has been shown by Narasimha (1957) how the original assumptions about the production of turbulence sources have to be modified in the light of new observations. The main feature of the modification stems from observations which suggest that laminar breakdowns in a two-dimensional flat plate boundary layer are very nearly point-like, and that the spots originate in only a restricted region. On physical grounds which have some support from stability theory, one may argue that the amplified laminar oscillations can be expected to lead to production of the turbulent spots at a fairly definite distance from the leading edge of the plate. Since the actual occurrence of spots is random, one can reason that there must be a region on the plate downstream of the point of instability where the origin of the spots is most probable. At points further downstream, the tendency for breakdown rapidly decreases on account of the state of flow behind a spot as well as the fact that most of the breakdowns have already occurred. Thus the source-rate density function describing spot production should have a maximum at some location. It turns out that the experimentally observed beginning of transition marks this location.

If one assumes a Gaussian error curve with its maximum at $x_t$ to describe the turbulence source-rate function, then Emmons' theory can be used to calculate the resulting $\gamma$ distributions. Here $x_t$ is the location where transition begins. It is interesting to note that the Gaussian curve which gives the best agreement with experimental data has a standard deviation approaching zero. This implies the form of the source-rate function to be very nearly the Dirac delta function. Figures 2 (*a*) and 2 (*b*) show representative cases of transition illustrating calculations based on the above arguments. An interesting and important feature of this hypothesis of localized laminar breakdown is the explanation it suggests for the observed statistical similarity in the transition distributions. Application of this hypothesis together with Emmons' theory gives

$$\gamma = 1 - e^{-A\xi^3}. \tag{1}$$

Here $\xi = (x - x_t)/\lambda$, a normalized stream-wise coordinate in the transition

zone, $\lambda$ being a measure of the extent of the transition region characterized by

$$\lambda = \{x\}_{\gamma=0.75} - \{x\}_{\gamma=0.25},$$

and $A$ is a constant equal to 0·412.

Equation (1) shows that whatever the cause of transition, all transition regions define a single universal intermittency distribution. Figure 3 shows the available data on intermittency during transition, and demonstrates the agreement between equation (1) and experiment. Further experimental

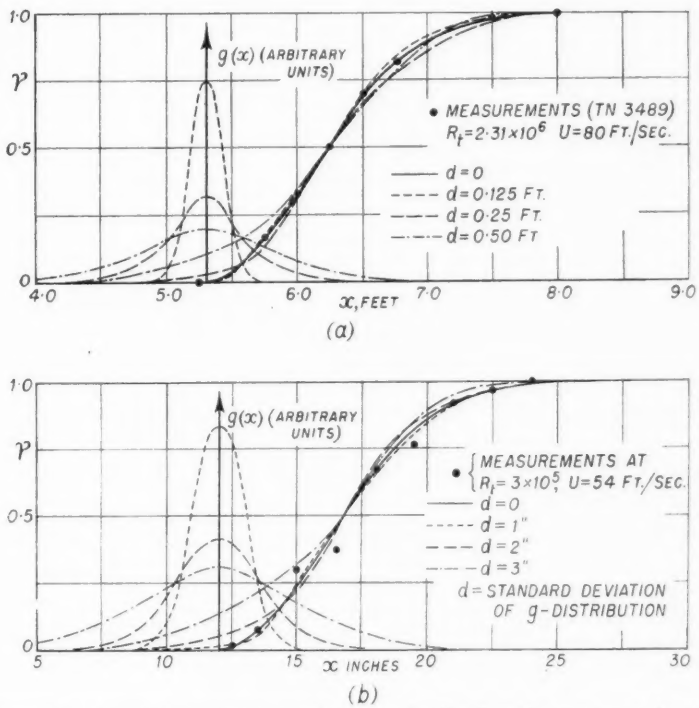


Figure 2. Calculated $\gamma$-distributions for normally distributed source-rate density.

evidence supporting the view that the origin of most of the turbulent spots is very close to the beginning of transition is given by observations of boundary layer thickness during transition. Figure 4 shows two representative cases. They reveal that the virtual origin of the resulting turbulent boundary layer is very nearly at $x_t$. The effect of pressure gradients on the $\gamma(\xi)$ distributions has not yet been investigated in detail, but preliminary measurements indicate that the distribution is modified mainly in the neighbourhood of $\gamma = 0$. Pressure gradients would thus appear to chiefly influence the manner of spot growth in the initial period.

Another point of interest is the distribution of $\gamma$ across the boundary layer, viz. normal to the plate surface. Note that $\gamma(y)$ is a function of the shape of the turbulent spots. The very detailed experiments of Schubauer & Klebanoff (1955) and measurements in this laboratory show that the spots

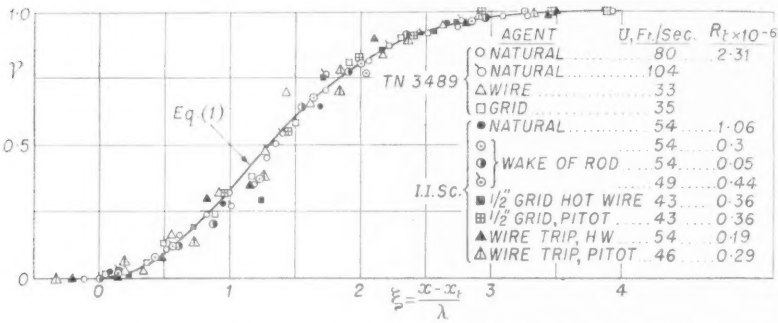


Figure 3. Universal distribution of $\gamma$ *vs* $\xi$ with transition due to different agents.

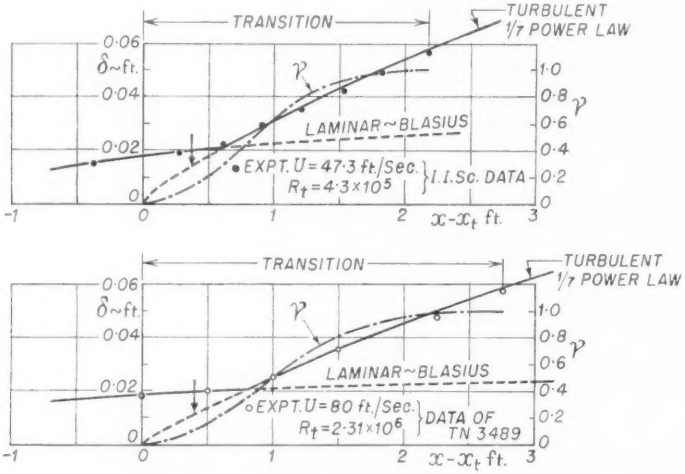


Figure 4. Boundary layer thickness in transition region (arrows mark limit of logarithmic turbulent boundary layer).

have a nearly constant cross-sectional area close to the surface, but they taper towards the outer edge. The measured $\gamma(y)$ distributions during transition are similar to those observed by Corrsin & Kistler (1954) in fully developed turbulent boundary layers, i.e. $\gamma$ varies from a constant maximum value close to the wall to zero towards the edge. While this $\gamma(y)$ variation is probably of importance to the detailed structure of the turbulent motion associated with the spots for all practical purposes, the $\gamma$ value near the wall is the characteristic property of importance for the

transition region. For instance, it is seen in § 3 that the $\gamma(y)$ variation has only a secondary influence in determining the mean velocity profiles in transition.

To sum up, it would appear that the almost point-wise breakdown of laminar flow in a boundary layer while occurring randomly in time takes place very nearly on a discontinuous line across the flow, whatever the cause of breakdown may be.

## 3. Details of transition flow

### (*a*) *Location and extent of the transition zone*

It has been observed in § 2 that the distribution of intermittency is universal on the $\gamma(\xi)$ plot, This implies that the transition zone has always the same extent in terms of the $\xi$-coordinate. This information tells us nothing about the physical location of the beginning of the transition region. So far it is not possible to predict theoretically, even in the simplest case, the Reynolds number of transition $R_t$. Since the mechanics of creation of the turbulent spots has yet to be formulated, attempts such as those by Liepmann (1945) and Lees (1952) to estimate $R_t$ from the development of amplified laminar oscillations lead to difficulties and have not yet been too successful. Experimental investigations have established useful correlations for the effect of particular types of disturbance agencies on $R_t$ (see Dryden (1953), Gazley (1953) and Lin (1955) for recent reviews of the available information). There are, however, unexplained discrepancies, and in any case these correlations are not general enough to predict $R_t$ when there is a combination of transition agencies.

A recent study of the experimental data on boundary layer transition available in the literature shows the possible existence of an interesting relation between the transition Reynolds number $R_t$ and $R_\lambda$, the Reynolds number based on the physical extent of the transition zone. Figure 5 shows a plot of $R_\lambda$ *vs* $R_t$ for the available experimental data. Since in many cases there were unspecified differences in experimental conditions, the data show considerable scatter; but in spite of this one can discern the dependence of $R_\lambda$ on $R_t$. The extent of the transition zone appears to decrease progressively with decreasing $R_t$, to some limiting value. Actually one would expect a family of $R_\lambda$ *vs* $R_t$ curves with each curve depending on the specific agency or agencies causing transition and each having perhaps different limiting values. Figure 5, however, shows that this dependency on the type of disturbance is not too marked, and that for rough estimates a single mean curve may be used. The data are represented on the average by the equation

$$R_\lambda = \alpha R_t^\beta \tag{2}$$

with $\alpha = 5{\cdot}0$ and $\beta = 0{\cdot}8$.

It should be noted that $R_\lambda$ is related to the turbulence source-rate production function of Emmons, and the possible existence of an $R_\lambda$ *vs* $R_t$ relation is probably of some significance to the transition problem. Using

equation (2), it is possible to calculate $\tilde{n}$, the average number of turbulence sources produced per second, as a function of the transition Reynolds number. The results of this calculation are shown as an $\tilde{n}$-scale in figure 5.

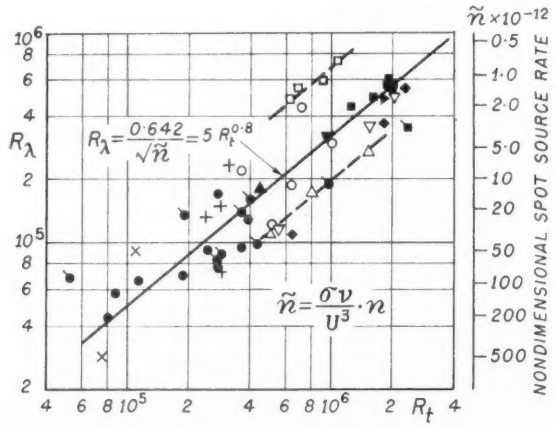


Figure 5. Correlation between $R_t$ and $R_\lambda$. (Flagged points are hot-wire measurements.)

*Subsonic measurements*

- ● Indian Inst. Sci.
- ■ Schubauer & Skramstad (1947), Schubauer & Klebanoff (1955).
- ▲ Dhawan (1953).
- ◗ Hunsaker (1939).
- + × Burgers (1925).

} flat plate

- ■ Wright & Bailey (1939), flat plate with pressure gradient.
- ▼ Silverstein & Becker (1939), aerofoil.

*Supersonic measurements*

- ○ Coles (1954), flat plate, $M = 1{\cdot}97$–$4{\cdot}54$.
- □ Higgins & Pappas (1951), flat plate, $M = 2{\cdot}4$.
- ▽ Chapman & Kester (1953), cone-cylinder, $M = 2{\cdot}9$.
- △ Winter *et al.* (1954), cone, $M = 2{\cdot}45$, $3{\cdot}25$.

### (*b*) *Mean velocity profiles in the boundary layer during transition*

Following the discussions of § 1 and § 2, we note that each point on the flat plate during transition is covered with a laminar boundary layer except during those intervals of time when turbulent spots pass over it. Two questions of immediate interest are: (i) what velocity profile is associated with a turbulent spot during its motion; and (ii) whether the mean velocity profiles during the intermittent transition process exhibit any similarity.

The clue to these and other related questions is contained in the observations which show that the turbulent spots are randomly created at a fairly definite $x$-wise location, and are on the average all similar in shape, their propagation cones being very nearly true cones with straight generators.

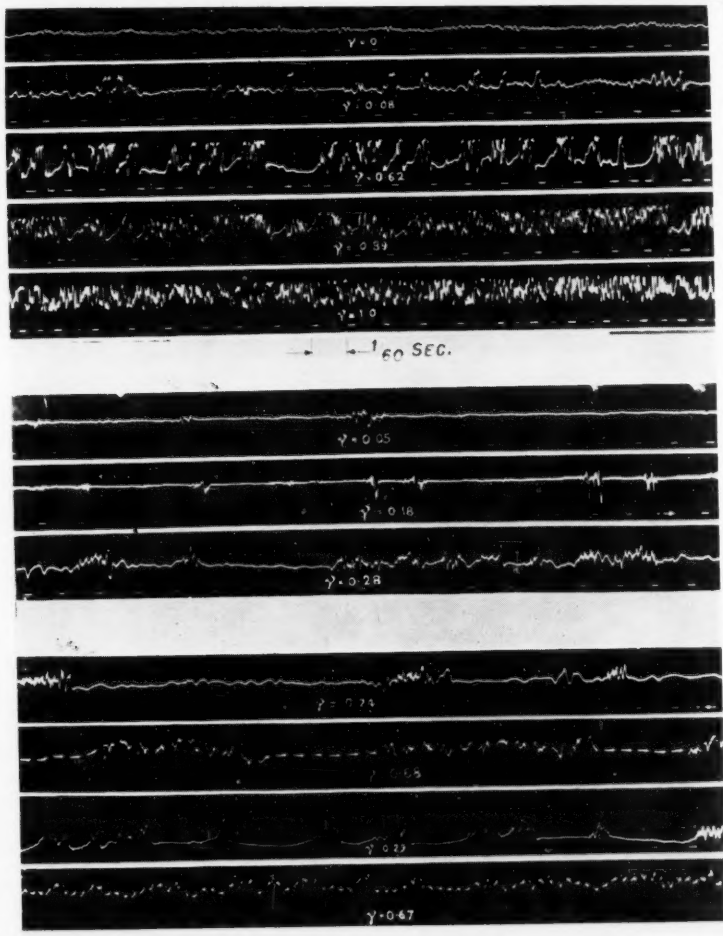


$\gamma(x)$ at $y = 0{\cdot}012$ in.
Transition due to 0·013 in. dia. wire trip

$\gamma(y)$ at $x = 4{\cdot}25$ ft. Natural transition

Natural transition

Transition due to 2 mesh screen

Transition due to isolated roughness element

Transition due to wake of $\frac{1}{8}$ in. dia. rod

Figure 1. Specimen hot-wire records.

The fully turbulent boundary layer on the plate which results after transition exhibits the characteristics of a two-dimensional turbulent layer, because it is a random mix-up of the turbulent spots originating from a narrow localized region. Within the transition zone one can similarly associate, on the average, a two-dimensional boundary layer with each spot, since the transition boundary layer is also a random mix-up of the spots but for smaller intervals of time. The overall effect, therefore, is approximately equivalent to a flow in which, at each point, the boundary layer alternates between a two-dimensional laminar and a two-dimensional turbulent layer, each at its appropriate Reynolds number, $\gamma$ representing the proportion of time spent in turbulent motion. The origin of the laminar layer is at the leading edge of the plate, while $\gamma$ departs from its zero value at some point further downstream. The thickness of the transition boundary layer would be equal to the laminar or the turbulent layer starting from $x_t$, whichever is the greater.

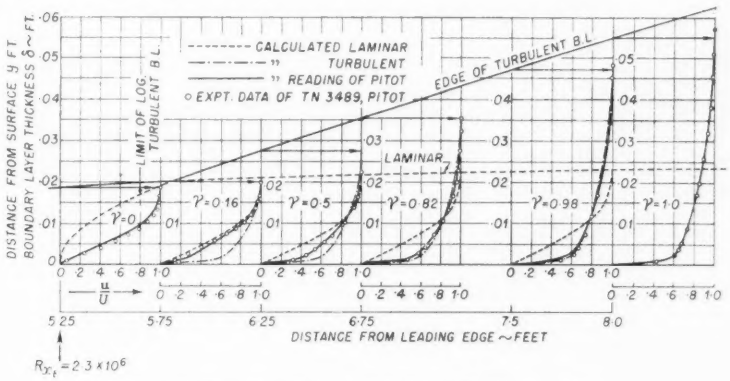


Figure 6. Boundary layer velocity profiles in transition.

Analysis of carefully obtained experimental data confirms the above observations. Figure 4 shows two representative cases of transition flow, and it is seen that the observed thickness of the transition boundary layer closely checks estimates based on the above reasoning. Figure 6 shows a case of transition analysed in detail. The calculated laminar and turbulent profiles between which the flow alternates are shown for each station on the plate where a mean profile was measured with a total-head tube. Also shown on the figure are the calculated mean Pitot profiles obtained by mixing the laminar and turbulent flows.

The agreement between the measurements and the calculations supports the basis of the arguments outlined above. The calculated turbulent boundary layer profiles are based on a combination of the well-known 'law of the wall' and the 'velocity defect law' as discussed by Clauser (1956). The constants entering into these laws were determined in each case from the measured fully developed turbulent profiles. Figures 4 and 6

show that the logarithmic turbulent profile is attained in the turbulent spots quite early in the transition process. The behaviour of turbulent boundary layers at low Reynolds numbers being not very well understood, the deviation of the calculated profiles from the experimental data at low $\gamma$ values is not surprising. The calculations can give only an approximate indication of the state of flow during the early history of a spot.

The Pitot profiles $u_P(y)$ during transition were calculated from the equation

$$u_P(y) = \{(1-\gamma)u_L^2 + \gamma u_T^2\}^{1/2}, \tag{3}$$

$\gamma$ being measured independently by hot-wire techniques and $u_L$, $u_T$ being the theoretical laminar and turbulent profiles respectively. Equation (3), incidentally, indicates that in regions of intermittent flow care must be exercised in interpreting the readings of averaging instruments such as Pitot tubes and hot-wire anemometers. The reading of a Pitot is proportional to pressure ($u^2$); hence the average velocity during transition flow indicated by a Pitot tube (i.e. equation (3)) is different from the true time mean $\bar{u}$, which is given by

$$\bar{u} = (1-\gamma)u_L + \gamma u_T. \tag{4}$$

Equations (3) and (4) are compared in figure 7, which shows a representative transition velocity profile measured carefully by means of a small flat total-head tube. A complete $\gamma(y)$ distribution measured across the boundary layer at the same location is also included.

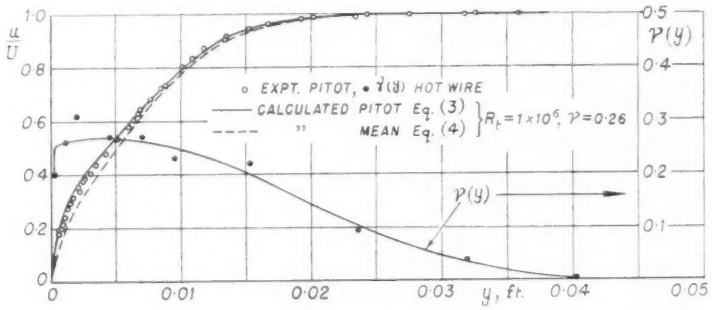


Figure 7. Transition profile.

Significant facts which emerge from the data and calculations of figures 6 and 7 are as follows:

(*a*) The calculated Pitot profiles are in remarkable agreement with the reading of the total-head tube. This agreement proves the soundness of the physical picture on which the analysis is based.

(*b*) Although $\gamma$ varies across the boundary layer, for purposes of profile calculation, the value measured close to the wall gives sufficiently accurate results for the whole profile. Thus the spot shape which is associated with the $\gamma(y)$ variation appears to have only a secondary influence on the transition flow, $\gamma(x)$ being the significant property.

(*c*) Transition velocity profiles measured with a total-head tube must be corrected to give the mean profile. The errors are specially significant close to the wall, and skin friction determinations from uncorrected measured profiles are likely to have large errors.

Before taking up the question of similarity of the mean velocity profiles during transition, it is useful first to consider the boundary layer parameters $\delta^*$, $\theta$, $H$ which are known to play an important part in the quantitative description of boundary layers. During transition the displacement and momentum thickness can be defined as

$$\delta_t^* = \int_0^{\delta_t} \left(1 - \frac{\bar{u}}{U}\right) dy, \tag{5}$$

and

$$\theta_t = \int_0^{\delta_t} \frac{\bar{u}}{U}\left(1 - \frac{\bar{u}}{U}\right) dy, \tag{6}$$

where $\delta_t$ is the thickness of the transition boundary layer, and $\bar{u}(y)$ is given by (4). $U$ is the uniform velocity outside the boundary layer.

Using (4) in (5) and (6), and recognizing that $\delta_t = \delta_L$ if $\delta_L > \delta_T$, or $\delta_t = \delta_T$ if $\delta_T > \delta_L$, we obtain after some simplification

$$\delta_t^* = (1-\gamma)\delta_L^* + \gamma(\delta_T^*), \tag{5a}$$

and

$$\theta_t = (1-\gamma)\{(1-\gamma)\theta_L - \gamma\delta_L^*\} + \gamma\{\gamma\theta_T - (1-\gamma)\delta_T^*\} + 2\gamma(1-\gamma)F(\delta_t), \tag{6a}$$

where $\delta_L^*$, $\delta_T^*$ are displacement thicknesses and $\theta_L$, $\theta_T$ are momentum thicknesses of the laminar and turbulent profiles respectively, and

$$F(\delta_t) = \int_0^{\delta_t} \left[1 - \left(\frac{u}{U}\right)_L \left(\frac{u}{U}\right)_T\right] dy.$$

Figure 8 shows two cases of transition flow for which equations (5a) and (6a) have been compared with experimental data obtained from corrected profiles and $\gamma$ measurements. One set of corrected profiles measured for $R_t = 4{\cdot}3 \times 10^5$ is shown in figure 9, while the other set for $R_t = 2{\cdot}3 \times 10^6$ is the same as that shown in figure 6. The analysis is seen to give good agreement with the measured distributions of $\delta_t^*$ and $\theta_t$. The profile-shape parameter $H$ is given by

$$H_t = \delta_t^*/\theta_t, \tag{7}$$

and this can be put in the form

$$H_t = \frac{(1-\gamma)H_L + \gamma H_T \dfrac{\theta_T}{\theta_L}}{(1-\gamma)^2\left[1 - \dfrac{\gamma}{1-\gamma} H_L\right] + \gamma^2\left[1 - \dfrac{1-\gamma}{\gamma} H_T\right]\dfrac{\theta_T}{\theta_L} + 2\gamma(1-\gamma)\dfrac{F}{\theta_L}}, \tag{7a}$$

where $H_L$ and $H_T$ are the form parameters for the laminar and turbulent boundary layers respectively.

The variation of $H_t$ is shown in figure 8 for the two cases studied. It is interesting to note that when plotted against the $\xi$-coordinate, the variation of $H_t$ in the transition region shows a near universality. Actually, as the

figure shows, one can notice a small Reynolds number effect on $H_t$ mainly towards the latter half of transition. This is to be expected since the turbulent boundary layer associated with the spots depends on $R_t$, the Reynolds number of transition, and $H$ for the turbulent layer is known to vary with Reynolds number. Figure 8 shows that the effect on $H_t$ is small

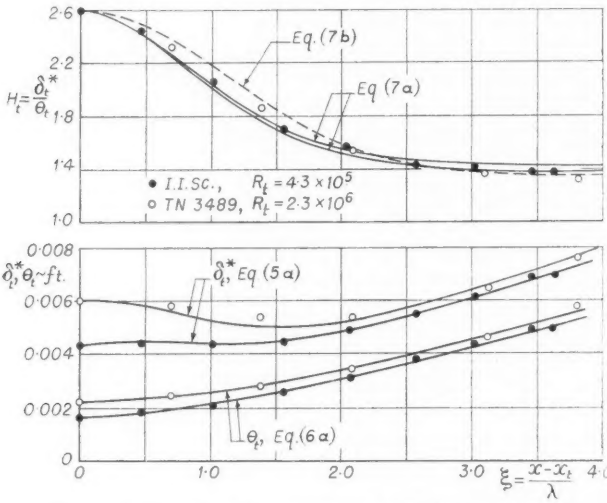
Eq. (7b)
Eq (7a)
$H_t = \frac{\delta_t^*}{\theta_t}$
• I.I.Sc., $R_t = 4{\cdot}3 \times 10^5$
○ TN 3489, $R_t = 2{\cdot}3 \times 10^6$
$\delta_t^*, \theta_t$ ~ ft.
$\delta_t^*$, Eq (5a)
$\theta_t$, Eq. (6a)
$\xi = \frac{x - x_t}{\lambda}$

Figure 8. Boundary layer parameters during transition.

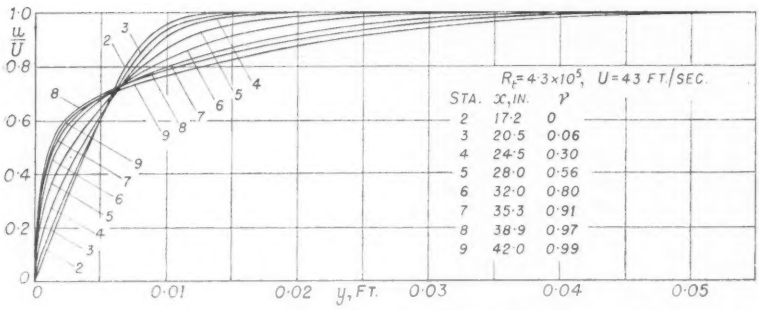


Figure 9. Corrected mean transition profiles (Indian Inst. Sci.).

for a wide range of $R_t$ values. For approximate calculations, a simple expression can be derived for the distribution of the transition-shape parameter. This is of the form

$$H_t = H_T + (H_L - H_T)e^{-A\xi^2}. \tag{7b}$$

This expression implies a linear relation between $H_t$ and $\gamma$, and is plotted in figure 8 for comparison.

Having seen that a knowledge of $R_t$ and $\gamma(x)$ for any case of transition leads to a calculation of the mean velocity profiles as well as the parameters $\delta_t^*$, $\theta_t$ and $H_t$, we now attempt to represent the profiles as far as possible in a unique manner. It is known from boundary layer theory that for steady flow past a flat plate with zero pressure gradient, both the laminar as well as the fully developed turbulent boundary layers exhibit similarity. This fact is usually expressed by the profiles being independent of Reynolds number effects when expressed in the form

$$\left(\frac{u}{U}\right)_L = f\left(\frac{y}{\theta_L}\right), \tag{8}$$

and

$$\left(\frac{u}{U}\right)_T = g\left(\frac{y}{\theta_T}\right). \tag{9}$$

The function $f(\ )$ is defined by the Blasius solution, while $g(\ )$ can be tabulated in terms of the nearly universal turbulent boundary layer logarithmic laws, of which the $\frac{1}{7}$th power law is an approximate representation. Since the mean transition profiles are a resultant of the

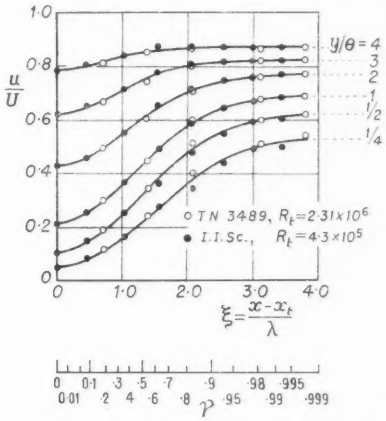


Figure 10. Similarity of transition profiles.

laminar and turbulent profiles combined in proportion to $\gamma$, it is logical to extend the similarity of equations (8) and (9) to transition flow by including the effect of $\gamma$. We thus postulate that

$$\left(\frac{\bar{u}}{U}\right)_t = h\left(\frac{y}{\theta_t}, \gamma\right). \tag{10}$$

In principle the function $h(\ )$ is defined by a solution of the differential equations governing the mean transition flow. Unfortunately, these have yet to be formulated. We resort to an examination of experimental data for information on the form of $h(\ )$.

In figure 10 two sets of mean transition profiles measured for widely differing $R_t$ have been plotted in the form $(\bar{u}/U)_t$ *vs* $\xi$ for fixed values of

$y/\theta$. Since $\xi$ is a function of $\gamma$, a $\gamma$-scale is also shown. Figure 10 shows that the transition profiles do indeed define, at least approximately, a function $h(y/\theta, \gamma)$ which for all practical purposes is independent of Reynolds number. Figure 11 is a cross-plot from figure 10, and shows the universal laminar and turbulent transition profiles as well as the one-parameter family of profiles. Persh (1955) has noted, from an examination of experimental data, that transition profiles exhibit approximate parametric similarity when plotted as $u/U$ *vs* $H$ for fixed $y/\theta$. We recall from (7 b) that $H_t(\xi)$ is nearly independent of Reynolds number effects. Since the functions $\gamma(\xi)$ and $h(y/\theta_t, \gamma)$ are universal, the reasons for the correlation observed by Persh become clear. The representation of transition profile data in the form of equation (10) is to be preferred as it shows the dependence on intermittency explicitly.

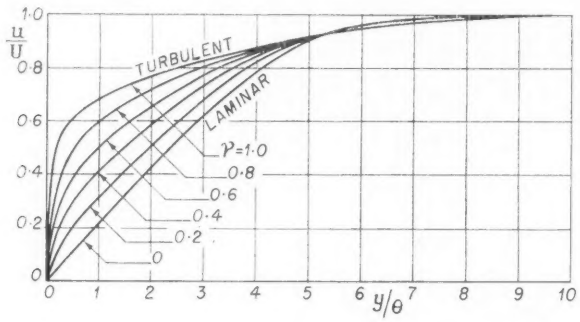


Figure 11. Similarity of transition profiles; $(\bar{u}/U)_t = h(y/\theta_t, \gamma)$.

*(c) Skin friction*

*Local skin friction*

If $c_{f_L}$ and $c_{f_T}$ are the local skin friction coefficients for laminar and turbulent flow respectively, then the mean local skin friction during transition is given by

$$c_{f_t} = (1-\gamma)c_{f_L} + \gamma c_{f_T}. \tag{11}$$

This equation is plotted in figure 12 for the two cases of transition analysed earlier. The transition $c_f$-curves, which fair smoothly into those for laminar and turbulent flow, show a more rapid increase of wall friction than is usually assumed. At the end of transition the local skin friction is seen to be considerably higher than the values given by the turbulent skin friction laws based on the turbulent boundary layer starting at the leading edge of the plate. The usual presentation of skin friction data on a plot of the total friction coefficient $C_F$ *vs* $R_x$ obscures the fact that the origin of the turbulent boundary layer is approximately coincident with the beginning of transition and the onset of intermittency. The usual skin friction curve for turbulent flow must be translated along $R_x$ so that its virtual origin coincides with the foot of transition.

Independent evidence supporting this is provided by the transition local skin friction data of Coles (1954), which is shown in figure 13. Coles' experiments measured $c_{f_t}$ directly, and were conducted at supersonic speeds so that the final turbulent boundary layer curves must include compressibility corrections. In figure 13 the Frankl–Voishel (1943) theoretical curve for $c_{f_T}$ has been used as this is known to give reasonably accurate predictions of supersonic skin friction. The characteristic shape

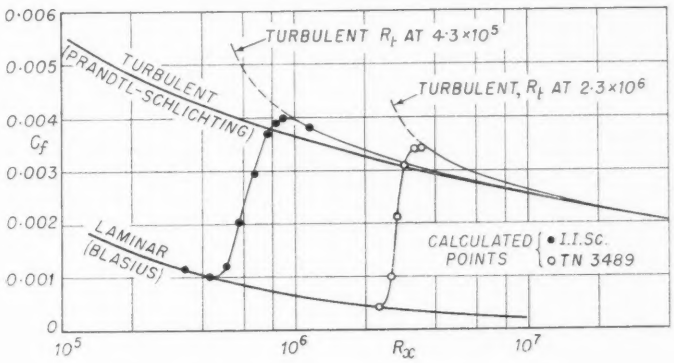


Figure 12. Local skin friction in transition region.

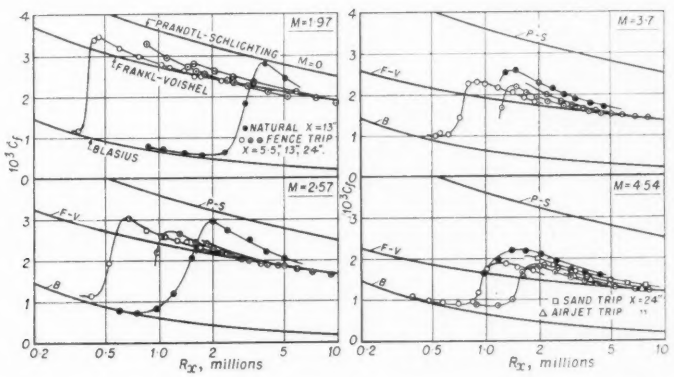


Figure 13. Local skin friction during transition in supersonic flow (from Coles 1954).

of the local $c_f$ curves rising above the turbulent friction curves is seen again. These data also suggest that the mechanism of transition is not altered at supersonic speeds. The fact that after the breakdown of laminar flow the resulting turbulent boundary layer has an effective origin close to the beginning of transition resulting in high $c_f$ values is probably also the reason why measurements of transition recovery factors show values higher than expected (Shoulberg, Hill & Rivas 1954).

Another interesting feature of the transition local skin friction curves is brought out by figure 14, which shows that the difference $\{c_{f_t} - c_{f_t}|_{\gamma=0}\}$ is independent of Reynolds effects during transition. Here $c_{f_t}|_{\gamma=0}$ is the value of $c_{f_L}$ at $x_t$. The points shown on figure 14 were calculated from the corrected experimental profiles used elsewhere in this paper. They approximately define a single curve with $\xi$ as the variable. While it is difficult to give an *a priori* theoretical justification for this observed correlation, a reasonable explanation is as follows.

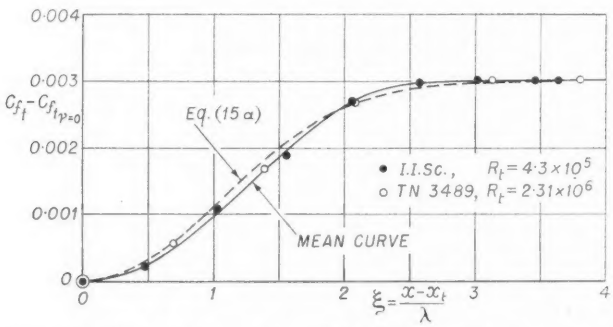


Figure 14. Similarity in variation of skin friction during transition.

We have that in (11) $c_{f_L}$ and $c_{f_T}$ may be represented as

$$c_{f_L} = K_1/R_x^{1/2}, \tag{12}$$

$$c_{f_T} \doteq K_2/R_x^{1/5}, \tag{13}$$

where $K_1$, $K_2$ are constants. Using the definition of $\xi$ and equations (1), (12) and (13), we can write (11) as

$$c_{f_t} = F\{R_t, R_\lambda, \xi\}. \tag{14}$$

Now if $R_t$ and $R_\lambda$ are related as suggested by the experimental data of figure 5, equation (14) becomes

$$c_{f_t} = F\{R_t, \xi\}. \tag{14a}$$

The correlation observed in figure 14 shows this function to have the form

$$F\{R_t, \xi\} = \Phi(R_t) + \Psi(\xi) \tag{14b}$$

with $\Phi(R_t) = c_{f_t}|_{\gamma=0}$, the value of laminar skin friction at the beginning of transition.

We thus get

$$c_{f_t} - c_{f_t}|_{\gamma=0} = \Psi(\xi), \tag{15}$$

function of the $\xi$-coordinate alone. We note that figure 14 implies, once again, that the main Reynolds number effect on transition is through the location of the region of laminar breakdowns. Subsequent events are

controlled by the intermittency and its distribution. An approximate expression for the function $\Psi$ is

$$\Psi(\xi) = 0{\cdot}003(1-e^{-\frac{1}{2}\xi^2}). \tag{15a}$$

This equation is plotted in figure 14.

*Total skin friction*

The behaviour of the local skin friction coefficient during transition discussed above can be used for engineering purposes to calculate the total skin friction of a plate on which transition occurs at some location. Integration of (11) for a plate of length $l$ with transition starting at $x = x_t$ and ending at $x = x_t'$ gives

$$\left.\begin{aligned} C_F &= \frac{1}{l}\int_0^l c_f\,dx \\ &= \frac{x_t}{l}\int_0^{x_t} c_{f_L}\,dx + \frac{\lambda}{l}\int_0^{\xi} c_{f_t}\,d\xi, \qquad \text{for } l \leqslant x_t', \\ &= \frac{x_t}{l}\int_0^{x_t} c_{f_L}\,dx + \frac{\lambda}{l}\int_0^{4\cdot0} c_{f_t}\,d\xi + \frac{1}{l}\int_{x_t'}^{l} c_{f_T}\,dx, \qquad \text{for } l > x_t'. \end{aligned}\right\} \tag{16}$$

Here the upper limit of the second integral for $l > x_t'$ has been taken to be $\xi = 4{\cdot}0$ in accordance with figure 3.

These expressions may be put in a more convenient form by utilizing the approximate relation (15a) and the $R_t$ *vs* $R_{\lambda}$ relation of (2). The total skin friction coefficient $C_F$ is then given by

$$\left.\begin{aligned} C_F &= \frac{a+bR-C\,\mathrm{erf}(dR'/R_t^{\beta})}{R_l}, \qquad \text{for } l \leqslant x_t', \\ \text{and} \\ C_F &= \frac{R'C_{F_T}-k}{R_l}, \qquad \text{for } l > x_t', \end{aligned}\right\} \tag{16a}$$

where

$$a = R_t\{C_{F_L}|_{\gamma=0}\}, \qquad b = 0{\cdot}003 + C_{F_L}|_{\gamma=0},$$

$$C = 0{\cdot}00376\alpha R_t^{\beta} = 0{\cdot}0188R_t^{0{\cdot}8}, \qquad d = 0{\cdot}707/\alpha = 0{\cdot}141,$$

$$k = C-a+4\alpha R_t^{\beta}\{C_{F_T}|x_t'-b\} = 5\{0{\cdot}00376+4(C_{F_T}|x_t'-b)\}R_t^{0{\cdot}8}-a,$$

$$\alpha = 5{\cdot}0, \qquad \beta = 0{\cdot}8, \qquad R' = R_x - R_t,$$

$$\mathrm{erf}\,z = \frac{2}{\sqrt{\pi}}\int_0^z e^{-s^2}\,ds.$$

Equation (16a) is plotted for a range of $R_t$ values in figure 15. For one case a comparison is shown with Emmons' calculations, the usual Prandtl–Schlichting estimation, and Geber's experimental data (see Schlichting 1955). The present analysis shows a sharper rise of $C_F$ due to transition than is indicated by Emmons and shows a rounding-off of the transition curve at the beginning of transition unlike the Prandtl–Schlichting semi-empirical curve.

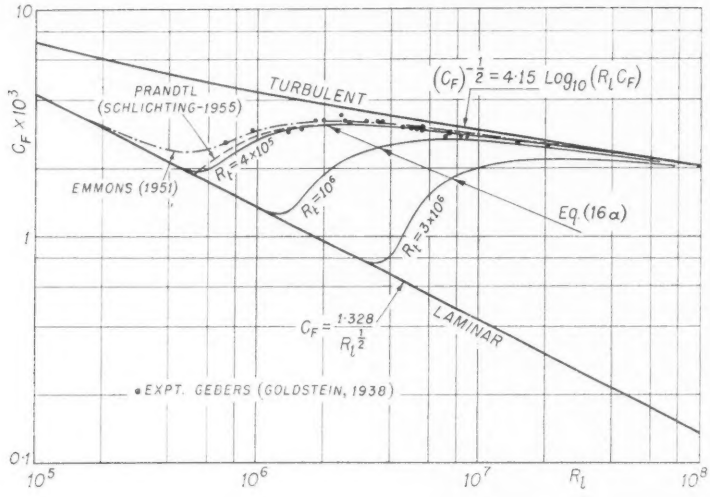


Figure 15. Mean friction coefficient of a flat plate with transition at $R_t$.

## 4. Estimation of $\gamma$ by a Pitot tube

It has been shown in § 3 that fairly good agreement is obtained between the velocity profiles measured by a Pitot tube and those calculated from the formula (obtained immediately from (3))

$$\left(\frac{u}{U}\right)_P = \left\{(1-\gamma)\left(\frac{u}{U}\right)_L^2 + \gamma\left(\frac{u}{U}\right)_T^2\right\}^{1/2}$$

using measured values for $\gamma$ and the theoretically known values for $(u/U)_L$ and $(u/U)_T$. This immediately suggests the possibility of experimentally obtaining $\gamma$ without having to use the hot wire and associated equipment. From the measured velocity profile, or indeed from a single measurement of $(u/U)_P$ in the transition region at a certain height from the surface, $\gamma$ can be obtained as

$$\gamma = \frac{\left(\frac{u}{U}\right)_P^2 - \left(\frac{u}{U}\right)_L^2}{\left(\frac{u}{U}\right)_T^2 - \left(\frac{u}{U}\right)_L^2}, \tag{17}$$

where $(u/U)_P$ is the reading of the Pitot tube.

A suitable procedure for determining the $\gamma$-distribution by this method is to traverse a Pitot tube along the transition region at a fixed height above the surface. To get the best results, the height should be such that the difference in the velocity, at that height, between the laminar and turbulent profiles is as large as possible throughout the transition region. From an examination of figures 9 and 10, it seems that this height should be of the order of $\theta$. A surface tube is not likely to give satisfactory results, as its readings cannot always be quantitatively interpreted.

Figure 16 compares intermittency measurements obtained for the same flow by the hot wire and Pitot methods. For the latter, the velocities $(u/U)_p$ were read off, for a height from the surface of 0·024 in., from measured Pitot velocity profiles. Figure 17 shows the results obtained from a Pitot traverse at a height of 0·035 in., together with the calculated laminar and turbulent curves. The origin for the turbulent boundary layer was chosen as the point where the measured curve departs from the

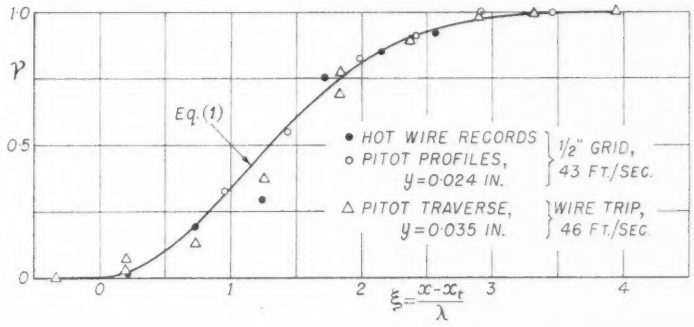


Figure 16. Estimation of $\gamma$ using a Pitot tube.

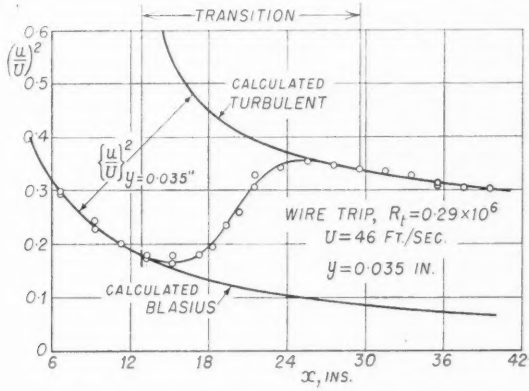


Figure 17. Pitot traverse along plate to estimate $\gamma$.

laminar. Incidentally, a simple method of obtaining the 'turbulent' curve in figure 17 is to plot the measured fully-turbulent points on logarithmic paper against $(x-x_t)$ and draw a straight line through them extending upstream. This line then gives the $(u/U)_T$ values for the $\gamma$ determination in the transition region. This procedure gives good results and would be completely justified if the turbulent profiles followed a power law with a constant index throughout. The values of the intermittency obtained from this experiment are also plotted in figure 16.

## Concluding remarks

In spite of the origin of turbulence remaining obscure, Emmons' picture of transition in a laminar boundary layer supplemented by experimental information allows a detailed physical model of the process to be set up. From this a relatively adequate calculation of the macroscopic effects can be carried out.

One of us (R. N.) wishes to acknowledge his indebtedness to the National Institute of Sciences of India for a Fellowship held during the course of this research.

## References

Burgers, J. M. 1925 *Proc. 1st Internat. Cong. Appl. Mech., Delft*, 113.

Chapman, D. R. & Kester, R. H. 1933 *J. Aero. Sci.* **20,** 441.

Charters, A. C. 1943 *Nat. Adv. Comm. Aero., Wash., Tech. Note* no. 891.

Clauser, F. H. 1956 Article in *Advances in Applied Mechanics*, Vol. 4. New York : Academic Press.

Coles, D. 1954 *J. Aero. Sci.* **21,** 433.

Corrsin, S. & Kistler, A. L. 1954 *Nat. Adv. Comm. Aero., Wash., Tech. Note* no. 3133.

Dhawan, S. 1953 *Nat. Adv. Comm. Aero., Wash., Rep.* no. 1121.

Dryden, H. L. 1953 *J. Aero. Sci.* **20,** 477.

Emmons, H. W. 1951 *J. Aero. Sci.* **18.** 490.

Frankl, F. & Voishel, V. 1943 *Nat. Adv. Comm. Aero., Wash., Tech. Mem.* no 1053.

Gazley, C., Jr. 1953 *J. Aero. Sci.* **20,** 19.

Goldstein, S. (Ed.) 1938 *Modern Developments in Fluid Dynamics*, Vol. 2. Oxford University Press.

Hama, F. R., Long, J. D. & Hagerty, J. C. 1957 *J. Appl. Phys.* **28,** 388.

Higgins, R. W. & Pappas, C. C. 1951 *Nat. Adv. Comm. Aero., Wash., Tech. Note* no. 2351.

Hunsaker, J. C. 1939 *J. Aero. Sci.* **6,** 104.

Lees, L. 1952 *Consolidated Aircraft Corporation Rep.* no ZA–7–006.

Liepmann, H. W. 1945 *Nat. Adv. Comm. Aero., Wash., A.C.R.* no. 4J28.

Lin, C. C. 1955 *The Theory of Hydrodynamic Stability*. Cambridge University Press.

Mitchner, M. 1954 *J. Aero. Sci.* **21,** 350.

Narasimha, R. 1957 *J. Aero. Sci.* **24,** 711.

Persh, J. 1955 *J. Aero. Sci.* **22,** 443.

Schubauer, G. B. & Klebanoff, P. S. 1955 *Nat. Adv. Comm. Aero., Wash., Tech. Note* no. 3489.

Schubauer, G. B. & Skramstad, H. K. 1947 *J. Aero. Sci.* **14,** 69.

Schlichting, H. 1955 *Boundary Layer Theory*. London : Pergamon Press.

Shoulberg, R. H., Hill, J. A. R. & Rivas, M. A., Jr. 1954 *J. Aero. Sci.* **21,** 763.

Silverstein, A. & Becker, J. V. 1939 *Nat. Adv. Comm. Aero., Wash., Rep.* no. 637.

Tani, I. & Hama, F. R. 1953 *J. Aero. Sci.* **20,** 289.

Winter, K. G., Scott-Wilson, J. B. & Davies, F. V. 1954 *Aero. Res. Counc., Lond., Curr. Pap.* no. 212.

Wright, E. A. & Bailey, G. W. 1939 *J. Aero. Sci.* **6,** 485.

# REVIEWS

**Jets, Wakes and Cavities,** by GARRETT BIRKHOFF and E. H. ZARANTONELLO. New York : Academic Press, 1957. 353 pp. $10.00 or 80*s*.

There can be little doubt that Helmholtz, with his paper " Über discontinuerliche Flüssigkeitsbewegungen " (1868), laid one of the cornerstones of modern fluid mechanics. He himself, with the editors of *The Philosophical Magazine*, who published a translation of the paper in the same year, was confident of its importance—just as, thirty-six years later, Prandtl was confident in his paper on the boundary layer. Yet, Helmholtz seems not to have known which cornerstone he was laying, and probably he imagined that he was laying Prandtl's.

Certainly the discontinuous solutions of Laplace's equation constructed by Helmholtz, and by his successors such as Kirchhoff (who introduced the name ' free streamline ') and Rayleigh, have found effective application almost exclusively to flows of liquid bordered by regions of gas or vapour—notably, liquid jets in a gaseous atmosphere, and liquid flows about obstacles with cavity formation—whereas the flows of a single homogeneous fluid, to which the authors originally intended the solutions to apply, have proved too complicated for detailed study by these means. Meanwhile, the theory and practice of constructing such discontinuous solutions have been developed to a high degree of virtuosity by an army of workers, and many interesting phenomena have been illuminated as a result. Nevertheless, too few of those writing on the subject have grasped its true relation to physical phenomena, and many have repeated almost word for word the errors of the founders of the theory, such as Helmholtz's ascription of flow separation from a solid surface to causes which really are those underlying cavitation. Especial harm has been done by the writers of hydrodynamical textbooks, who have actively propagated false views of the significance of free-streamline theory.

The vast structure built upon Helmholtz's original paper—comprising the mathematical theory of the existence and uniqueness of flows with free streamlines ; the techniques of obtaining analytical expressions for such flows in particular cases and then translating them into numerical results ; the use of the solutions to throw light on jet collisions, on planing, on the effectiveness of shaped charges, on vapour-filled and air-filled cavities, on contraction coefficients and flows over weirs and waterfalls ; the experimental and theoretical study of the physical conditions in flows involving jets and cavities and the relation between these conditions and aspects of the mathematical solutions ; the further study of possible relationships between separated flows of a homogeneous fluid and particular types of free-streamline solution—all this is a structure spanning the widely different disciplines of pure and applied mathematics, and involving substantial parts of physics and engineering. The need for a unified account of all this varied material, which would help those working on isolated parts of it to see the material as a whole, and reduce the danger of

their misinterpreting its significance, has long existed, as has the difficulty of finding anyone competent to undertake such a synthesis.

Now Professors Garrett Birkhoff and E. H. Zarantonello, both distinguished workers in the field, have collaborated to produce just such a unified account, and it is a real pleasure to report that they have succeeded, achieving both the necessary breadth and the necessary depth. Professor Birkhoff is to be congratulated on having made the difficult transition from pure to applied mathematics, at least for the purpose of writing parts of this book; and those applied mathematicians who found their enjoyment of his *Hydrodynamics* spoilt by its oversimplified view of the relations between natural science and mathematics can be assured that this experience will not be repeated.

The authors are particularly strong adherents to the view that free streamlines are valuable only as representations of liquid–gas boundaries. With the principal object of emphasizing this, they include three chapters on wakes and jets in the flow of homogeneous fluid (for example, air jets in air), chapters which summarize rather briefly the knowledge in these fields but at least make clear to any doubters that an approach to them by means of free-streamline solutions must be quite inadequate. With the exception of these chapters (12–14) the book is a study of cavities and liquid jets, and of the theory of the mathematical determination of free-streamline solutions.

The authors are careful not to give an oversimplified view of the cavitation phenomenon, and they devote their final chapter to its many complexities as well as to descriptions of the various instabilities which lead to the break-up of jets.

Naturally, one of the most useful features of the book is the ' zoo ' of basic free-streamline flows, that is, two-dimensional irrotational flows with either the magnitude or the direction of the velocity uniform along each portion of the boundary. The zoo is well arranged, in three chapters (2, 3 and 5) dealing with types of flow in increasing order of complexity. In these chapters there are some sixty sketches of particular configurations, showing simply the solid boundaries and the free streamlines in each case, which, with a sentence or two in the text, identify the flow clearly. In addition, the analytical expressions for the solution are given, and remarks about its utility, if any. In chapter 9 the numerical computation of these flows is systematically discussed. Streamline shapes and other details of the internal flow are obtained in many cases and exhibited in a series of plates at the back of the book. This is a big advance, since, in previous work, details only of the boundary streamlines had been computed for flows of this kind. In addition, many tables and graphs are given of the relations between the defining parameters for particular types of flow.

The general theory of the existence, uniqueness and nature of free-streamline flows, including those with curved solid boundaries, is treated in chapters 4, 6 and 7. A knowledge of at least the results of this material is of the greatest help to those using free-streamline solutions. Readers wishing to understand the proofs will have to make a very real effort,

but fortunately they are set out in a civilized way which does not prevent a reader skimming the cream of the results while only sipping at the difficult ideas underlying their demonstration.

The first half of chapter 8 is devoted to the Chaplygin compressible-flow free-streamline theory of gaseous jets, a subject included somewhat inconsistently in view of the authors' general contention that only liquid jets are well represented by free-streamline theory. This chapter ends with some remarks about the problem of including gravitational effects. However, it gives no account of perturbation methods in this connection, and computations by the relaxation method are not mentioned, being only briefly treated in a section at the end of chapter 9, whereas they have proved especially fruitful for calculating free streamline flows under gravity. Chapter 10 is a good account of what is known about axisymmetric free-streamline flows, and chapter 11 takes us rapidly, but with references, through an extensive miscellany of unsteady flows with free boundaries.

When one looks back over this book, which is such a welcome addition to the shelf of really good hydrodynamical treatises, it is difficult to find any general questions on which one would like to challenge the authors. However, I will try. Perhaps the one possible fault is an inevitable consequence of one of the book's chief virtues, namely its insistence (so necessary in view of the errors of the past) that flows of homogeneous fluid with separation are too complicated to be represented by free-streamline solutions. At the end of the book, on the other hand, one would like to ask: "Given that this is indisputably true in the main, are there not still occasional points where free-streamline theory can throw some light on flows of homogeneous fluid?" In other words, was Helmholtz completely wrong?

For example, the authors' figure 3 in chapter 2 indicates that the pressure distribution on a flat plate, at an angle of incidence of 15° or more, is close to that given by one of the cavitation models (such as that with a re-entrant jet, but admittedly all the models give much the same distribution over the plate), with a cavity pressure equal to that found experimentally on the leeward side of the plate. Also, figures 2 in both chapter 1 and chapter 14 indicate that a re-entrant jet model is a reasonable qualitative representation of the flow near the plate, although the real flow becomes fuzzier and fuzzier (relative to the model) as one goes away from the plate.

Again, there are experimental indications that vortex sheets in the neighbourhood of solid boundaries are fairly stable, so that free-streamline models may be more useful for representing 'separation bubbles' (that is, finite dead-air regions produced by boundary-layer separation followed by reattachment) than, say, wakes. The choice of model for a separation bubble would involve boundary-layer considerations to determine the position of separation.

But it probably needs to be pointed out that the authors of this book are at their weakest in boundary-layer considerations. Fortunately, the main sections of the book do not lose much from this, since on most solid boundaries in the free-streamline solutions which are discussed the flow is accelerating, so that boundary layers should be thin and should not separate.

However, there are several flows illustrated involving flow round a corner in a wall (see chapter 2, figures 4a, 4b, 6d ; chapter 3, figures 10b, 12a ; chapter 5, figures 7a, 7b, 8a, 8b, 8c, 8d, 8e, 10a, 10b, 10c). In all of these, boundary-layer separation would cause large inaccuracies in the solution—a circumstance to which the reader's attention should have been drawn more explicitly.

Actually, there is no evidence in the book itself that the authors are aware of this fact in the case of corners concave to the flow. If they had been, they would presumably not have delayed the only discussion of boundary layers and separation until chapter 14, where a single page is devoted to the subject. This page, indeed, is a peculiar one, apparently designed to play down the role of the boundary layer, and it fails to state clearly that separation will not occur at all in flows with sufficiently small adverse pressure gradients along solid boundaries.

It is surprising that authors who have written at such length on irrotational flows should wish to play down the boundary layer, by whose presence alone irrotational flows are made possible in the face of the hydrodynamic boundary condition of zero relative velocity at a solid boundary. The Navier–Stokes equations for incompressible flow are exactly satisfied by irrotational flow fields, but these are compatible with the boundary condition only if a boundary layer intervenes between them and any solid boundary. A flow irrotational outside this thin layer will be possible only if the equations governing the dynamics of the layer, in the environment of the given irrotational flow, permit a steady solution without such a singularity as is implied by the separation condition. Divergences between theory and experiment for boundary layers which do separate (that is, for which the equations reach this singularity) constitute no criticism of a theory whose most important conclusion is the condition under which separation will be absent.

However, this condition is not satisfied by any flow along a wall up to a stagnation point (like a concave corner). It is for this reason that flows involving separation bubbles (see for example chapter 5, figures 2b, 2c, 2d in this book) have been proposed to describe such cases. The present reviewer has argued for such a model in the case of flow up a step (apparently without convincing Professor Birkhoff, for one cannot, alas, suppose the reference unknown to such an accomplished bibliographer !). In addition, there is reason to hope that free-streamline theories of separation bubbles on thin aerofoils at high angle of incidence may gradually achieve greater accuracy.

Still, it must be confessed that the authors' case remains a tenable one, and that Helmholtz's vindication is yet to come. In the meantime, the appearance of this powerful critical survey of the present position in the whole subject may be regarded as bearing witness to the vitality of his original conception. Our thanks are due to the authors for making such a book as pleasant to read as it is comprehensive and instructive.

M. J. Lighthill

JOURNAL OF FLUID MECHANICS

Volume 3, Part 4 January 1958

## CONTENTS

Flow past a flat plate at low Reynolds numbers
by E. JANSSEN .. .. .. .. .. .. 329

Further space-time correlations of velocity in a turbulent boundary layer
by A. J. FAVRE, J. J. GAVIGLIO and R. J. DUMAS .. .. 344

A simple derivation of Lighthill's heat transfer formula
by H. W. LIEPMANN .. .. .. .. .. 357

Turbulent flow in a stably stratified atmosphere
by A. A. TOWNSEND .. .. .. .. .. 361

The minimum Reynolds number for a turbulent boundary layer and the selection of a transition device
by J. H. PRESTON .. .. .. .. .. .. 373

Two-dimensional flow at high subsonic speeds past wedges in channels with parallel walls
by J. B. HELLIWELL .. .. .. .. .. 385

Slow motion of a paraboloid of revolution in a rotating fluid
by L. V. K. VISWANADHA SARMA .. .. .. .. 404

On the series that represent tides and surges in an estuary
by J. PROUDMAN .. .. .. .. .. .. 411

Some properties of boundary layer flow during the transition from laminar to turbulent motion
by S. DHAWAN and R. NARASIMHA .. .. .. .. 418

*Reviews* .. .. .. .. .. .. .. .. 437

Printed in Great Britain by Taylor & Francis Ltd.